CACNB4 Overexpression and Dendritic Spine Loss in Schizophrenia

by

Emily Meredith Parker

A.B., University of Georgia, 2011

M.A., Columbia University, 2015

Submitted to the Graduate Faculty of the

School of Medicine in partial fulfillment

of the requirements for the degree of

Doctor of Philosophy

University of Pittsburgh

2020

UNIVERSITY OF PITTSBURGH

SCHOOL OF MEDICINE

This dissertation was presented

by

Emily Meredith Parker

It was defended on

September 22, 2020

and approved by

Robert Sweet, UPMC Endowed Professor, Department of Psychiatry

Michael Gold, Professor, Department of Neurobiology

Maria Rubio, Professor, Department of Neurobiology

Srivatsun Sadagopan, Assistant Professor, Department of Neurobiology

Zachary Wills, Assistant Professor, Department of Neurobiology

Peter Penzes, Professor, Department of Physiology, Northwestern University

Dissertation Director: Stephen Meriney, Professor, Department of Neuroscience

CACNB4 Overexpression and Dendritic Spine Loss in Schizophrenia

Emily Meredith Parker, Ph.D.

University of Pittsburgh, 2020

Reduced density of dendritic spines is an intermediate anatomical phenotype for schizophrenia (Sz). This dissertation is a collection of descriptive studies about dendritic spines and the voltage-gated calcium channel protein β4, a study of a Sz-related β4 manipulation, and the impacts of this manipulation on dendritic spine density and morphology. Chapter 2 is a descriptive study of sex differences in dendritic spines in murine sensory cortex over adolescent neurodevelopment. Chapter 3 is an in-depth assessment of the impacts of CACNB4 overexpression (β4OE) on dendritic spines of male and female adult mice. Chapter 4 is a final descriptive study of sex differences in the β4 interactome of adult mice. Sex differences were deliberately assessed at baseline and in the study of the impacts of β4OE on dendritic spines given the importance of sex as a biological factor and known sex differences in the clinical presentation and expression of Sz. In Chapter 2, we identified sex differences in spine density, and in Chapter 3 evidence for volume- as well as sex-specific β4OE-mediated spine loss; small spines were reduced in female β4OE mice only. These findings provide a model for the intermediate phenotype of small spine loss in primary auditory cortex in Sz and support both our group's previous suggestion to rethink the Feinberg hypothesis, but also the possibility that small mature spines are eliminated excessively in Sz during adolescence, as Feinberg predicted. In Chapter 4 we found that β1b is significantly enriched in the β4 interactome of male mice only, the presence of which may confer protection for males from the effects of β4OE. Moreover, we detail three pathways through which β4OE could reduce small spine density in female mice. These proposed pathways nominate

kinases and MAPs in β4-related spine alterations. Overall, the findings described herein underscore the importance of evaluating the biological sex at baseline, over normal neurodevelopment and following a disease-related manipulation, particularly neurodevelopmental disorders, including Sz.

Table of Contents

List of Tables

List of Figures

List of Equations

Preface

This document is based on multiple published or in preparation manuscripts.

Chapter 1 includes modified text and a figure from:
Parker, E. M., & Sweet, R. A. (2018). Stereological Assessments of Neuronal Pathology in Auditory Cortex in Schizophrenia. *Frontiers in Neuroanatomy*, *11*, 131. https://doi.org/10.3389/fnana.2017.00131

Chapter 2 is a modified version of:
Parker, E. M., Kindja, N. L., Cheetham, C. E.J., & Sweet, R. A. (2020). Sex differences in dendritic spine density and morphology in auditory and visual cortices in adolescence and adulthood. *Scientific Reports*, *10*, 9442. https://doi.org/10.1038/s41598-020-65942-w

Chapter 3 and 4 are modified versions of:
Parker, E. M., Kindja, N. L., MacDonald, M. E., Salisbury, R., Krivinko, J. M., Cheetham, C. E.J., & Sweet, R. A. (2020). CACNB4 overexpression leads to dendritic spine loss like observed in schizophrenia. *In preparation.*

1.0 Introduction

1.1 Schizophrenia Overview

Schizophrenia (Sz) is a serious mental illness that besets approximately 1% of the global population (A. Wong & H. Van Tol, 2003). Sz diagnosis is determined primarily based on symptom presentation, guided by information regarding family history and illness course gathered in standardized structural interviews (Andreasen, 1995). Two or more of the following symptoms must be present for diagnosis: 1) delusions, 2) hallucinations, 3) disorganized speech, 4) grossly disorganized or catatonic behavior, 5) negative symptoms. One of these must be a positive/psychotic symptom (delusions, hallucinations or disorganized speech). Along with core Sz symptoms, several notable associated features support diagnosis: cognitive deficits, sensory processing deficits and socio-cognitive impairment (American Psychiatric Association, 2013).

Lifetime prevalence rates of Sz are fairly consistent, however variation has been reported based on race/ethnicity, across countries and by geographic origin for immigrants and their children (American Psychiatric Association, 2013; A. Wong & H. Van Tol, 2003). Sz is a neurodevelopmental disorder with onset typically occurring during late adolescence or early adulthood (Ziermans, Schothorst, Sprong, & van Engeland, 2011). Presence of cognitive deficits often precedes onset. The typical course begins with attenuated nonspecific or negative symptoms and progresses to the development of subthreshold or brief positive symptoms in prodromal Sz. Attenuated positive symptoms usually intensify or become more frequent before individuals transition to full-blown psychosis, the latter of which marks illness onset as a general rule (Larson, Walker, & Compton, 2010). Positive symptoms tend to lessen as individuals age, whereas negative

and cognitive symptoms often are not mitigated over illness course (Lieberman et al., 2001; Lieberman et al., 2005; Ojeda et al., 2007; Schultz et al., 1997). Atypical antipsychotic drugs are often prescribed for mitigating positive/psychotic symptoms in Sz. Discontinuation is extremely common. Atypical antipsychotics are often not well-tolerated, with severe side effects, and are largely ineffective for treating negative symptoms and cognitive deficits (Lally & MacCabe, 2015).

Sz is a polygenic disorder for which liability is conferred by common and rare risk alleles, with single alleles contributing very little to the population variance. Many of the alleles identified that confer susceptibility for Sz fall into two broad categories: genes associated with synaptic signaling and genes that encode proteins involved in Ca^{2+} signaling (Purcell et al., 2014; Schizophrenia Working Group of the Psychiatric Genomics Consortium, 2014), both of which are of high interest in the current discussion. Epigenetic and environmental factors converge on multiple genetic variants to result in Sz expression (MacDonald et al., 2017). Prenatal maternal infection, stress or malnutrition in utero may confer considerable susceptibility for Sz. In particular, maternal influenza increases the risk for Sz by 3-8 times (Goff, 2013). Twin and adoption studies are demonstrative of the presence of gene by environment interactions in Sz. In dizygotic twin pairs, an unaffected sibling has a 17% incidence of Sz, whereas among monozygotic twins incidence for the unaffected twin is close to 50% (Gottesman, 1991). Adoption studies have revealed that Sz risk is associated with presence of the disorder in biological but not adoptive parents (Lewis & Lieberman, 2000).

Sex differences are observed in the clinical presentation, incidence, and illness course in Sz (Abel, Drake, & Goldstein, 2010; Aleman, Kahn, & Selten, 2003). Males tend to present with more negative symptoms, disorganization, and social cognition impairment whereas women

typically display more mood-related and psychotic symptoms. Additionally, males have poorer premorbid adjustment, lower educational achievement and more prominent negative symptoms and cognitive deficits. Lifetime prevalence of Sz is approximately equal in men and women, although general incidence tends to be higher in males. Sz onset typically occurs during late adolescence/early adulthood, with mean age of onset in males earlier than in females. The peak age of onset for first episode psychosis in males is in the early to mid-twenties, whereas the first psychotic episode typically occurs in females in the late-twenties. There is an additional risk period for Sz onset in females after age forty years (American Psychiatric Association, 2013).

1.2 Auditory Sensory Processing Deficits in Sz

Individuals with Sz experience auditory sensory processing deficits that can manifest, for instance, in impaired ability to distinguish between auditory tones (Kantrowitz et al., 2011; O'Donnell, Vohs, Hetrick, Carroll, & Shekhar, 2004; Pekkonen et al., 2002; Petkova et al., 2014). Auditory sensory processing deficits in turn contribute to socio-cognitive dysfunction (Javitt & Sweet, 2015; Kantrowitz et al., 2016; Kantrowitz et al., 2015; Leitman et al., 2005; Leitman et al., 2007; Leitman et al., 2008; Leitman et al., 2010). Unlike the positive symptoms of Sz, socio-cognitive dysfunction is not targeted by available pharmacological interventions. Among individuals with Sz, those with prominent socio-cognitive dysfunction have the poorest functional outcomes (Fett, Viechtbauer, Penn, van Os, & Krabbendam, 2011; Green, Horan, & Lee, 2015; Green, Kern, & Heaton, 2004; Green & Leitman, 2008; Javitt & Sweet, 2015; Kantrowitz et al., 2016).

Auditory sensory processing deficits typically emerge in Sz around the time of the first psychotic episode and persist over the course of the illness (Gold et al., 2012; Javitt, Strous, Grochowski, Ritter, & Cowan, 1997; Kantrowitz et al., 2011; Leitman et al., 2005; Leitman et al., 2010; McCarley, Faux, Shenton, Nestor, & Adams, 1991; Wexler, Stevens, Bowers, Sernyak, & Goldman-Rakic, 1998). Electroencephalography studies reveal that individuals with Sz exhibit reduced auditory mismatch negativity (MMN) responses (Javitt, 1993; K. Kasai et al., 2003; Michie et al., 2000; Shelley et al., 1991). MMN is an event-related potential recorded immediately following a stimulus that differs in characteristic from preceding stimuli (for example a tone of a deviant pitch among a series of tones of the same pitch) and, in the auditory system, reflects pre-attentive auditory sensory processes. In Sz, reduced auditory MMN is correlated with impaired auditory tone discrimination (Javitt, Shelley, & Ritter, 2000; Javitt, Steinschneider, Schroeder, & Arezzo, 1996; Javitt, Steinschneider, Schroeder, Vaughan, & Arezzo, 1994; Leitman et al., 2010). Electroencephalography methods likewise indicate that individuals with Sz exhibit impaired auditory steady-state response entrainment, predominantly in the gamma frequency range (Brenner et al., 2009; Hamm et al., 2015; Hamm, Gilmore, Picchetti, Sponheim, & Clementz, 2011). Altered fast GABAergic inhibition in auditory circuits is presumed to underlie impaired aSSR entrainment in Sz (Krishnan et al., 2009; Kwon et al., 1999; Light et al., 2006).

1.3 Neuronal Pathology in Auditory Cortex in Sz

Cortical gray matter loss is a hallmark anatomical feature of Sz (Shenton, Dickey, Frumin, & McCarley, 2001). The most pronounced gray matter loss is observed in frontal and temporal regions (A. Wong & H. Van Tol, 2003), most notably in the superior temporal gyrus (STG)

(Honea, Crow, Passingham, & Mackay, 2005; McCarley et al., 1999; Shenton et al., 2001). Gray matter volume reduction in the STG ranks among the most consistent findings from studies reporting gray matter loss in Sz (McCarley et al., 1999). Gray matter loss is apparent around the time of Sz onset and in the years following first episode psychosis (Hirayasu et al., 2000; Hirayasu et al., 1998; Kasai, Matsuzaki, Noguchi, Yasumatsu, & Nakahara, 2003; K. Kasai et al., 2003; Kubicki et al., 2002; Vita, De Peri, Deste, & Sacchetti, 2012). Gray matter reductions occur within the STG in Heschl's gyrus and the planum temporale (Barta et al., 1997; Hirayasu et al., 2000; Kwon et al., 1999), where the primary auditory cortex (A1) and auditory association cortex (A2) are located, respectively.

Functional MRI studies reveal that auditory MMN reductions in Sz subjects are correlated with gray matter loss in Heschl's gyrus (Salisbury, Kuroki, Kasai, Shenton, & McCarley, 2007). Similarly, auditory MMN and tone discrimination are thought to depend on the integrity of cells in supragranular layers (L1–L3) of A1 (Javitt et al., 1994). Thus, we have hypothesized that neurons within supragranular layers of A1 are altered in Sz (Javitt & Sweet, 2015). Electroencephalography and *in vivo* imaging approaches do not have the resolution to test this prediction directly, requiring human postmortem studies to assess gray matter alterations at the neuronal level. In theory, a wide array of neuronal aberrations could lead to reduced gray matter volumes in Sz, as gray matter has multiple constituents, including, neurons, glia and endothelial cells, the cell bodies of these cells and their neuropil, which is made up of the unmyelinated portions of axons, dendrites and the processes of glia. Therefore, it is conceivable that auditory cortical neurons could be altered in Sz due to: 1) fewer total cells, 2) reduced neuron somal size, 3) reduced number of axon boutons, 4) reduced number of dendritic spines, or 5) a combination of any two or more of these possibilities.

The following subsections review findings from human postmortem studies conducted by our lab that reveal neuronal abnormalities in auditory cortex in Sz (Figure 1.1). These studies provide direct evidence that morphological features of neurons in the human auditory cortex are implicated in the pathology of this illness. Likewise, these findings provide potential neural correlates for auditory sensory processing deficits and cortical gray matter loss in primary and secondary auditory regions in Sz.

1.3.1 Pyramidal Cell Number

A1 layer III (L3) pyramidal cell density was increased in Sz, relative to unaffected comparison cases. In contrast, pyramidal cell number did not differ significantly across diagnostic groups, in agreement with previous reports that found no change in neuron number in cerebral cortex, PFC nor anterior cingulate in Sz (Pakkenberg, 1993; Stark, Uylings, Sanz-Arigita, & Pakkenberg, 2004; Thune, Uylings, & Pakkenberg, 2001). Neither L3 A1 volume, nor total A1 volume were found to be significantly reduced in Sz. Increased pyramidal cell density, with no change in pyramidal cell number, was interpreted to mean that STG gray matter loss in Sz is due to the loss of neuropil components such as dendritic spines, rather than to the loss of the number of pyramidal cells (Dorph-Petersen et al., 2009).

1.3.2 Pyramidal Cell Somal Volume

Mean somal volume of deep layer 3 (L3) pyramidal cells was reduced in Sz by 13.1% in A2 (Sweet, Pierri, Auh, Sampson, & Lewis, 2003). Similarly, mean pyramidal cell somal volume was decreased in Sz by 10.4% in deep L3 of A1, with no change in the somal volume of Layer 5

pyramidal cells in A2 (Sweet et al., 2004). These data implicated feedforward but not feedback auditory circuits in Sz and provided evidence for neuronal morphological abnormalities consistent with gray matter loss in auditory cortex in Sz.

1.3.3 Axon Boutons

L3 axon bouton density was significantly reduced in A1 in Sz based on synaptophysin-immunoreactivity (SYP-IR) (Sweet et al., 2007). Synaptophysin is found in approximately 95% of cortical boutons and does not distinguish between excitatory and inhibitory boutons (Navone et al., 1986). Excitatory bouton density did not appear to be altered in A1 in Sz based on assessments of vesicular glutamate transporter 1-immunoreactivity (VGluT1)- and VGluT2-IR in two independent cohorts of cases (Moyer et al., 2013). Glutamic Acid Decarboxylase-immunoreactivity (GAD65-IR) bouton density was also not altered in two independent cohorts, but GAD65-IR fluorescent intensity was significantly reduced, suggesting that within-bouton GAD65 enzyme levels are reduced in A1 in Sz (Moyer et al., 2012).

1.3.4 Dendritic Spines

In the first study of dendritic spines, density of spinophilin-immunoreactive (SP-IR) puncta was reduced by 27.2% in deep L3 of A1 and reduced by 22.2% in deep L3 of A2 in Sz. These findings were consistent with previous reports of reduced dendritic spine density (DSD) in regions of neocortex and of hippocampal formation in Sz (Moyer, Shelton, & Sweet, 2015). Reduced DSD was interpreted to reflect a reduction in spine number, despite the fact that A1 volume was not estimated in the subjects in this initial study.

Both DSD and spine number were significantly reduced in deep L3 in A1 in Sz in a follow-up study, which reported 19.2% reduction in mean spine density (Shelton et al., 2015). The second study utilized co-labeling of SP-IR and phalloidin (mushroom toxin that binds f-actin (Capani, Ellisman, & Martone, 2001)) to identify and measure spines. Off-target labeling of the anti-spinophilin antibody could explain the discrepancy in the magnitude of spine density reductions observed across the initial versus follow-up studies. Importantly, the finding of reduced DSD in deep L3 in A1 in Sz was then replicated in independent assessments using separate cohorts of Sz and non-psychiatric control cases in two additional follow-up studies. These studies demonstrated decreased DSD in deep L3 in A1 in Sz is selective for and driven by loss of the smallest dendritic spines (MacDonald et al., 2017; McKinney et al., 2019).

Reduced DSD is proposed to function as an intermediate, anatomical phenotype for Sz, a key component that could link genetics to functional outcomes. Many Sz risk genes encode synaptic proteins and those involved in excitatory Ca^{2+} signaling in dendrites (Heyes et al., 2015; Purcell et al., 2014; Schizophrenia Working Group of the Psychiatric Genomics Consortium, 2014). Thus, one promising future direction for assessment of A1 neuronal pathology in Sz is investigation of potential mechanisms associated with known genetic risk for Sz that could lead to reduced small DSD, as is observed in A1 in Sz. Our group recently showed that levels of a peptide shared among voltage-gated calcium channel (VGCC) β subunits was inversely correlated with the density of spines with the smallest volumes. Overexpressing *CACNB4*, the gene that encodes the β4 VGCC subunit, which is present in the temporal cortex, and is a critical regulator of VGCC activity (Dolphin, 2012, 2016), in primary neuronal culture resulted in reduced density of small volume, but not large volume, dendritic spines (MacDonald et al., 2017).

Functional outcomes of individuals with Sz have remained largely unchanged since the introduction of antipsychotics, likely due in part to the fact that we do not fully understand the pathophysiology of this illness (Insel, 2010). Probing relationships between β4 and dendritic spine morphology has the potential to elucidate an important, anatomical phenotype of Sz, which may be a final common pathway for auditory impairment in Sz. Finally, examining such relationships could lead to the identification of drug targets or provide other critical information for the development of superior strategies to treat or prevent auditory sensory processing deficits in Sz.

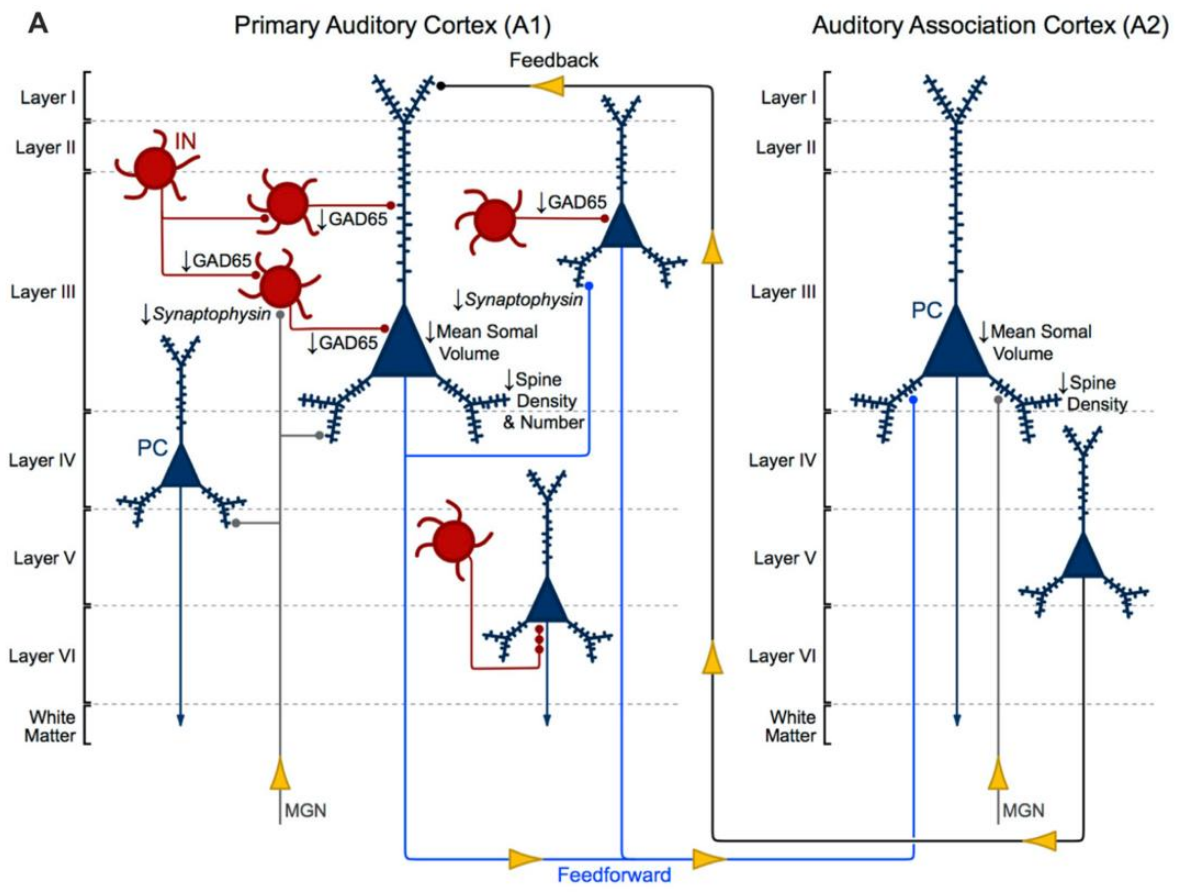

Figure 1.1: Pyramidal cell morphological alterations in auditory cortex in Sz

Morphometric alterations in auditory cortex in Sz superimposed on feedforward and feedback auditory circuits. Thalamic projections from the medial geniculate nucleus (MGN) synapse onto pyramidal cells (PCs, blue) and interneurons (INs, red). Layer III (L3) pyramidal cells in A1 send local intralaminar projections to other L3 pyramidal cells in this region and longer-range feedforward projections to pyramidal cells in L3 of A2. L5 pyramidal cells in A2 in turn send excitatory feedback projections to neurons in L1 in A1. Mean somal volume of pyramidal cells in deep L3 in A1 and A2 in Sz were significantly reduced. GAD65 levels were reduced in deep L3 boutons in A1 in Sz, although the specific interneuron cell types affected are not currently known DSD was reduced in deep L3 of A1 and A2, reflecting reduced number of dendritic spines in deep L3 of A1 in Sz. Recently, decreased DSD in deep L3 in A1 in Sz was demonstrated to be selective for and driven by loss of the smallest dendritic spines. Note: this figure is Figure 6A in (Parker & Sweet, 2018).

1.4 Dendritic Spines and the Feinberg Hypothesis of Sz Pathogenesis

Santiago Ramón y Cajal discovered dendritic spines 1890 proposing they may be dynamic three years later (Ramón y Cajal, 1888, 1890, 1893). For over a hundred years these small structures have been the source of much curiosity among many scientists. The canonical dendritic spine is a mushroom-shaped protrusion attached to the shaft of a dendrite with a narrow neck and large, bulbous head, supported by a dynamic actin-cytoskeleton. Dendritic spines are the major postsynaptic recipient sites for excitatory synaptic transmission in the brain (Gray, 1959). Excitatory inputs to pyramidal cells almost exclusively synapse onto dendritic spines, whereas interneurons primarily synapse onto the dendritic shaft of pyramidal cells and less frequently onto spines (Arellano, Benavides-Piccione, DeFelipe, & Yuste, 2007; J. L. Chen et al., 2012; Javier DeFelipe, Hendry, & Jones, 1989; Somogyi & Cowey, 1981; Spacek & Harris, 1998; Yuste, 2011). Spine number and morphology are mediated by activity-dependent actin remodeling as a consequence of synaptic plasticity and synapse remodeling that occurs during neurodevelopment. These short- and long-term processes generate substantial diversity in spine number and morphology, and implicate many upstream mediators and signaling pathways (Arellano et al., 2007; Javier DeFelipe, 2015; Gray, 1959; Spacek & Harris, 1998).

Spines are rapidly motile structures that undergo activity-dependent morphological alterations (Dunaevsky, Tashiro, Majewska, Mason, & Yuste, 1999; Fischer, Kaech, Knutti, & Matus, 1998). During the lifetime of a single spine, it will undergo spine dynamics: addition and subtraction/elimination (primarily referred to as "elimination" in spine dynamics studies and referred to in this dissertation as such). The term "elimination" implies active removal but in the context of spine dynamics studies, the word elimination is a synonym for simple subtraction. Addition and elimination are normally balanced in adulthood (Holtmaat et al., 2005). Spine

lifetimes are categorized as transient or persistent. After a transient spine is initially formed, it is subsequently removed within ~48h to four days, whereas once a persistent spine is added it can remain for years. If a spine disappears and gone forever it is additionally considered a persistent spine (Holtmaat et al., 2005).

Spines are divided into two categories based on synapse maturity: immature spines, which lack the scaffolding protein post-synaptic density protein 95 (PSD-95) and mature spines defined by the presence of PSD-95. PSD-95 enters a new spine within 24h of its initial formation, is required for activity-dependent excitatory synapse stabilization, and PSD-95 levels positively correlate with spine density (De Roo, Klauser, Mendez, Poglia, & Muller, 2008; Ehrlich, Klein, Rumpel, & Malinow, 2007; Lambert, Hill, Park, Culp, & Zito, 2017; Taft & Turrigiano, 2014). Thus, discussions included in this dissertation focus on immature versus mature, rather than transient versus persistent status of dendritic spines. Although immature spines account for the majority of spine dynamics (i.e. adding and eliminating/subtracting), the remodeling of these spines is not likely to engender long-term effects on network structure, at least not in the context of normal neurodevelopment (Berry & Nedivi, 2017).

Spines are separately classified based on morphological shape. Morphologies include mushroom, stubby, thin, branched and atypical, the latter of which is a catch-all category of spines that do not conform to any of the previously mentioned types (see Appendix A Figure 1A and Appendix B Figure 2B for examples). Dendritic spine form and function are linked. However, the role of dendritic spines in shaping neuronal system function has been extensively debated (Yuste, 2011). One view holds that on the population level spine synaptic molecular profiles and morphologies are tuned to regulate the gain of pyramidal cell input/output properties toward the reorganization of neural networks.

Finally, dendritic spine number is altered over the neurodevelpmental lifecourse and in psychiatric disorders. Decreased DSD is not pathognomonic to Sz. Spine loss is also observed in Alzheimer's disease. In contrast, spines are generally reported to be pathologically increased in Autism Spectrum Disorder (ASD). ASD and Sz are both classified as neurodevelopmental disorders with onset in childhood or adolescence/early adulthood, respectively (Xiao et al., 2014; Ziermans et al., 2011). Against the background of synapse remodeling and concurrent spine number fluctuations that occur during normal neurodevelopment, in Sz spine numbers are proposed to increase during the perinatal period and childhood and begin to decrease at the end of childhood. A substantial drop in spine number is proposed to occur in Sz around disease onset in late adolescence/early adulthood, significantly deviating from normal by magnitude of loss during this period (Penzes, Cahill, Jones, VanLeeuwen, & Woolfrey, 2011). These changes are predicted to account for significantly reduced DSD in adult Sz, particularly in deep L3 of A1 (Figure 1.2).

In 1982 Irwin Feinberg proposed a theory of Sz pathogenesis to account for Sz onset during adolescence following highly heterogeneous childhoods, in some cases characterized by premorbid behavioral abnormalities and in other cases characterized by ostensibly normal childhood neurodevelopment (Feinberg, 1983; Keshavan, Anderson, & Pettergrew, 1994). This hypothesis is now widely referred to as the "overpruning" hypothesis of Sz. According to Feinberg's theory, Sz results from excessive elimination of mature synapses during adolescence in brain areas involved in cognitive neurodevelopment (Feinberg, 1983; Keshavan et al., 1994). Others later added to this model, for example proposing axon collaterals are hyper-pruned in prefrontal cortex in Sz (Keshavan et al., 1994). In the 1990s and 2000s, a number of MRI and postmortem studies demonstrated cortical gray matter volume loss and significantly reduced DSD in frontal and temporal cortices in Sz (Moyer, Shelton, et al., 2015; Vita et al., 2012). In vivo

imaging methods utilized in human studies lack the spatial resolution needed to observe the synaptic plasticity and spine dynamics that ultimately result in reduced DSD in adult Sz. For many years Feinberg's theory has been used in conjunction with the studies reporting gray matter and synapse reductions in Sz to explain Sz pathogenesis.

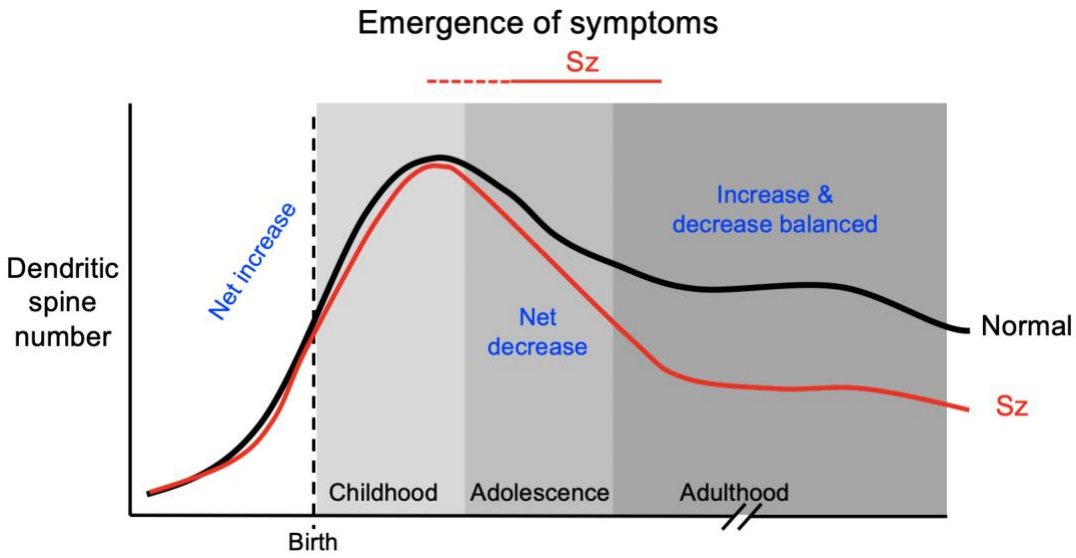

Figure 1.2: Model for dendritic spine number in human neurodevelopment

Proposed trajectory of dendritic spine number in normal human neurodevelopment (black line) and Sz (red line). Prodromal period of Sz (dashed horizontal line) and emergence of symptoms (solid horizontal line) are indicated in red at the top. Note: this figure is modeled after portions of Figure 1 in (Penzes et al., 2011).

1.5 Voltage-Gated Calcium Channel β4 Subunits

Voltage-gated calcium channels (VGCCs) are comprised of an α1 (ion permeable channel) subunit (Figure 1.3) and three auxiliary subunits, β, $\alpha_2\delta$ and γ, which combine in a 1:1:1:1 reversible stoichiometry (Buraei & Yang, 2010, 2013; Dolphin, 2016). β is the best understood auxiliarly VGCC subunit. There are four β protein subfamilies (β1-4) (Castellano & Perez-Reyes,

1994). Each β subtype is encoded by a separate gene with multiple splice variants, all of which are highly expressed in mouse brain, except β1a, β1d, β2d, and β2e (Buraei & Yang, 2010; Schlick, Flucher, & Obermair, 2010). β4a expression is limited to the cerebellum (Buraei & Yang, 2010). Particular β subunits predominate in neuronal subcellular compartments depending on the α1 subunits they preferentially bind to and modulate (Buraei & Yang, 2010). β subunits are "highly promiscusous" meaning each can bind to any high-voltage activated (HVA) α1 VGCC subunit. The binding affinity of β to α1 is high, ranging from 2–54nM. α1-β reshuffling may occur via competitive replacement or to compensate for β subunit loss (Buraei & Yang, 2013; Burgess et al., 1999; Burgess, Jones, Meisler, & Noebels, 1997; Dolphin, 2016; Yeon, Park, Hille, & Suh, 2018).

β subunits are required for forward trafficking of the α1 subunit of HVA VGCCs to the plasma membrane, potentially acting as chaperones, and inserting the α1 subunit into the plasma membrane (Gonzalez-Gutierrez, Miranda-Laferte, Naranjo, Hidalgo, & Neely, 2008; Jones, Wei, & Yue, 1998; Josephson & Varadi, 1996; Maltez, Nunziato, Kim, & Pitt, 2005). More recent work has indicated that β could be essential for proper folding of the I-II linker of α1 VGCC subunits. β subunits strongly regulate VGCC channel gating kinetics (Buraei & Yang, 2010). β subunits generally hyperpolarize the voltage-dependent threshold of channel activation and promote closed state of voltage-dependent inactivation (Buraei & Yang, 2010; Patil, Brody, & Yue, 1998; T. Yasuda, Lewis, & Adams, 2004). β subunits are required for RGK- and G protein βγ subunit-mediated inhibition of HVA VGCCs (Meir, Bell, Stephens, Page, & Dolphin, 2000; Yun Zhang et al., 2008).

CACNB4 encodes β4 VGCC subunits and has five known splice variants (Etemad et al., 2014). β4 isoforms vary in size, ranging from 37-58 kilodaltons. Generally, β4 is expressed highly in brain, where transcript and protein levels have been demonstrated to fluctuate in several brain

regions as a function of age (Buraei & Yang, 2010; Ferrándiz-Huertas, Gil-Mínguez, & Luján, 2012; Ludwig, Flockerzi, & Hofmann, 1997). β4 preferentially binds the presynaptic $Ca_V2.1$ VGCC (Tanaka, Sakagami, & Kondo, 1995; Wittemann, Mark, Rettig, & Herlitze, 2000) and has also been demonstrated to bind to ~40% of Ca_V1 VGCCS, as well as $Ca_V2.2$ and $Ca_V2.3$ (Buraei & Yang, 2010; McEnery, Vance, et al., 1998; Scott et al., 1996). Neuronal subcellular distribution of β4 appears diffuse. β4 is detected at the plasma membrane, intracellularly, in axons and dendrites and dendritic spines of pyramidal cells. Electron Microcopsy assessment revealed mouse cerebellar and hippocampal β4 levels are significantly higher in neurons in intracellular space than in specific subcellular compartments (Ferrándiz-Huertas et al., 2012). β4 and VGluT1 colocalize in presynaptic terminals of glutamatergic neurons, and β4 has been identified in synaptosome preparations in mass spectrometry experiments (Etemad et al., 2014; Klemmer, Smit, & Li, 2009). Unique among β4 subunits, β4b has been shown to exhibit nuclear targeting potentially implicating it in transcription regulation (Subramanyam et al., 2009).

β subunits have been demonstrated to compensate for one another, in cases of scientific manipulation, injury or disease (Berggren et al., 2004; Buraei & Yang, 2013; Heyes et al., 2015; Namkung et al., 1998; Neef et al., 2009). "Lethargic" β4-knockout mice result from a naturally occurring null mutation in CACNB4 and are characterized by α1-β reshuffling (Burgess et al., 1999; Burgess et al., 1997). Increased pairing of $Ca_V2.1$ and $Ca_V2.2$ with β1-3 are observed in lethargic mice, with increased pairing of $Ca_V2.2$ and β1b particularly prevalent (Burgess et al., 1999). Despite the apparent α1-β reshuffling that occurs in lethargic mice, compensation appears partial, as α1-β reshuffling does not fully rescue loss of β4 or reverse the epilepsy-like phenotype of these mice (Buraei & Yang, 2010, 2013; Burgess et al., 1999; Burgess et al., 1997). Lethargic mice exhibit upregulated thalamic LVA current density, reduced excitatory neurotransmission in

thalamus and lower forebrain and cerebellar $Ca_V2.2$ expression (Caddick et al., 1999; McEnery, Copeland, & Vance, 1998; Yi Zhang, Mori, Burgess, & Noebels, 2002). Clear evidence of partial compensation, despite α1-β reshuffling in lethargic mice highlights the fact that β4 performs distinct functions among the β subtypes, mediated potentially via interactions involving the NH_2 and COOH termini of β4 with α1 VGCCs (Brice & Dolphin, 1999; De Waard, Witcher, Pragnell, Liu, & Campbell, 1995; Stotz et al., 2004; Walker, Bichet, Campbell, & De Waard, 1998; Walker et al., 1999; Wittemann et al., 2000).

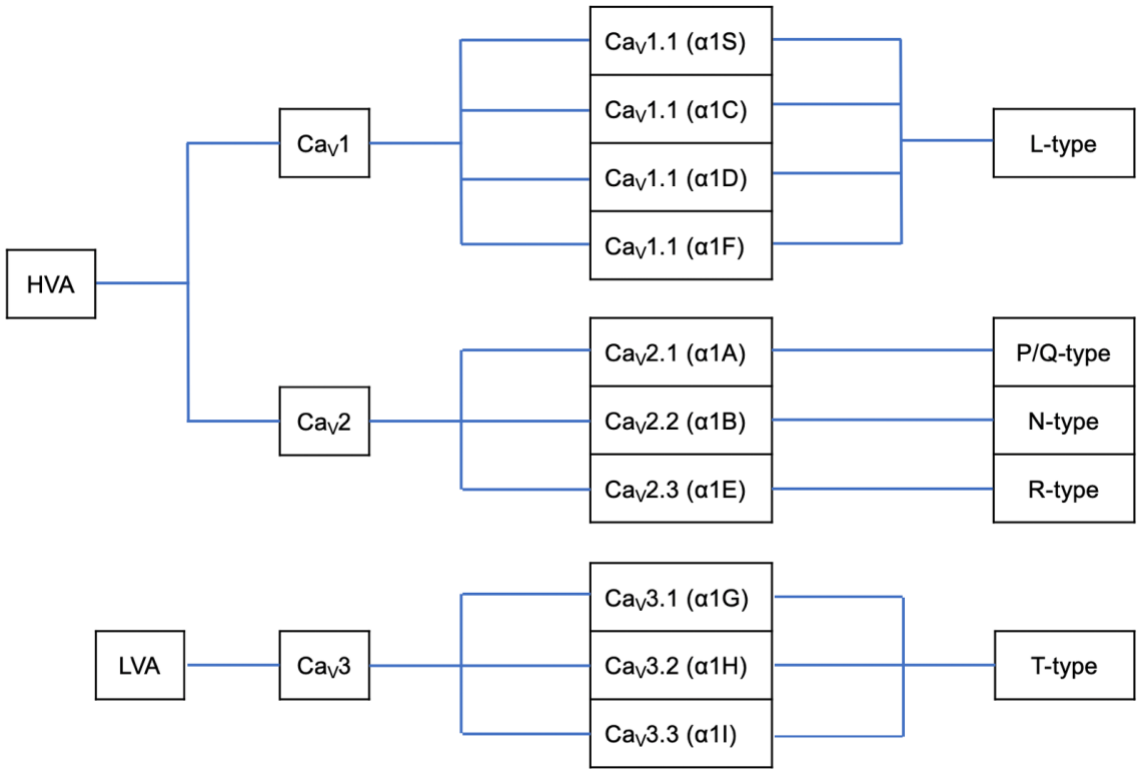

Figure 1.3: α1 VGCC subtype nomenclature

α1 VGCC subtypes, including ten members partitioned into two classes, high voltage-activated (HVA) VGCCs (Ca_V1 and Ca_V2) and low voltage-activated VGCCs (Ca_V3). Ca^{2+} current type nomenclature provided far right. Note: this figure is included as a tool for reading studies described in this dissertation given the history and complexity of α1 VGCC subunit nomenclature.

1.6 Purpose of Studies

In this dissertation, we first characterized dendritic spines and VGCC β subunits over murine adolescent brain development of male and female mice to provide a background for our Sz-related manipulation of dendritic spines. We then dissected the impact of overexpressing CACNB4 during brain development on the spines of adult male and female mice. Finally, we reported sex differences in the β4 interactome of adult mice. Chapter 2 includes a descriptive study of sex differences in dendritic spine density and morphology in murine sensory cortex over adolescent neurodevelopment. Chapter 3 revealed that overexpressing CACNB4 during brain development significantly decreased small spine density of female but not male mice. Chapter 4 characterized sex differences in the adult murine β4 interactome. A model for how β4 overexpression might lead to small spine loss in female but not male mice is outlined in the overall discussion. Taken together, these findings provide descriptive information about dendritic spines and β4 levels, reveal the volume- and sex-specific impact of a VGCC-focused Sz-related manipulation on dendritic spines in murine sensory cortex and identify sex differences in the murine β4 interactome in mice with relevance to theories of Sz spine pathophysiology and potential implications for development of treatment for treating auditory sensory processing deficits and improving socio-cognitive functioning in Sz.

2.0 Sex Differences in Dendritic Spine Density and Morphology in Auditory and Visual Cortices in Adolescence and Adulthood

2.1 Introduction

Dendritic spines are the predominant postsynaptic sites of excitatory input onto pyramidal cells in the cerebral cortex. Neuroscience pioneer Santiago Ramón y Cajal discovered dendritic spines in 1890 (Ramón y Cajal, 1888, 1890). In the 85 years between Ramón y Cajal's death and the present day, we have learned a great deal about these micron-sized dendritic protrusions. The canonical dendritic spine is a mushroom-shaped structure protruding from the shaft of a dendrite, supported by a dynamic actin cytoskeleton, with a narrow neck and large, bulbous head. This spine contacts a single pre-synaptic axon terminal and contains the constitutive molecular machinery, receptors, channels and signaling molecules, required for transmitting incoming glutamatergic signals to the dendritic shaft. The number of dendritic spines on a neuron and the morphology of single spines are altered via actin remodeling as a consequence of synaptic plasticity and circuit refinement that occurs during neurodevelopment or as a result of sensory experience. Such plasticity and structural remodeling generate substantial diversity in spine number and morphology through a myriad of context- and activity-dependent mediators (Arellano et al., 2007; Javier DeFelipe, 2015; Gray, 1959; Spacek & Harris, 1998).

A growing body-of-work has established that dendritic spine density (DSD), significantly differs based on sex. Sex is an important biological variable that has recently become an important priority in biomedical research (McCarthy, Arnold, Ball, Blaustein, & De Vries, 2012). Sex differences in DSD in adult animals have so far been reported in subcortical brain regions and

medial prefrontal cortex. DSD is significantly increased in female rats in the posterodorsal medial amygdala, nucleus accumbens, CA1 hippocampus (during proestrus), arcuate nucleus of the hypothalamus and medial prefrontal cortex. DSD is significantly lower in female rats in two regions of the hypothalamus, the preoptic area and the ventromedial nucleus (Brusco et al., 2014; Calizo & Flanagan-Cato, 2000; de Castilhos, Forti, Achaval, & Rasia-Filho, 2008; Delevich et al., 2019; Forlano & Woolley, 2010; Frankfurt, Gould, Woolley, & McEwen, 1990; Koss, Belden, Hristov, & Juraska, 2014; Markham & Juraska, 2002; Mong, Roberts, Kelly, & McCarthy, 2001; Schwarz, Liang, Thompson, & McCarthy, 2008; Shors, Chua, & Falduto, 2001; Todd, Schwartz, Mong, & McCarthy, 2007; Weinhard et al., 2018; Wissman, May, & Woolley, 2012; Wright, Burks, & McCarthy, 2008; Wright, Schwarz, Dean, & McCarthy, 2010). DSD was recently reported to be increased on apical dendrites in medial prefrontal cortex in female mice (Delevich et al., 2019). To our knowledge, there is yet no existing published data providing evidence for sex differences in morphology or DSD in mouse auditory and visual sensory regions.

Spine formation and morphology are altered as a result of sensory experience. Sensory cortex adapts as diverse sensory stimuli shape perception and motor planning (Nimchinsky, Sabatini, & Svoboda, 2002). In vivo calcium imaging experiments reveal that visual and auditory cues evoke Ca^{2+} signaling cascades in individual dendritic spines in first-order sensory areas including primary visual and primary auditory cortices (X. Chen, Leischner, Rochefort, Nelken, & Konnerth, 2011; Jia, Rochefort, Chen, & Konnerth, 2010). Ca^{2+} signaling in activated spines leads to activity-dependent actin remodeling and altered spine morphology (Majewska & Sur, 2006). Long-term potentiation has been shown to precipitate spine head enlargement (Lang et al., 2004; Matsuzaki, Honkura, Ellis-Davies, & Kasai, 2004; Okamoto, Nagai, Miyawaki, & Hayashi, 2004), whereas long-term depression precipitates spine shrinkage (Okamoto et al., 2004; Zhou,

Homma, & Poo, 2004). Sensory deprivation experiments demonstrate that sensory cues are required for normal patterning of dendritic spines over neurodevelopment, including reduction in dendritic spine number observed over the adolescent period (Majewska & Sur, 2006). A caveat of many of these studies is that they included male animals only. It remains unclear if interplays between sensory experience and alterations to spine density and morphology take place over adolescent brain development in sensory regions in female animals, as they have been shown to in males.

The goal for the current study was to characterize dendritic spines in male and female mice at the start of adolescence (P28) and in early adulthood (P84) to identify potential sex differences in spine complement and synaptic remodeling that take place during adolescence. We focus on sensory regions of the posterior cortex, first-order sensory areas: primary auditory cortex (A1), primary visual cortex (V1), plus secondary auditory cortex (A2), secondary visual cortex (V2), and temporal association cortex (TeA). Our data reveal evidence for lower DSD in auditory and visual regions of female compared to male mice for the very first time, with this effect appearing to be driven, at least in part, by fewer short stubby, long stubby and short mushroom spines in female mice. Although age did not significantly affect mean DSD in our primary statistical model, as it has been shown to in male mice, we found a significant age by layer interaction. When examining DSD from P28 to P84 in different cortical layers separately, we found that mean DSD was significantly decreased in L4, with a trend for a reduction in L5/6 from P28 to P84. There was also a trend level reduction in long mushroom spine density from P28 to P84, providing additional evidence of synaptic remodeling over the adolescent period.

2.2 Methods

2.2.1 Experimental Animals

E16 pregnant C57BL/6J dams were acquired from The Jackson Laboratory (Bar Harbor, ME) and singly housed in BSL-2 biocontainment in standard microisolator cages (Allentown Caging Equipment, Allentown, NJ) on a 12h light/dark cycle with food and water provided ad libitum. The adeno-associated virus (AAV) AAV2-CaMKII-eGFP-WPRE (titer = 1.088e13gc/ml), which is designed to selectively express the fluorescent protein eGFP in glutamatergic neurons (pyramidal cells), was obtained from Penn Vector Core. AAV injectate was prepared by diluting AAV in sterile filtered 1x PBS at 1:10 (Gholizadeh, Tharmalingam, MacAldaz, & Hampson, 2013; Stoica, Ahmed, Gao, & Esteves, 2013). Diluted AAV was used in order to achieve sparse AAV transduction in A1, A2, V1, V2 and TeA. P0-P2 C57BL/6J mouse pups were exposed to AAV injectate using the bulk regional AAV injection (BReVI) procedure (Cheetham, Grier, & Belluscio, 2015). Briefly, neonates were cryoanesthesized (Phifer & Terry, 1986) to induce brief hypothermia until response to toe pinch was absent. 1μL AAV solution was injected intracranially 1mm rostral to the left earbud and 1mm lateral from the midline using a custom injector: a 1mL Luer-lock syringe connected to a pulled glass micropipette with a sharp tip. Toe amputation was performed for group identification. Pups were returned to the home cage with the dam following thrombus at site of toe amputation and 10-12m rewarming on a heating pad. Experimental mice were housed with littermates following the BReVI procedure until 3-weeks following birth (P21), at which point mice were weaned and housed with same-sex littermates until P28 or P84. Each cage of weaned animals was provided environmental enrichment (a hut and exercise wheel) at P21, in accordance with a new policy set by the Institutional Animal

Care and Use Committee (IACUC) at the University of Pittsburgh. These experiments were approved by the IACUC at the University of Pittsburgh in accordance with the guidelines outlines in the USPHS Guide for Care and Use of Laboratory Animals.

2.2.2 Perfusion and Tissue Processing

Mice were euthanized at either P28 (4 males and 3 females) or P84 (4 males and 3 females). Mice were weighed, deeply anesthetized with Nembutal (150mg/kg) and transcardially perfused with ice-cold 1x PBS followed by 4% PFA. Brains were rapidly extracted and post-fixed in 4% PFA for 24h and then moved to 18% sucrose for 24h and stored at -30°C in 30% ethylene glycol and 30% glycerol in phosphate buffer (cryoprotectant) until sectioning. 60μm-thick coronal tissue sections were cut on a cryostat directly into 12-well plates containing cryoprotectant and then placed in -30°C for long-term storage.

2.2.3 Immunohistochemistry

Free-floating sections corresponding to plates 55 and 59 in Franklin and Paxinos's ***The Mouse Brain In Stereotaxic Coordinates*** (Franklin & Paxinos, 2004) were selected for immunohistochemistry. Plates 55 and 59 correspond to -2.92mm and -3.4mm from bregma, respectively. A1, A2, V1, V2 and TeA are each found at both of these stereotaxic coordinates. Free-floating sections were washed in 0.1M PB to remove Tissue-Tek O.C.T. compound (Sakura Finetek Europe, Alphen aan den Rijn, Netherlands), then incubated for 30m in 1% $NaBH_4$ to reduce autofluorescence. After thorough rinsing, sections were blocked for 3h in a solution of 1% normal goat serum, 3% Triton X-100, 1% bovine serum albumin, 0.1% lysine and 0.1% glycine.

Sections were then incubated in the primary antibodies guinea pig anti-NeuN (Millipore ABN90 lot:2834791, 1:2000) and chicken anti-GFP (ThermoFisher A10262 lot: 1972783, 1:1000) for 24h and 96h respectively. Anti-NeuN was utilized to label neurons and Anti-GFP to amplify the eGFP signal. Pilot experiments demonstrated that amplifying the eGFP signal with a 568 secondary antibody rather than a 488 secondary antibody produced dendrites with superior signal-to-noise characteristics (Figure 2.1A). Therefore, following primary antibody incubation, sections were washed and incubated in the secondary antibodies goat anti-guinea pig 405 (Abcam Ab175678 lot:1972783, 1:500) and goat anti-chicken, Alexa Fluor 568 (ThermoFisher A11041 lot:1963088, 1:500). After a 24h incubation in secondary antibodies, sections were washed and mounted on TruBond 380 micro slide glass (Matsunami, Osaka, Japan) using ProLong Gold antifade mountant (Invitrogen, ThermoFisher Scientific, Waltham, MA).

2.2.4 Sampling and Confocal Imaging

Images were captured using an Olympus BX51 WI upright microscope (Center Valley, PA) with an Olympus spinning disk confocal, Hamamatsu ORCA R2 CCD camera (Bridgewater, NJ), BioPrecision2 XYZ motorized stage with linear XYZ encoders (Ludl Electronic Products Ltd., Hawthorne, NY), Lumen 220 light source (Prior Scientific, Cambridge, United Kingdom), excitation and emission filterwheels (Ludl Electronic Products Ltd.) and a Sedat Quad 89000 filter set (Chroma Technology Corp., Bellows Falls, VT). 1.25x 2-D images of each tissue section were acquired in SlideBook 6 software (Intelligent Imaging Innovations, Denver, CO) using 405 nm and 568 nm excitation. Franklin and Paxinos's ***The Mouse Brain In Stereotaxic Coordinates*** (Franklin & Paxinos, 2004) was used to establish the region of interest (ROI) and estimate the regional location (A1, A2, V1, V2 or TeA) of the cell body of each pyramidal cell imaged (Figure

2.1B). The region we define as A2 here includes both Franklin and Paxinos regions: secondary auditory cortex, dorsal region (2ary auditory cx, dorsal) and secondary auditory cortex, ventral region (2ary auditory cx, ventral). V1 refers to primary visual cortex, monocular region (primary visual cx, monocular) and primary visual cortex, binocular region (primary visual cx, binocular). Our definition of V2 includes all 3 subregions of secondary visual cortex (2ary visual cx, lat area, 2ary visual cx, mediolat and 2ary visual cx, mediomed). Collectively, the regions we assayed are primary and secondary auditory and visual cortices in ascending sensory pathways, with the exception of TeA, which is thought to be a multisensory region that processes complex auditory stimuli downstream from A1 (Tasaka et al., 2019). Fluorescent pyramidal cells transduced with AAV were identified at 1.25x magnification in *both hemispheres* and systematically numbered in the aforementioned 1.25x 2-D image captures (Figure 2.1B). Numbered cells were then randomly sampled and captured in 3-D image stacks using an Olympus PlanApo N 60x/1.40 N.A. oil immersion super-corrected objective on. Each capture site comprised of the cell body of one randomly selected (numbered) pyramidal cell, plus all basal dendrites visible within the capture window (Figure 2.1C). Neutral density (ND) filter and exposure time for the 568 nm channel were optimized for one randomly selected minor basal dendritic segment at each site. Minor basal dendritic segment is defined here as any dendritic segment branching directly off of a major or primary basal dendrite. Total tissue thickness was estimated at each site by measuring anti-NeuN labeling in the z-dimension. 1024x1024 pixel 3-D image stacks were acquired through the entire thickness of the tissue (mean tissue thickness=40.36μm, standard deviation tissue thickness=3.53μm; 0.25μm between each z-plane) in SlideBook 6 software.

2.2.5 Image Processing and Analysis

SlideBook 6 and Stereo Investigator (MicroBrightField, Inc., Natick, MA) software were used for image processing and analysis. 1024x1024 image stacks were first transformed using a no-neighbors smoothing algorithm in SlideBook 6. All minor basal dendritic segments >10μm away from the cell body and >3μm from a dendrite branch point were identified in 1024x1024 image stacks (Figure 2.1C) and cropped into individual image stacks containing one minor basal dendritic segment each. Minor basal dendritic segments were proximately located, with mean distance from soma 19.34μm. Mean distance from soma was not significantly different across age or sex (data not shown). Signal-to-noise ratio (SNR) was calculated for each individual dendritic segment to compute fluorescent intensity of the dendritic segment (signal) relative to the background (noise) (Figure 2.1D). The threshold for reliably distinguishing spines from fluorescent non-spine objects was set at SNR=2. Segments that either failed to meet this SNR=2 threshold or otherwise did not allow for reliable distinction between spines and non-spines were excluded. The length of each dendritic segment was measured in SlideBook 6 using the line tool. Individual dendritic segments were exported as TIFF series from SlideBook 6 and opened in Stereo Investigator for spine counting and categorization. Examination of anti-NeuN labeling was used to estimate laminar location, post-hoc (Bopp, Holler-Rickauer, Martin, & Schuhknecht, 2017; Li et al., 2003; W. Zhang, Peterson, Beyer, Frankel, & Zhang, 2014) (Figure 2.1E). Spine density for each neuron was calculated using Equation 1.

$$Dendritic\ spine\ density\ (DSD) = \frac{\text{total \# dendritic spines}}{\Sigma\ dendrite\ lengths}$$ **Equation 1**

In 1970 Peters and Kaiserman-Abramof introduced what is currently accepted as the traditional classification of morphological types: stubby, thin and mushroom dendritic spines (Peters & Kaiserman-Abramof, 1970). We included these types in our analysis of dendritic protrusion morphology along with branched dendritic spines (Basu et al., 2018), filopodia, and atypical dendritic spines (Arellano et al., 2007), a catch-all category which includes protrusions that do not conform to any of the aforementioned morphological types. Dendritic protrusions were manually counted and classified into one of eight types (short stubby, long stubby, short mushroom, long mushroom, thin, branched or atypical dendritic spine or filopodia) based on morphological characteristics described by other groups at length (Arellano et al., 2007; Risher, Ustunkaya, Alvarado, & Eroglu, 2014) (Appendix A Figure 1A). Short dendritic spines had maximal width greater than length, and long spines had maximal length greater than width. Mushroom spines had >0.4μm head diameter with a clear distinction between spine head and neck. Stubby spines were dendritic protrusions with no significant distinction between head and neck. Thin spines had ≤0.3μm head diameter and <2μm total length. Branched spines had 2 spine heads attached to 1 spine neck. Atypical spines were <2μm long and did not fall into any of the abovementioned types (Arellano et al., 2007; Risher et al., 2014). Filopodia were defined as >2μm long dendritic protrusions with no distinction between spine head and neck (Risher et al., 2014). Filopodia were not included in the total count of dendritic spines and thus not built into DSD for each neuron (MacDonald et al., 2017). Long mushroom spines made up the highest proportion of dendritic protrusions counted in our study (66.03%). Long stubby spines accounted for 14.66%. The remaining dendritic protrusion types collectively accounted for less than 10% of the total spines counted, with filopodia accounting for 1.33%, thin spines 1.52%, and branched and atypical spines collectively making up <1% (Appendix A Figure 1B).

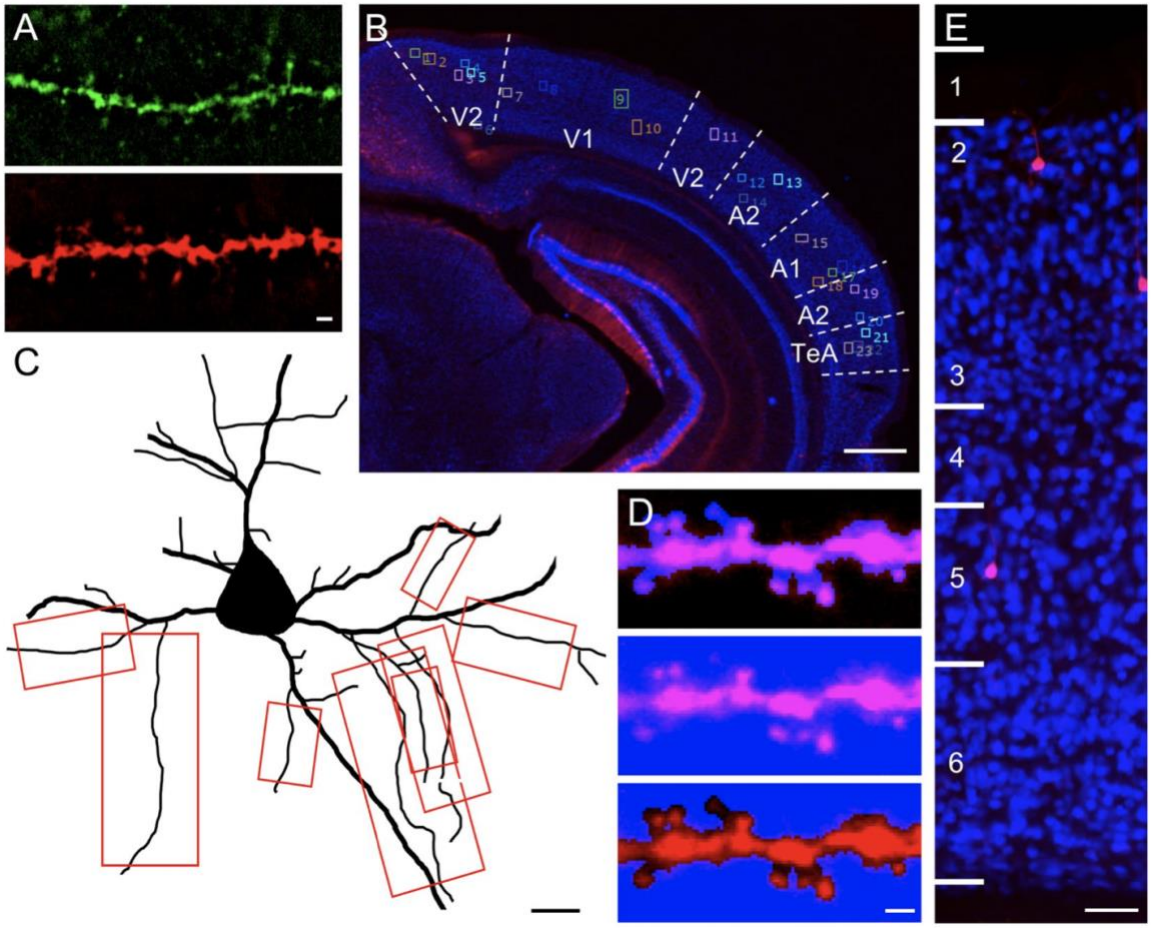

Figure 2.1: Immunohistochemical, sampling and image processing methods

(A) Fluorescent signal amplification using an AlexaFluor 568 secondary antibody (bottom panel) achieved superior SNR characteristics compared to amplification with AlexaFluor 488 (top panel) after no neighbors smoothing. Scalebar = 1μm. (B) Numbering strategy for fluorescent pyramidal cells in ROI of a representative 60μm thick tissue section corresponding to plate 59 in Franklin and Paxinos's ***The Mouse Brain In Stereotaxic Coordinates*** (Franklin & Paxinos, 2004). ROI comprises the following regions, clockwise from top left: mediomedial and mediolateral secondary visual cortex (V2), monocular and binocular primary visual cortex (V1), lateral secondary visual cortex (V2), dorsal secondary auditory cortex (A2), primary auditory cortex (A1), ventral secondary auditory cortex (A2) and temporal association cortex (TeA). Numbered neurons were imaged in random order. Scalebar = 500μm. (C) Illustration of pyramidal cell with all secondary minor basal dendritic segments outlined in red meeting criteria for segment inclusion (>10μm from soma and >=3μm from dendrite branch point or termination). Scalebar = 10μm. (D) Quantitative strategy used to exclude dim dendritic segments. 10μm sampling area of each dendritic segment assayed

was masked in SlideBook 6. Top panel shows manually generated mask using thresholding and the brush tool for "signal" of the dendritic segment. Middle panel shows the mask covering 100% of the pixels in the capture window. Bottom panel shows the mask created using the masks in the 2 panels on the left and Boolean math. This mask represents the "noise." SNR was calculated as mean intensity of the signal divided by mean intensity of the noise. SNR for the segment in this example = 3.205. Segments with SNR>2 were included in data analysis. Scalebar = 1μm. (E) Assessment of NeuN labeling in 10x images were used to estimate region and determine laminar location of cell bodies of red fluorescent pyramidal cells. This example from region A2. Scalebar = 50μm.

2.2.6 Statistics

Statistical tests were performed in SPSS software (IBM, Armonk, NY). The Shapiro-Wilk test was used to confirm normality. Breusch-Pagan test was used to confirm that variances were equal regardless of age or sex. Tissue thickness, layer and region were built into ANCOVA models as covariates, and the effects of age, sex, region, layer and age by layer interaction, and significance were tested using a univariate general linear model. Total number of fluorescent cells in ROI, mean distance from soma, ND filter and 568 exposure time were identified as measures that did not significantly affect mean DSD and thus were not built into statistical models. Since layer was highly significant in the primary model, indicating layer strongly predicted mean DSD, this variable was included as a main effect in a secondary ANCOVA along with age and sex (with covariates: tissue thickness and region). Main effect of layer and age by layer, sex by layer and age by sex by layer interactions were Bonferroni corrected (p=0.05) in the secondary model. Fitting the data to a mixed effects model with mouse as the random effect revealed that the within mouse correlation is not significant (p=0.1125), ruling out the possibility that mean DSD of individual mice drove the group findings. Thus, DSD is reported throughout the paper at the level

of individual neurons. In addition, mean DSD was calculated for each animal, and the descriptive statistics are provided in Figure 2.2C. Group mean DSD was tested using an ANCOVA (covariate: mean tissue thickness) with main effects of age and sex and age by sex interaction. Levene's Test was used to test the possibility that the variance among female mean DSD was significantly different than the variance among male mean DSD. The latter was used as a proxy to determine if estrous stage could underlie variability in female mouse mean DSD.

MANCOVA (α=0.05) with Bonferroni correction was used to detect significant differences in mean densities among dendritic protrusion types. Main effects of age and sex, and age by sex interaction were tested. Tissue thickness, layer and region were built into a multivariate analysis of variance as covariates with eight dependent variables: short stubby, long stubby, thin, short mushroom, long mushroom, branched, atypical and filopodia densities and age and sex fixed factors.

2.3 Results

2.3.1 DSD Did Not Differ by Region

Dendritic spines in five adjacent regions: A1, A2, V1, V2 and TeA were assessed in the current study, and regional identity of each pyramidal cell was estimated using anatomical landmarks and Franklin and Paxinos demarcations (Franklin & Paxinos, 2004). Region did not significantly impact DSD (F=1.829, DF=4, p=0.131) after Bonferroni adjustment. There were no significant region by sex nor region by age interactions (Appendix A Figure 2A).

2.3.2 DSD Differed Based on Cortical Layer

Our survey included dendritic spines on pyramidal cells with cell bodies located in supragranular (layer 2/3 (L2/3)), granular (layer 4 (L4)) and infragranular (layer 5/6 (L5/6)) cortical layers of five adjacent auditory and visual cortical regions in a secondary statistical model with layer included as a fixed factor. Layer significantly impacted DSD after Bonferroni adjustment, and the laminar pattern of DSD: L2/3 > 4=5/6 was preserved across ages and sexes (L2/3 and 4 $p=0.001$; L2/3 and 5/6 $p<0.001$; L4 and 5/6 $p=0.100$), without a significant sex by layer interaction (Appendix A Figure 2B).

2.3.3 DSD Lower in Females

We reasoned that there would be no difference in DSD in auditory and visual brain regions in male versus female mice. In contrast to this prediction, ANCOVA ($\alpha=0.05$) revealed a highly significant decrease in DSD of neurons from female, compared to male mice ($F=14.838$, $DF=3$, $p<0.001$) in A1, A2, V1, V2 and TeA. There were no significant sex by age, sex by region nor sex by layer interactions (Figure 2.2A). In a confirmatory analysis, mean DSD was calculated for each animal (i.e. collapsing across regions and layers), and yielded complementary evidence of lower mean DSD of female mice (Figure 2.2C).

Stage of estrous has been shown to modulate DSD in the ventromedial nucleus of the hypothalamus (Frankfurt et al., 1990) and hippocampal regions (J.-R. Chen et al., 2009; McCarthy & Konkle, 2005; Smith, Vedder, & McMahon, 2009) but not in the anterior cingulate of female rats (Markham & Juraska, 2002). Although we did not specifically record and evaluate DSD in female mice in different stages of the estrous cycle, we did calculate coefficient of variation (CV)

to evaluate variation of DSD measurements in male versus female mice and test for homogeneity of variances using Levene's Test (Bowman et al., 2018). If DSD significantly differed in females based on the stage of estrous cycle, one would reasonably predict that variation of DSD measured in female mice would be higher than in males. Although we did find that CV was higher in P84 females (CV=21.49) than in males (CV=19.29), Levene's Test revealed that the variances were not significantly different ($F(1,44)=0.010$, $p=0.919$).

2.3.4 Stubby Spine and Short Mushroom Spine Densities Lower in Females

Short stubby ($F=12.408$, $DF=1$, $p=0.001$), long stubby ($F=10.338$, $DF=1$, $p=0.002$) and short mushroom ($F=5.834$, $DF=1$, $p=0.018$) spine densities were significantly reduced in female compared to male mice, with no significant age by sex interactions (Figure 2.2B). Short stubby, long stubby and short mushroom spines collectively make up 30.83% of the total dendritic protrusions counted in our study (Appendix A Figure 1B). Sex did not appear to influence density of any of the other spine types, nor filopodia.

2.3.5 DSD Differed Across Adolescence in Layer-Specific Manner

We hypothesized that DSD would be significantly reduced during adolescent development, from P28 to P84, consistent with our previously published findings of reduced spine number in layers 2-4 of male mouse A1 across adolescent neurodevelopment (Moyer, Erickson, et al., 2015). In contrast to this hypothesis, we found no significant change in DSD over adolescent development ($F=0.001$, $DF=1$, $p=0.971$) in auditory and visual brain regions in male and female mice in our primary statistical model (Figure 2.3A). The age by sex interaction was also not significant.

However, the age by layer interaction was significant (F=0.777, DF=2, p=0.043). Mean DSD was significantly lower at P84 in L4 (n=19 neurons)(F=5.880, DF=1, p=0.026), with no change in mean DSD in L2/3 (n=31 neurons)(F=1.516, DF=1, p=0.229) nor in mean DSD in L5/6 (n=47 neurons) (F=3.082, DF=1, p=0.086) (Figure 2.3B). The age by sex by layer interaction was not significant (Figure 2.3C).

2.3.6 Long Mushroom Spine Density Across Adolescent Development

Long mushroom spine density was lower at P84 in male and female mice. This observation was a trend that approached statistical significance (F=3.615, DF=1, p=0.060) (Fig. 2-3D). Long mushroom spines made up 66.91% of the total dendritic protrusions counted in our study (Appendix A Figure 1B). Densities of the other spine types and of filopodia were not significantly different comparing P28 to P84.

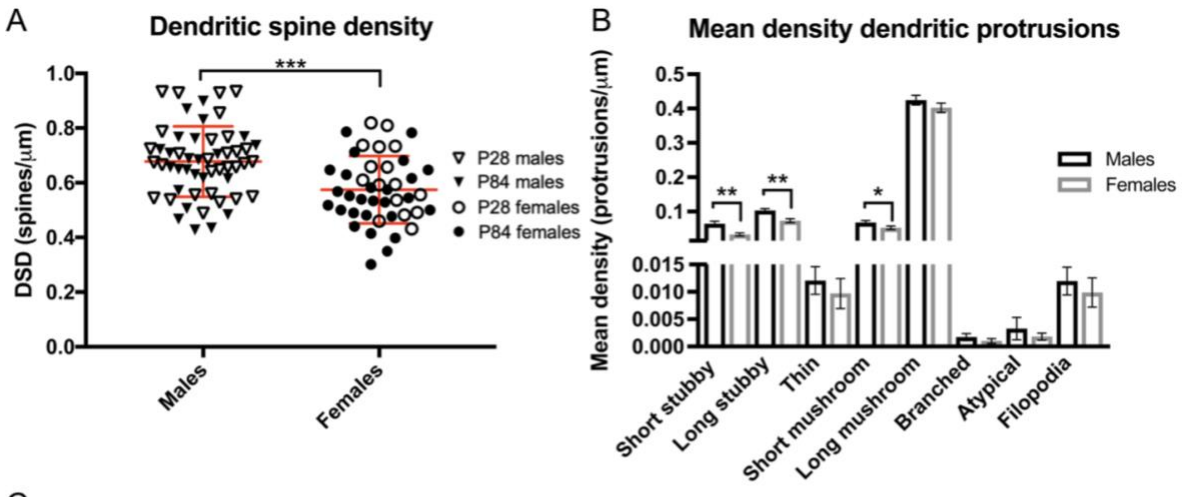

C

	Mouse number	Mean DSD (spines/µm)	SD (spines/µm)
P28 Males (n=30 cells)	401	0.7279	0.1425
	411	0.7919	0.0993
	424	0.6662	0.0994
	431	0.5371	0.0211
	Group	**0.6855**	**0.1306**
P84 Males (n=23 cells)	1210	0.6760	0.0399
	1215	0.7410	0.0316
	1216	0.5937	0.1551
	1227	0.6856	0.1359
	Group	**0.6673**	**0.1286**
P28 Females (n=16 cells)	423	0.5031	0.0288
	425	0.6638	0.1207
	432	0.6035	0.1287
	Group	**0.6186**	**0.1231**
P84 Females (n=27 cells)	1203	0.5065	0.0765
	1218	0.5264	0.1104
	1230	0.7320	0.0660
	Group	**0.5480**	**0.1178**

Figure 2.2: Sex differences in dendritic spine density (DSD) and mean density dendritic protrusions

(A) DSD is significantly reduced in female, compared to male mice ($F=14.838$, $DF=3$, $p<0.001$). There were no significant sex by age, sex by region nor sex by layer interactions. Data points are DSD from individual neurons. Mean DSD and SD represented by red lines. (B) Short stubby ($F=12.408$, $DF=1$, $p=0.001$), long stubby ($F=10.338$, $DF=1$, $p=0.002$) and short mushroom ($F=5.834$, $DF=1$, $p=0.018$) densities are significantly reduced in female mice with no significant age by sex interactions. Error bars = SEM. (C) Mean DSD for each animal. There is a trend level reduction in mean DSD in female, compared to male mice ($F=4.846$, $DF=1$, $p=0.055$). Mean DSD is not significantly different from P28 to P84 ($F=0.005$, $DF=1$, $p=0.943$). The age by sex interaction was not significant.

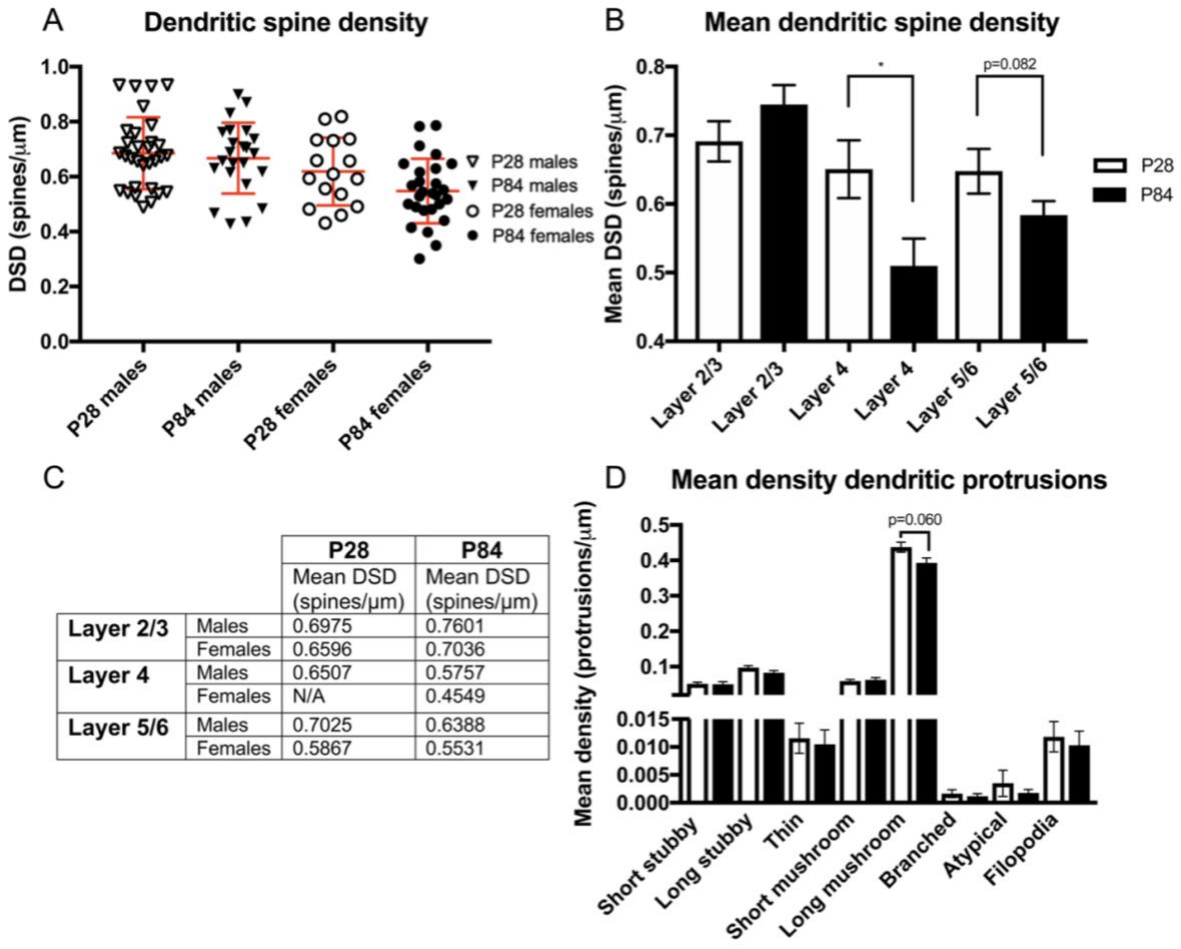

		P28	P84
		Mean DSD (spines/μm)	Mean DSD (spines/μm)
Layer 2/3	Males	0.6975	0.7601
	Females	0.6596	0.7036
Layer 4	Males	0.6507	0.5757
	Females	N/A	0.4549
Layer 5/6	Males	0.7025	0.6388
	Females	0.5867	0.5531

Figure 2.3: DSD and mean density dendritic protrusion findings over adolescent brain development

(A) DSD is not significantly changed in male and female mice from P28 to P84 (F=0.001, DF=1, p=0.971). Data points are DSD from individual neurons. Mean DSD and SD represented by red lines. (B) There is a significant age by layer interaction (F=0.777, DF=2, p=0.043). Mean DSD is unchanged from P28 from P84 in L2/3 (F=1.516, DF=1, p=0.229), significantly decreased in L4 (F=5.880, DF=1, p=0.026) and unchanged in L5/6 (F=3.082, DF=1, p=0.086) over this period. Error bars = SEM. (C) Table demonstrating mean DSD of males and females at P28 and P84 show same laminar patterns of mean DSD shown in Fig.2B; the age by sex by layer interaction was not significant. (D) Long mushroom mean density is nearly significantly reduced over adolescent neurodevelopment (F=3.615, DF=1, p=0.060) with no significant age by sex interactions. Error bars = SEM.

2.4 Discussion

In the current study, we set out to assess DSD and dendritic spine morphology in auditory and visual brain regions of male and female mice at P28 and P84 to determine if sex differences in dendritic spines are present at these ages and to acquire a more comprehensive understanding of synaptic remodeling across adolescence. We reasoned that sex would not significantly impact DSD in the regions we surveyed given that auditory and visual cortices do not fundamentally drive sex behaviors and that there are no established links between sex hormones and spine dynamics in these regions in mice. In contrast, we show for the first time that DSD on minor basal dendritic segments of pyramidal cells in A1, A2, V1, V2 and TeA is significantly lower in female mice. Lower DSD in female mice was robust; this effect was present even after calculating mean DSD for each animal, which included DSD from neurons located in different cortical layers.

Existing published reports of lower DSD in females are limited to two brain regions: preoptic area and ventromedial nucleus of rat hypothalamus (Calizo & Flanagan-Cato, 2000; Frankfurt et al., 1990; Schwarz et al., 2008; Wright et al., 2008). Preoptic area and ventromedial nucleus are hypothalamic regions that undergo sex differentiation in the juvenile period of postnatal rat development and support the emergence of sex characteristics and sexual behavior. The hormone 17 β-estradiol (E2) plays a formative role in developmental patterning in each of these areas and this patterning leads to sex differences in DSD. In the medial preoptic area, E2 in male rats promotes prostaglandin synthesis to facilitate masculinization, which results in dendritic spine formation. In the ventromedial nucleus of male rats, E2 promotes glutamate release to facilitate defeminization, resulting in increased dendrite branching and spine formation (Wright et al., 2010). It seems plausible that the sex differences in DSD we observed in our study occur as a consequence of sex differentiation during early developmental patterning of auditory and visual

regions given that DSD was detectably lower in female mice at P28, an age at which activational effects of gonadal steroids would be limited. Whether the patterning in mouse auditory and visual brain regions is mediated by E2 through mechanisms similar to those that occur in rat hypothalamus remains to be determined.

Coefficient of variation calculations confirmed that variation in mean DSD is greater in female than in male mice, consistent the possibility that stage of estrous could mediate mean DSD in female mice. However, Levene's Test demonstrated that the variances among males and females are not significantly different, indicating that estrous stage is unlikely to mediate mean DSD in females in our study. It should also be noted that our data do not reflect plastic changes that are associated with motherhood, including altered neuron firing properties in primary and association sensory regions (Cohen, Rothschild, & Mizrahi, 2011; Galindo-Leon, Lin, & Liu, 2009; Liu, Linden, & Schreiner, 2006; Liu & Schreiner, 2007; Marlin, Mitre, D'amour, Chao, & Froemke, 2015; Shepard, Chong, & Liu, 2016; Tasaka et al., 2019; Tasaka et al., 2018); males and females were housed separately after weaning at P21 and none of the female mice in our study produced offspring.

Short stubby, long stubby and short mushroom spine densities were significantly reduced in female mice. Dendritic spine morphology is widely variable (Arellano et al., 2007; Gray, 1959; Spacek & Harris, 1998). Despite this, all dendritic spines share two features: a spine head harboring synaptic machinery and a neck region connecting the spine head to the dendritic shaft. Spine head volume and spine neck diameter are thought to be regulated independently (Benavides-Piccione, Ballesteros-Yáñez, DeFelipe, & Yuste, 2002). The spine neck region acts as a biochemical and electrical bottleneck. The narrower the neck region, the higher the resistance for molecules moving toward or away from the synapse. Stubby spines were defined in our study as dendritic protrusions

lacking a clear distinction between the head and neck. These spines would, in theory, lack the neck resistance that other spines (like mushroom spines) can provide, and since single spines are hypothesized to play active roles in dendritic integration through linear and non-linear mechanisms (Grienberger, Chen, & Konnerth, 2015), lower density of stubby spines in female mice could impact integration dynamics of synaptic inputs in single pyramidal cells (Palmer, 2014). Future studies are required to determine if there are sex-based differences in dendritic integration or gain in cortical pyramidal cells at sites where spine morphology profiles differ in male and female mice.

We previously observed lower dendritic spine number at P84, compared to P28, in L2-4 of A1 in male mice (Moyer, Erickson, et al., 2015). In contrast to our previous reported findings, our current data reveal that age does not significantly impact DSD. We reason for the discrepancy in our findings could be due to one or more of the following factors: spine labeling method, sampling, and measurement. Labeling method is unlikely to account for the lack of agreement across the two studies since the co-labeling strategy employed in the previous study to identify spine objects clearly labeled GFP-positive dendritic protrusions in tissue from the current study (Appendix A Figure 1C). In terms of sampling, we previously sampled from L2-4, counting all spine objects, whereas in the current study we sampled from L2/3, L4 and L5/6, only counting spines on proximal (minor) basal dendrites on a subset of systematically randomly sampled pyramidal cells. We observed stark differences in DSD on proximal (minor) basal dendrites of pyramidal cells located in different cortical layers (Appendix A Figure 2B). Although spines from basilar dendrites of L5/6 neurons were included in the current but not prior study, differences in laminar sampling alone is unlikely to explain the discrepancy in the findings from the two studies since the directionality of change in mean DSD with age in L2/3 differs between the two studies. Differences in measurement seem most likely to account for the discordant results observed. In our prior study we used an

immunohistochemical strategy that labelled all putative spine objects in L2-4 regardless of cell body location and location on dendritic tree. We then computed spine number which is dependent on both density of spines in tissue and tissue volume of the region of interest. Tissue volume is known to be affected by normal developmental patterning of structures other than spines themselves, including dendrite, axon, myelin and glial volumes. It seems likely that such differences in spine number/density measurement could account for the lack of agreement in results in the two studies, although it would be necessary to use both measurement methods to count spines in the same mouse subjects to confirm whether or not this is true.

Mouse strain and environmental enrichment are two additional factors that cannot be ruled out as potential contributors to discordant results. C57BL/6NJ mice were used in the prior study whereas C57BL/6J mice were used in the current. C57BL/6J is distinguished from C57BL/6NJ by five SNP differences and a deletion in the *Nnt* gene. Such subtle genetic differences could have accounted for the divergence in the results. Environmental enrichment (complex housing) (Bayne, 2018) has been shown to increase DSD in male rat occipital cortex (Alvarez, 2007; Hickmott & Ethell, 2006; Kolb, Gibb, & Gorny, 2003), supporting the possibility that environmental enrichment could have mediated DSD on basal dendrites in homologous regions in murine cortex in our study. Animals in our current study were exposed to environmental enrichment starting at P21. Interestingly, one study demonstrated that environmental enrichment increased the total length of basilar dendrites in visual cortex of male but not female rats (Juraska, 1984). If exposure to environmental enrichment increased DSD in addition to total dendrite length only in male (Kolb et al., 2003) but not female mice in our study, this may be able to explain why we found DSD was lower in females exposed to environmental enrichment and DSD was not significantly lower at P84 in males (compared with our prior report of reduced spine number from P28 to P84 in standard

housed male mice (Moyer, Erickson, et al., 2015)). However, although we can confirm that, unlike in our previously published study of DSD in A1, mice in the current study had access to environmental enrichment, we cannot confirm the frequency by which these mice specifically utilized this environmental enrichment nor if this enrichment had any direct impact on basal dendritic DSD.

Despite the fact that we did not find a significant lower DSD at P84 in our current study, our data did reveal important evidence of synapse remodeling across adolescence. Given the impact of layer on DSD (Appendix A Figure 2B), we built a secondary statistical model to further probe the impact of layer and age on DSD. This assessment revealed a significant age by layer interaction and that mean DSD is unchanged across adolescence in L2/3 (n=31 neurons) ($F=1.516$, $DF=1$, $p=0.229$), significantly lower at P84 in L4 (n=19 neurons) ($F=5.880$, $DF=1$, $p=0.026$) and lower at P84 in L5/6, although the difference was not statistically significant (n=47 neurons) ($F=3.082$, $DF=1$, $p=0.086$). Lower mean DSD at P84, compared to P28, in L4 is consistent with our previous finding of reduced spine number in layers 2-4 across adolescent development. Overall, these data provide evidence that different layers in auditory and visual sensory regions undergo divergent neurodevelopmental trajectories of DSD during adolescent brain development.

Region did not significantly impact DSD (Appendix A Figure 2A) consistent with a growing body-of-work demonstrating that regional differences in DSD do not exist across adjacent or similar cortical mouse brain regions (Arellano et al., 2007; Benavides-Piccione et al., 2002; Hsu, Luebke, & Medalla, 2017; Luebke, 2017). Despite the fact that pyramidal cells in mice and higher mammals share the same subcellular compartments and many of the same features (Harris & Shepherd, 2015), the finding that DSD does not significantly differ across adjacent cortical regions in mice does not translate to non-human primates and humans, as dendrite arbor size and

DSD have been shown to differ extensively based on regional location within cortex in these higher mammals (Amatrudo et al., 2012; Clemo & Meredith, 2012; Gilman, Medalla, & Luebke, 2016; Jacobs et al., 2001).

We assessed DSD on proximal basal dendrites of pyramidal cells located in different cortical layers. DSD in L2/3 was significantly higher than DSD in both L4 and L5/6, but no difference was found in DSD in L4 versus in L5/6 (Appendix A Figure 2B). These data agree with the well-documented diversity of cortical pyramidal cell morphology, connectivity and functional properties based on the laminar location of pyramidal cell somata (Feldmeyer, 2012; Harris & Shepherd, 2015; Larkman, 1990; Petersen & Crochet, 2013; Rojo et al., 2016; Tija, Yu, Jammu, Lu, & Zuo, 2017). Heterogeneous morphology of pyramidal cells across cortical layers is thought to support the diversity of roles characteristic of dendritic spines (Tija et al., 2017). The laminar pattern of DSD we observed was preserved across ages and sexes, supporting the notion that pyramidal cells in different layers perform specific roles in information processing within cortical circuits. One implication of these findings is a cautionary note. DSD appears to depend on the layer in which a pyramidal cell is located, consistent with previous reports (Feldmeyer, 2012; Harris & Shepherd, 2015; Larkman, 1990; Petersen & Crochet, 2013; Rojo et al., 2016; Tija et al., 2017), and definitive evidence for synaptic remodeling across adolescence was not found until a secondary analysis was performed, which analyzed DSD in the layers separately. Future studies that assess DSD in more than one cortical layer should specifically analyze DSD in the layers separately. For studies that use immunohistochemical methods and fluorescence microscopy, a marker is needed to reliably distinguish adjacent layers from one another. This can easily be achieved by counterstaining for NeuN as others have done in previous studies (Bopp et al., 2017; W. Zhang et al., 2014), and we have done here.

Collectively, these results provide important evidence of sex differences and layer-specific refinement of DSD over adolescent brain development in sensory brain regions located in posterior cortex. We demonstrate for the first time that DSD is lower in female mice in cortical brain regions that have not yet been discussed in the sex differences literature and are not thought to directly drive sex behavior. One may speculate that sex differences in DSD in auditory and visual cortices generate behavioral consequences. Links between divergent developmental patterning of DSD in male and female mice and behavior should be explored in future studies. Potential roles for gonadal steroids in the modification of DSD in auditory and visual brain regions in male and female, defined by gonadal anatomy, should also be examined.

Finally, although it is known that the organization of auditory and visual cortices are largely conserved across primates (Hackett, 2008; Homman-Ludiye & Bourne, 2014), it remains unclear if the sex differences we observed in mouse DSD translate to higher mammals, and future studies are required to confirm this prediction. If the sex differences finding does translate to human, this work could inform our understanding of sex differences in normative and in abnormal adolescent neurodevelopmental trajectories. First, as discussed above, lower DSD in auditory and visual regions in females could have consequences for behavior during normative neurodevelopment. Again, this possibility must be specifically tested. Potentially more interestingly, if this finding translates to humans, this could have implications for studying the prodromal period and/or emergence of neurodevelopment disorders, for instance Sz. Postmortem studies have revealed that DSD is significantly lower adults with Sz including in A1, however the relative reduction of DSD in Sz did not differ by sex (McKinney et al., 2019). Many believe that individuals that develop Sz experience accelerated spine loss during adolescent synaptic remodeling, over and beyond the normal spine reduction that occurs during this period; this accelerated reduction in DSD across

adolescence may underlie, in part, the significantly lower number of spines observed in Sz in adulthood (MacDonald et al., 2017; McKinney et al., 2019; Shelton et al., 2015; Sweet, Henteleff, Zhang, Sampson, & Lewis, 2009). Despite no apparent sex difference in DSD in Sz in A1 in adult postmortem tissue, sex differences are well described in Sz including mean age of onset and clinical presentation of symptoms (American Psychiatric Association, 2013; Leung & Chue, 2000). The data in our current study suggest that sex differentiation in DSD occurs prior to the start of adolescence (P28) in auditory and visual brain regions in mouse, presumably prior to Sz onset in humans. Further experimental work is necessary to determine if sex differentiation processes are or are not intact in auditory and visual brain regions of human individuals at-risk for developing, or those who go on to develop, Sz and whether and how such differences are associated with age of onset or symptom presentation of Sz.

3.0 CACNB4 Overexpression Decreased Dendritic Spines of Female Mice

3.1 Introduction

Schizophrenia (Sz) is a severe and complex neurodevelopmental disorder (Insel, 2010; Lewis & Levitt, 2002) that besets approximately 1% of the global population (A. H. C. Wong & H. H. Van Tol, 2003). Sz onset typically occurs during adolescence and early adulthood, with a peak onset age of 18-25 years-old (Insel, 2010; Ziermans et al., 2011). Though onset usually occurs earlier in males than in females and general incidences tend to be higher in males, SZ's lifetime prevalence is approximately equal in men and women (Abel et al., 2010). Males also tend to have more negative symptoms and disorganization, whereas females typically display more mood-related and psychotic symptoms while better preserving their social functioning (American Psychiatric Association, 2013).

Psychotic symptoms are core Sz symptoms (American Psychiatric Association, 2013), and the most widely recognized among these are auditory hallucinations. Individuals with this disorder present with lesser-known sensory processing deficits in both visual and auditory domains (Javitt, 2009; Javitt & Freedman, 2015). Sensory processing deficits impair socio-cognitive functioning (Javitt & Sweet, 2015; Kantrowitz et al., 2016), which is not targetable by current treatments and, when prominent, is associated with the poorest functional outcomes among individuals living with Sz (Fett et al., 2011; Green et al., 2015; Green et al., 2004; Green & Leitman, 2008; Javitt & Sweet, 2015; Kantrowitz et al., 2016). Grey matter loss and dendritic spine loss in primary auditory cortex (A1) in Sz are both presumed to contribute to the impaired ability to discriminate between auditory inputs (Javitt & Sweet, 2015; Parker & Sweet, 2018). Two decades of postmortem studies

assessing the cellular architecture of individuals with Sz have revealed that synaptic pathology is a key feature of Sz pathology (Moyer, Shelton, et al., 2015). Substantial evidence indicates that dendritic spine density (DSD) is significantly reduced in Sz in key cortical areas in the frontal-temporal network linked with Sz symptoms and associated features, including in A1 (MacDonald et al., 2017; McKinney et al., 2019; Shelton et al., 2015; Sweet et al., 2009).

In multiple independent comparisons of spines in postmortem Sz relative to non-psychiatric control subjects, our group has demonstrated that DSD is significantly reduced in deep layer III of A1 in Sz (MacDonald et al., 2017; McKinney et al., 2019; Shelton et al., 2015; Sweet et al., 2009). We use a dual label immunohistochemical approach to detect putative spines in postmortem brain tissue. Specifically, spine objects are identified based on colocalization of phalloidin, a mushroom toxin that binds f-actin, and spinophilin, which is highly enriched in spine heads (Allen, Ouimet, & Greengard, 1997; Muly, Smith, Allen, & Greengard, 2004; Shelton et al., 2015). Using this approach, our group recently demonstrated that loss of spines in A1 appears to be selective for and driven by the loss of the smallest dendritic spines (MacDonald et al., 2017; McKinney et al., 2019).

In normal neurodevelopment, dendritic spines begin to emerge during the third trimester of pregnancy in humans, with spine number peaking during the juvenile period. Circuits are refined, and a substantial number of spines are decreased during adolescent pruning, a process that leads to a net loss in the number of spines in adulthood (Penzes, Buonanno, Passafaro, Sala, & Sweet, 2013; Penzes et al., 2011). Spines are largely maintained in adulthood, with rates of addition and elimination being approximately equal, with modest reductions in spine number in mid- to late-adulthood (Penzes et al., 2013; Penzes et al., 2011). In the early 1980s, Feinberg famously hypothesized that synapses could be “excessively pruned” during adolescent neurodevelopment in

Sz (Feinberg, 1983; Keshavan et al., 1994). Currently, the consensus is that an overall net reduction in spine number in Sz, whether it be due to insufficient spinogenesis, stability or excessive elimination during adolescence, or some combination of these, results in symptom onset in adolescence and reduced DSD observed in adulthood.

Ca^{2+} signaling is critical for the structural and functional plasticity of dendritic spines (Higley & Sabatini, 2012; H. Kasai et al., 2003; Yuste, Majewska, & Holthoff, 2000). Ca^{2+} is critically important for several important biological processes including neurotransmitter release, excitation-transcription coupling and the structural remodeling of dendritic spines. Voltage-gated calcium channels (VGCCs) provide regulated Ca^{2+} influx into neurons and localize within the plasma membrane of dendritic spines (Higley & Sabatini, 2012; Sabatini & Svoboda, 2000; R. Yasuda, Sabatini, & Svoboda, 2003). These channels comprise the $\alpha 1$ subunit, which is the ion-permeable pore, plus regulatory, auxiliary subunits: β, γ, and $\alpha_2\delta$. Each subunit protein has multiple associated isoforms (Buraei & Yang, 2010). VGCCs contribute to Ca^{2+} signaling in dendrites, and genes that regulate VGCC function confer risk for Sz (Heyes et al., 2015; Purcell et al., 2014; Ripke et al., 2013; Schizophrenia Working Group of the Psychiatric Genomics Consortium, 2014).

Consistent with this, our lab recently performed an exploratory mass spectrometry study focusing on postmortem human tissue from Sz and non-psychiatric control subjects to nominate candidate proteins for small spine loss in Sz. DSD of small but not large spine objects was negatively correlated with levels of the tryptic peptide ALFDFLK, which is found in the $\beta 4$ subunit of VGCCs, encoded by the gene *CACNB4* (MacDonald et al., 2017). The primary function of β subunits is to regulate the activity of $\alpha 1$ VGCC subunits: β subunits are required for cell surface expression of high voltage activated $\alpha 1$ subunits, regulation of channel gating, and facilitation of $G_{\beta\lambda}$-, RGK-, phospho- and lipid-mediated inhibition of $\alpha 1$ subunits (Buraei & Yang, 2010;

Dolphin, 2012). After identifying increased β4 as a candidate driver for small spine loss in Sz, our group demonstrated that CACNB4 overexpression (β4OE) significantly reduced small spines in primary cortical neuronal culture (MacDonald et al., 2017).

The current study's goal was to characterize dendritic spines in male and female mice at the adult timepoint of postnatal day 84 (P84) following β4OE in the developing brain. We hypothesized that β4OE during neurodevelopment decreases DSD of small spines in adult mice, mirroring the reduction observed in A1 in postmortem Sz. Interestingly, β4OE significantly reduced DSD in layer 5 (L5) of sensory cortex of female but not male P84 mice, and loss of the smallest spines drove this reduction. This manipulation largely did not discriminate between spine type; in nearly all dendrite protrusion categories asssessed, density of spines was reduced in β4OE females. DSD appears to be significantly reduced in A1 of female *and* male postmortem Sz subjects, relative to non-psychiatric controls (McKinney et al., 2019). So, although our β4 calcium channel manipulation recapitulated cellular pathology reminiscent of spine loss observed in Sz, it did not do so in both sexes in mice.

3.2 Methods

3.2.1 Experimental Animals

E16 pregnant C57BL/6J dams were acquired from The Jackson Laboratory (Bar Harbor, ME) and singly housed in BSL-2 biocontainment in standard microisolator cages (Allentown Caging Equipment, Allentown, NJ) on a 12h light/dark cycle with food and water provided ad libitum. The Synapsin-driven mCherry fluorescent adeno-associated virus (AAV) AAV2-hSyn-

mCherry (Titer≥$5x10^{12}$vg/ml), which confers long-term transgene expression of mCherry expression in neurons, was obtained from AddGene (#114472-AAV2). Two other AAVs were acquired, both from Penn Vector Core. AAV2-CaMKII-CACNB4-P2A-eGFP-WPRE (Titer = 4.94e13gc/ml) was designed to selectively express non-native β4 protein and eGFP in glutamatergic neurons (pyramidal cells). AAV2-CaMKII-eGFP-WPRE (Titer = 1.088e13gc/ml) is a control virus that expresses eGFP in pyramidal neurons.

A schematic of the summary study design and execution is found in Figure 3.1. Two versions of AAV injectate were prepared by adding 1μL AAV2-hSyn-mCherry to either 1μL AAV2-CaMKII-CACNB4-P2A-eGFP-WPRE or 1μL AAV2-CaMKII-eGFP-WPRE virus diluted in sterile filtered 1x PBS at 1:10 (Gholizadeh et al., 2013; Stoica et al., 2013). Diluted AAV was used to achieve sparse AAV transduction. β4 overexpression (β4OE) experimental mice were produced by exposure to injectate containing 1μL AAV2-CaMKII-CACNB4-P2A-eGFP-WPRE. Control (CN) mice were produced by exposure to injectate containing 1μL control GFP virus. Co-injection of AAV2-hSyn-mCherry was used to avoid biasing DSD measurement due to differences in GFP fluorescence produced by AAV2-CaMKII-CACNB4-P2A-eGFP-WPRE and the control virus, AAV2-CaMKII-eGFP-WPRE. AAV solutions were coded randomly “A” and “B” before exposure so that the investigator was blind to group during the exposure procedure. Approximately 50% of each litter was exposed to A and 50% to B. Twenty four P0-P2 C57BL/6J mouse pups were exposed to AAV injectate using the bulk regional AAV injection (BReVI) procedure (Cheetham et al., 2015). Neonates were first cryoanesthetized (Phifer & Terry, 1986) to induce brief hypothermia until response to toe pinch was absent. 1μL AAV injectate was injected intracranially 1mm rostral to the left earbud and 1mm lateral from the midline using a 1mL Luer-lock syringe connected to a pulled glass micropipette with a sharp tip. Toe amputation was

performed while pups were anesthetized for group identification. Mouse pups were returned to home cage with the dam following thrombus at site of toe amputation and 10-12m rewarming on a heating pad. Experimental mice were housed with littermates following the BReVI procedure until 3-weeks following birth (P21), at which point mice were weaned and housed with same-sex littermates until P84. Each cage of weaned animals was provided environmental enrichment (a hut and exercise wheel) starting at P21, in accordance with policies of the Institutional Animal Care and Use Committee (IACUC) at the University of Pittsburgh. These experiments were approved by the IACUC at the University of Pittsburgh in accordance with the guidelines outlines in the USPHS Guide for Care and Use of Laboratory Animals. β4 overexpression following injection with AAV2-CaMKII-CACNB4-P2A-eGFP-WPRE versus AAV2-CaMKII-eGFP-WPRE or saline was confirmed in mice using western blot (Appendix B.1 Methods and Appendix B Figure 1A).

3.2.2 Estrous Stage Assessment

Stage of estrous cycle was determined by evaluating vaginal cytology of P84 mice on day of sacrifice. Vaginal lavage was performed on each female mouse just prior to anesthesia. Briefly, the rear end of each mouse was elevated, gently grasped by the tail and 20 μL ddH_2O was dispensed onto the opening of the vaginal canal. The fluid was drawn back up into the tip of a pipette and transferred to a dry glass slide. After air drying, the slide was examined at 20x on a light microscope. Estrous stage (proestrus, estrus or metestrus/diestrus) was estimated based on ratio of cornified squamous epithelial cells, leukocytes and/or nucleated epithelial cells in samples (Byers, Wiles, Dunn, & Taft, 2012; McLean, Valenzuela, Fai, & Bennett, 2012).

3.2.3 Immunohistochemistry

Free-floating sections corresponding to plates 55, 57, 59 and 61 in Franklin and Paxinos's ***The Mouse Brain In Stereotaxic Coordinates*** (Franklin & Paxinos, 2004) (-2.92mm, -3.16mm, -3.4mm and -3.88mm from bregma, respectively) were selected for immunohistochemistry. The region of interest (ROI) is referred to here as sensory cortex and comprises the following regions: primary and secondary auditory (A1, A2) and visual (V1, V2) cortices plus temporal association cortex (TeA). Four free-floating sections per mouse were washed in 0.1M PB, then incubated for 30m in 1% $NaBH_4$ to reduce autofluorescence. After thorough rinsing, sections were blocked for 3h in a solution of 1% normal goat serum, 3% Triton X-100, 1% bovine serum albumin, 0.1% lysine and 0.1% glycine. Sections were incubated in the primary antibodies guinea pig anti-NeuN (Millipore #ABN90 lot:2834791, 1:2000) and rabbit anti-RFP (Rockland #600-401-376 lot: 39670, 1:1000), for 24h and 96h respectively. Following primary antibody incubation, sections were washed and incubated in the secondary antibodies goat anti-guinea pig 405 (Abcam #Ab175678 lot:1972783, 1:500) and goat anti-rabbit Alexa Fluor 568 (ThermoFisher #A11036 lot:997761, 1:500). After a 24h incubation in secondary antibodies, sections were washed and mounted on TruBond 380 micro slide glass (Matsunami, Osaka, Japan) using ProLong Gold antifade mountant (Invitrogen, Carlsbad, CA, USA).

3.2.4 Sampling and Confocal Imaging

Images were captured using an Olympus BX51 WI upright microscope (Center Valley, PA) with an Olympus spinning disk confocal, Hamamatsu ORCA R2 CCD camera (Bridgewater, NJ), BioPrecision2 XYZ motorized stage with linear XYZ encoders (Ludl Electronic Products

Ltd., Hawthorne, NY), Lumen 220 light source (Prior Scientific, Cambridge, United Kingdom), excitation and emission filterwheels (Ludl Electronic Products Ltd.) and a Sedat Quad 89000 filter set (Chroma Technology Corp., Bellows Falls, VT), controlled by SlideBook 6 software (Intelligent Imaging Innovations). 2-D images of each tissue section were acquired using an Olympus PlanAPO 1.25x/0.04 N.A. objective and epifluorescent 405nm and 568nm excitation. Franklin and Paxinos's ***The Mouse Brain In Stereotaxic Coordinates*** (Franklin & Paxinos, 2004) and examination of NeuN and mCherry fluorescence in the 2-D images were used to estimate the laminar and regional location (A1, A2, V1, V2 or TeA) of the cell body of each layer 5 (L5) pyramidal cell imaged (Bopp et al., 2017; Li et al., 2003; W. Zhang et al., 2014). Regions are defined as in (Parker, Kindja, Cheetham, & Sweet, 2020) (also see Appendix B Figure 1B). L5 mCherry+ pyramidal cells with somal GFP fluorescence (GFP+mCherry+ cells) were identified using an Olympus UPlanSApo 10x/0.40 N.A. objective and captured in 2-D at fixed exposure times (405nm=100ms, 488nm=1500ms and 568nm=150ms at 1.5% Neutral Density)(Appendix B Figure 1C). GFP+mCherry+ L5 pyramidal cells (n=170) were subsequently captured in a 3-D image stack using an Olympus PlanApo N 60x/1.40 N.A. oil immersion super-corrected objective with spinning disk unit engaged. Appendix B Figure 1D shows a single 2-D plane of a 60x stack. GFP-mCherry+ L5 pyramidal cells (n=86) in tissue sections from β4OE mice were also captured in 3-D image stacks and serve as the within mouse control for neurons in the β4OE group. Each 3-D stack is a capture site comprised of the cell body of one L5 pyramidal cell and all of its corresponding basal dendrites visible within the 1024x1024 pixel capture window (Figure 1C in (Parker et al., 2020)). ND filter and exposure time for the 568nm channel were optimized for one randomly selected minor basal dendritic segment at each site for each 3-D stack captured. Minor basal dendritic segments were defined as any dendritic segment branching directly off a major or

primary basal dendrite. Total tissue thickness was estimated by measuring anti-NeuN labeling in the z-dimension. 3-D image stacks were acquired through the entire thickness of the tissue (0.25μm between each z-plane).

3.2.5 Image Processing and Analysis

Slidebook 6 and Stereo Investigator (MBF Bioscience) softwares were used for image processing and analysis. 1024x1024 image stacks were first transformed using a no-neighbors smoothing algorithm in Slidebook 6. mCherry fluorescence was used to determine dendrite segment lengths and assess spines in CN and β4OE mice. Minor basal dendritic segments >50μm in length and arising >10μm away from the cell body and >3μm from a dendrite branch point were identified in 1024x1024 image stacks and cropped into individual image stacks containing one minor basal dendritic segment each. Mean (SD) distance from the soma of dendritic segments captured on GFP+mCherry+ cells were 15.85(4.48)μm indicative of proximal branches. Mean distance from soma did not significantly differ by genotype or sex (data not shown).

For determination of dendritic spine density dendritic segment lengths were measured in Slidebook 6 using the line tool. Individual dendritic segments were exported as TIFF series from Slidebook 6 and viewed in Stereo Investigator for spine counting and categorization. Spine objects were manually counted in Stereo Investigator and spine density for each neuron was calculated using Equation 1.

Two neurons per mouse were selected for further assessment to determine if the significant main effect of genotype on mean DSD could be driven by a significant difference in density of spines of a particular volume. Each neuron selected had DSD within 2 standard deviations of the

group mean. Spine objects included in the neuron DSD calculation were marked, files coded to blind investigator to neuron, and group, and each spine (n=1543 objects) manually masked using the brush tool in Slidebook 6 (Appendix B Figure 2A). Object volume (μm^3) statistics were extracted for each mask in Slidebook 6 using mask statistics. Spine objects were organized into objects of 10 size bins based on volume as in (MacDonald et al., 2017). The bin with the smallest putative spines comprises objects of volumes < $0.1\mu m^3$, the next bin of spines volumes from 0.1-$0.2\mu m^3$ and so on. The bin with the largest putative spines comprises objects measuring > $0.9\mu m^3$. Dendritic protrusions were classified into one of eight types in Stereo Investigator. Types included short stubby, long stubby, short mushroom, long mushroom, thin, branched or atypical dendritic spine or filopodia. Category was determined based on morphological characteristics described previously (Arellano et al., 2007; Parker et al., 2020; Risher et al., 2014) (Appendix B Figure 2B).

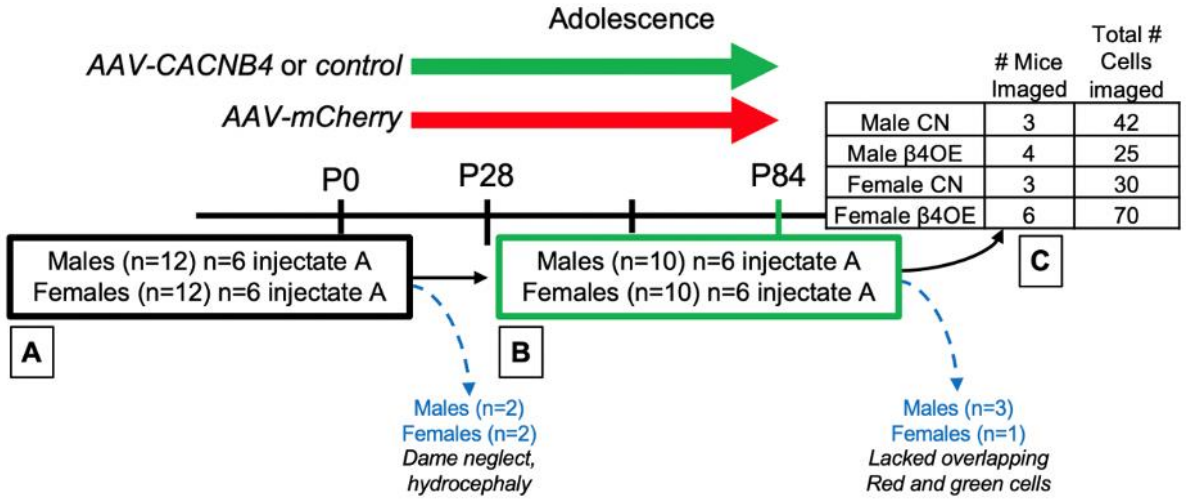

Figure 3.1: Study design and execution

(A) Two versions of AAV injectate were prepared by adding AAV-mCherry to either AAV-CACNB4 (to generate β4 overexpression [β4OE] mice) or AAV-control virus (to generate control [CN] mice). AAV solutions were randomly coded "A" and "B" before exposure to blind experimenter to group. Twenty-four P0-P2 C57BL/6J mouse pups were exposed to AAV injectate (50% to injectate A) using the bulk regional AAV injection (BReVI) procedure. Two males and two females perished prior to P84, due to either dame neglect (n=3) or hydrocephaly (n=1). (B) Stage of estrous cycle was estimated by evaluating vaginal cytology of P84 mice on day of sacrifice. Twenty mice were euthanized at P84: 4 male CN, 6 male β4OE, 4 female CN, and 6 female β4OE mice. Mice were anesthetized and transcardially perfused with ice-cold 1x PBS followed by 4% PFA. Brains were extracted, post-fixed in 4% PFA, moved to 18% sucrose and stored at -30°C in cryoprotectant until sectioning. (C) Layer 5 red (mCherry) fluorescent pyramidal cells with green (GFP) somal labeling were selected for imaging. We aimed for and used a sparse labeling approach for this study because it allowed us to visualize and evaluate spines without over-sampling. The major tradeoff for employing this sparse labeling approach is that we had to exclude 4 mice (1 male CN, 2 male β4OE and 1 female CN) before image analysis, due to fact that these mice lacked GFP+mCherry+ cells. Image stacks from P84 mice were assessed: 3 male CN (n=42 total cells), 6 male β4OE(n=25 cells), 3 female CN (n=30 cells), and 6 female β4OE mice (n=70 cells).

3.2.6 Statistics

Statistical tests were performed at two levels: 1) mouse level where n=16 mice and 2) neuron level where n=170 neurons in SPSS software (IBM, Armonk, NY). Shapiro-Wilk test was used to confirm normality. For statistical assessment at mouse level, an ANOVA (α=0.05) was used to test the main effects of genotype, sex, and the genotype by sex interaction on mean DSD.

These data were further examined at the neuron level in a separate statistical test. First, potential effects of mean distance of dendritic branch from soma, mean number of GFP+mCherry+ cells in ROI and region were evaluated for any association with DSD. None were significantly associated with DSD and were thus not included in the final model. An ANOVA (α=0.05) was used to test the main effects of genotype, sex, and the genotype by sex interaction on DSD.

An ANOVA (α=0.05) was used to test the main effects of genotype, sex, and the genotype by sex interaction on DSD of each individual spine mask size bin.

MANOVA (α=0.05) with Bonferroni correction was used to detect significant differences in mean densities among dendritic protrusion types. Main effects of genotype, sex, and the genotype by sex interaction were tested. The eight dependent variables were: mean short stubby, long stubby, thin, short mushroom, long mushroom, branched, atypical and filopodia densities.

3.3 Results

3.3.1 β4OE Reduced DSD of L5 Pyramidal Cells in Sensory Cortex

At the mouse level, β4OE significantly reduced mean DSD on minor basal branches of L5 pyramidal cells in five regions (V1, V2, A1, A2, and TeA) of sensory cortex ($F=9.249$, $DF=3$, $p=0.01$, Figure 3.2A). Sex did not significantly impact DSD. Similarly, there was a non-significant genotype by sex interaction. At the neuron level, β4OE significantly reduced DSD ($F=30.922$, $DF=3$, $p<0.001$, Figure 3.2B). Although main effect of sex on DSD was not significant, there was a significant genotype by sex interaction ($F=16.372$, $DF=3$, $p<0.001$). In a secondary analysis focusing on neurons from the two sexes separately, β4OE significantly reduced DSD in female ($F=61.899$, $DF=1$, $p<0.001$) but not male mice (Figure 3.2C-D).

3.3.2 β4OE-Mediated Spine loss in Females was Independent of Estrous Stage

Female CN and β4OE mice assessed in this study were in the following estrus stages: proestrus, estrus and metestrus/diestrus. Neuron DSD of female mice is displayed broken down by estrous stage in Figure 3.3A. Metestrus/Diestrus was the only stage with neurons from both CN and β4OE mice. DSD was significantly reduced in female β4OE mice in Metestrus/Diestrus alone ($F=6.190$, $DF=1$, $p=0.017$, Figure 3.3B). We performed a within mouse internal control assessment to determine if estrous stage significantly impacted neuron DSD within individual female β4OE mice. DSD of GFP+mCherry+ neurons was significantly decreased compared to DSD of GFP-mCherry+ internal control neurons in three β4OE mice: Ms10-87, Ms5-10 and Ms16-169. β4OE significantly reduced DSD within each mouse, regardless of estrous stage; Ms10-87 was in Estrus

(F=67.688, DF=1, p<0.001), and Ms5-10 (F=9.502, DF=1, p=0.004) and Ms16-169 (F=126.518, DF=1, p<0.001) were in Metestrus/Diestrus (Figure 3.3C). DSD of GFP-mCherry+ internal control neurons in the three β4OE mice assessed in Figure 3.3C did not significantly differ based on estrous stage (F=2.108, DF=1, p=0.154)(Figure 3.3D).

3.3.3 β4OE Selectively Reduced Density of Spines with Small Volumes in Females

Because spine density reductions due to β4OE were limited to females, we focused subsequent analyses on females (corresponding analyses in males available in Appendix B Supplemental Methods). Mean DSD of small < 0.1μm^3 spines were significantly decreased in neurons from female β4OE mice, relative to female CN (F=5.276, DF=1, p=0.035). Mean DSD of larger spine objects > 0.1μm^3 did not significantly differ based on genotype in female mice (Figure 3.4A). β4OE significantly decreased mean DSD of small spines 0.1μm^3 - 0.2μm^3 in volume (F=6.748, DF=1, p=0.032) in female β4OE mice in Metestrus/Diestrus alone (Figure 3.4B). The effect of reduced small spine objects was observed in female but not male mice (Appendix B Figure 3A).

3.3.4 β4OE Decreased Density of Four Morphologic Types of Spines in Females

β4OE significantly decreased mean density of four dendritic spine morphologic categories: short stubby, long stubby, short mushroom and long mushroom in female mice (Figure 3.4C). These four categories comprised the majority (95.19%) of all dendritic spines observed in females at P84. Focusing exclusively on females in Metestrus/Diestrus, β4OE significantly decreased mean density of short mushroom spines (F=20.160, DF=1, p<0.001) (Figure 3.4D). In contrast to effects

observed in females, alterations to the spine morphologic categories of males were slight. β4OE significantly increased mean density of long stubby spines in male mice (F=4.202, DF=1, p=0.044). There was a trend level increase in mean density of short mushroom (F=3.332, DF=1, p=0.072) and a trend level decrease in mean density of long mushroom (F=3.215, DF=1, p=0.077) spines in male β4OE mice (Appendix B Figure 3B).

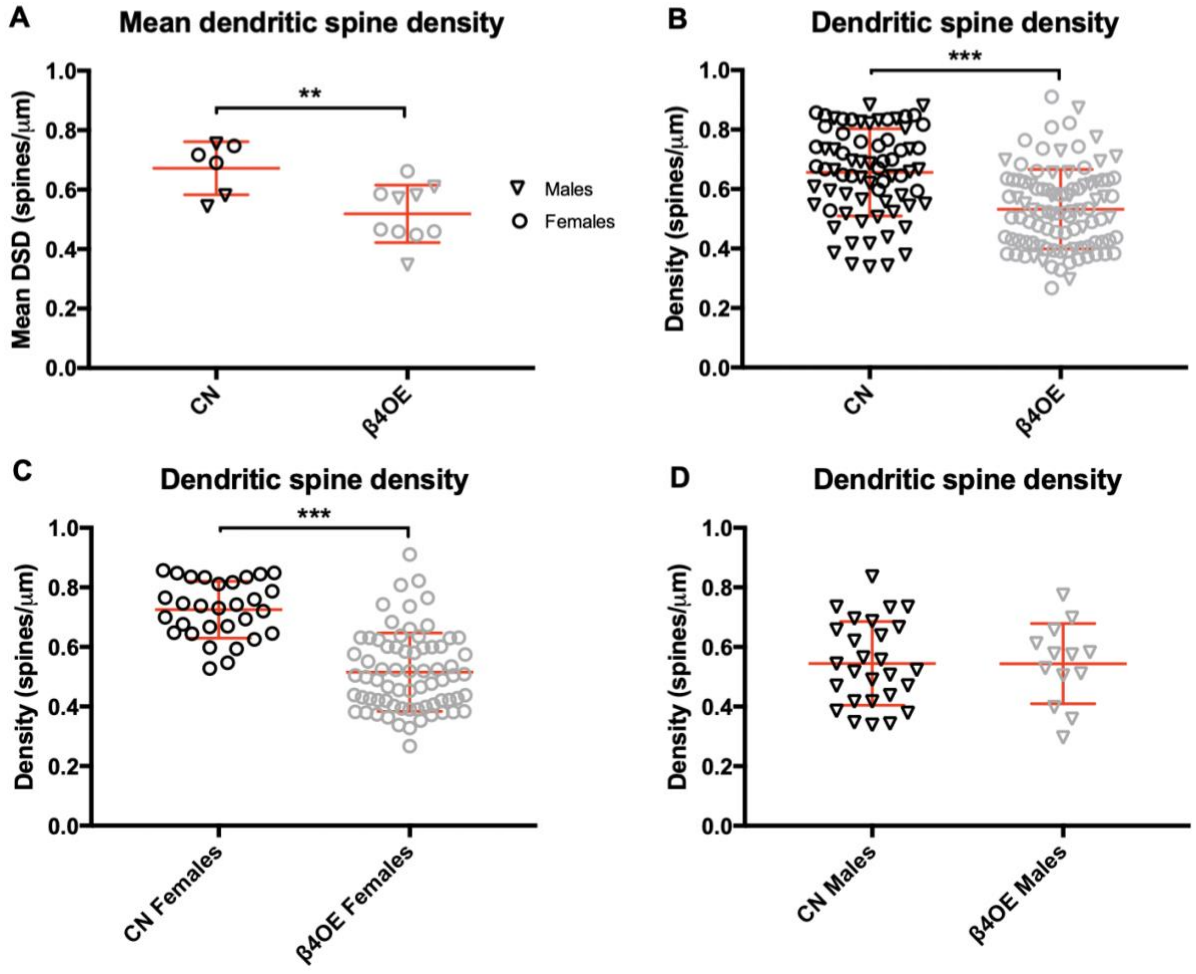

Figure 3.2: β4 overexpression (β4OE) significantly reduced dendritic spine density (DSD) on minor basal branches of layer 5 (L5) pyramidal cells in sensory cortex

(A) β4OE significantly reduced mean DSD at mouse level ($F=9.249$, $DF=3$, $p=0.01$). Main effect of sex on mean DSD was not significant ($F=0.612$, $DF=3$, $p=0.449$). Genotype by sex interaction was also not significant ($F=1.129$, $DF=3$, $p=0.309$). Data points are mean DSD values from individual mice. Error bars = SD. (B) DSD was significantly reduced in β4OE, compared to control (CN) mice at the neuron level ($F=30.922$, $DF=3$, $p<0.001$) (n=42 from CN males, n=28 from β4OE males, n=30 from CN females and n=70 from β4OE females). Main effect of sex on DSD was not significant ($F=1.812$, $DF=3$, $p=0.180$). There was a significant genotype by sex interaction ($F=16.372$, $DF=3$, $p<0.001$). Data points are DSD from individual neurons. Error bars = SD. (C) β4OE significantly reduced DSD in neurons from female mice ($F=61.899$, $DF=1$, $p<0.001$) (D) In contrast, β4OE did not significantly impact DSD in neurons from male mice ($F=0.838$, $DF=1$, $p=0.363$). Data points in C and D are DSD from individual neurons. Error bars = SD.

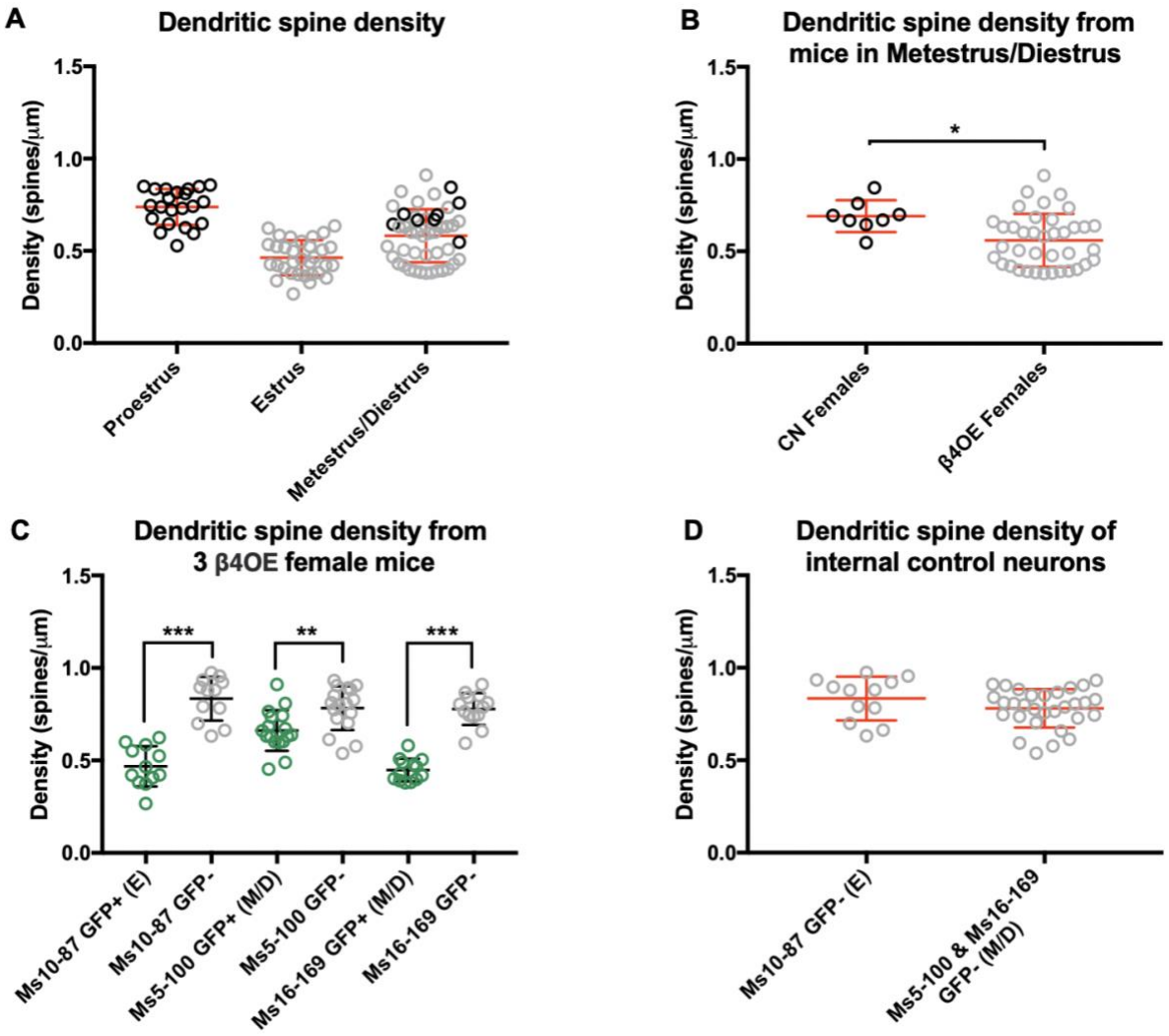

Figure 3.3: β4OE significantly reduced DSD in female mice regardless of estrous stage

(A) Estrous stage breakdown of DSD of neurons from female CN and β4OE mice. Data points are from individual neurons. Error bars = SD. (B) β4OE significantly reduced DSD in female mice in Metestrus/Diestrus (F=6.190, DF=1, p=0.017). Data points are from individual neurons. Error bars = SD. (C) Within mouse internal control comparison. DSD of GFP+mCherry+ (abbreviated GFP+) neurons was significantly decreased relative to DSD of GFP-mCherry+ (abbreviated GFP-) internal control neurons in three β4OE mice. Mice were in different estrous stages (L-R): Ms10-87 was in Estrus (E) (F=67.688, DF=1, p<0.001), and Ms5-10 (F=9.502, DF=1, p=0.004) and Ms16-169 (F=126.518, DF=1, p<0.001) were in Metestrus/Diestrus (M/D) on day of sacrifice. Data points are from individual neurons. Error bars = SD. (D) DSD of GFP- internal control neurons in the three β4OE mice (in C) did not significantly differ based on estrous stage (F=2.108, DF=1, p=0.154). Data points are from individual neurons. Error bars = SD.

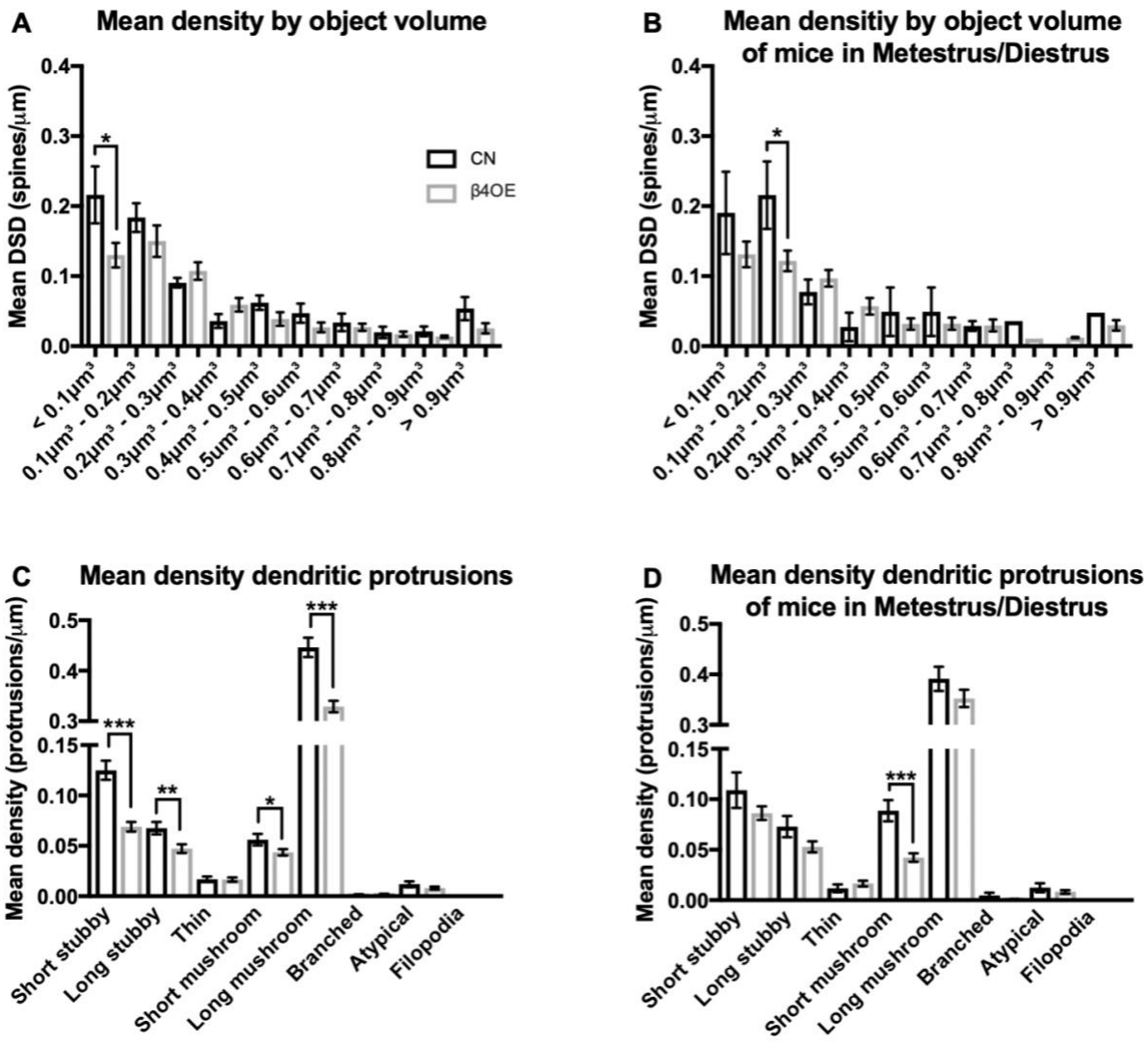

Figure 3.4: β4OE selectively reduced mean density of small volume spines and of distinct morphologic types in females mice

(A) Mean DSD of small objects of < 0.1μm^3 volume was significantly reduced in neurons from female β4OE mice, relative to CN (F=5.276, DF=1, p=0.035). Mean DSD of larger objects with volumes > 0.1μm^3 did not significantly differ based on genotype in female mice. Error bars = SEM. (B) Focusing exclusively on female mice in Metestrus/Diestrus, β4OE significantly decreased mean DSD of small objects of 0.1μm^3 - 0.2μm^3 volume (F=6.748, DF=1, p=0.032). Error bars = SEM. (C) β4OE significantly reduced mean density of short stubby (F=33.939, DF=1, p<0.001), long stubby (F=7.043, DF=1, p=0.009), short mushroom (F=4.342, DF=1, p=0.040) and long mushroom (F=30.354, DF=1, p<0.001) spines in female mice (all estrous stages represented) after Bonferroni correction. Collectively, spines in these four categories made up 95.19% of all protrusions observed in female mice. Error bars =

SEM. (D) Focusing exclusively on female mice in Metestrus/Diestrus, β4OE significantly decreased mean density of short mushroom spines ($F=20.160$, $DF=1$, $p<0.001$). Error bars = SEM.

3.4 Discussion

In the current study, we tested the hypothesis that overexpressing CACNB4 in the developing brain decreases DSD in adult mice, mirroring the spine loss intermediate anatomical phenotype observed in A1 in postmortem Sz (MacDonald et al., 2017; McKinney et al., 2019; Shelton et al., 2015; Sweet et al., 2009). β4OE significantly reduced DSD in primary cortical neuronal culture (MacDonald et al., 2017) and DSD was significantly reduced in A1 in postmortem Sz subjects (McKinney et al., 2019). With this evidence, we reasoned that β4OE would significantly decrease DSD of male and female mice. In contrast, β4OE significantly reduced DSD in L5 of sensory cortex of female but not male mice. We evaluated estrous stage of female mice on day of sacrifice, reported DSD of CN and β4OE females during all estrous stages and during Metestrus/Diestrus alone, and carefully compared DSD of GFP+ to DSD of GFP- (internal control) pyramidal cells in female β4OE mice. The results from these assessments provide complementary evidence that the spine loss we observed in β4OE female mice was not an artifact of estrous stage differences between genotypes. Spine volume assessment revealed β4OE-driven spine loss in female mice is selective for loss of the smallest spines, mirroring the recent finding of small spine loss in A1 in postmortem Sz (MacDonald et al., 2017; McKinney et al., 2019; Shelton et al., 2015; Sweet et al., 2009). Furthermore, β4OE-driven spine loss appeared relatively undiscriminating in terms of morphological type of spines lost in female mice, but notably included short and long

mushroom spines, which are characterized by large spine head volume and presumed to accommodate a mature postsynaptic density (Arellano et al., 2007).

Two methodological limitations encountered in this study warrant discussion. First, we intentionally employed a sparse labeling approach to assess dendritic spines on pyramidal cells to clearly visualize spines (with optimal signal-to-noise characteristics) and avoid over-sampling spine objects in our tissue. A minor downside of sparse labeling in the current study was that this necessitated expanding the ROI from A1, the region that is specified in our scientific premise, to sensory cortex (V1, V2, A1, A2, and TeA). In other words, the ROI we focused on herein was not perfectly aligned to the tightly focused A1 studies in our scientific premise (MacDonald et al., 2017; McKinney et al., 2019; Shelton et al., 2015; Sweet et al., 2009). Importantly, we and others have shown that unlike in higher mammals (Amatrudo et al., 2012; Clemo & Meredith, 2012; Gilman et al., 2016; Jacobs et al., 2001), there are little to no differences in cortical spine density based on region in mice (Arellano et al., 2007; Benavides-Piccione et al., 2002; Harris & Shepherd, 2015; Hsu et al., 2017; Luebke, 2017). Therefore, ROI does not diminish the translatability of our findings to human A1. Sparse labeling led to an uneven number of mice and neurons per group, which is a significant downside to the approach. Further reducing the size of the groups before image processing to equalize the numbers was not sensible, so we did everything in our power to carefully analyze the data by reporting DSD at both mouse and neuron levels, including as many controls as possible, probing potential confounds and performing rigorous statistics. The second methodological limitation concerns the β4OE AAV we employed. The P2A element included in the β4OE AAV was not 100% efficient, resulting in the expression of a β4-GFP fusion protein in addition to non-native β4 and GFP (Appendix B Figure 2A). One concern is that the heavier fusion protein may not translocate to and behave like native β4. We can be fairly confident that β4-GFP

translocates to dendrites, where it has the potential to alter DSD, given that a similar fusion protein, GFP-β4, co-localized with the dendritic protein Map2 in cultured hippocampal neurons (Wittemann et al., 2000). Regardless, it is unlikely the effect of β4OE on DSD was due to the fusion protein as β4OE did not significantly reduce DSD in male mice.

Several highly influential light and electron microscopy studies have demonstrated that circulating hormone levels across the estrous cycle shape spine dynamics in hippocampus of female rats (Alexander et al., 2018) with high levels of 17β-estradiol (E_2) during proestrus corresponding with higher DSD (A. Kato et al., 2013; Woolley, Gould, Frankfurt, & McEwen, 1990; Woolley & McEwen, 1992). Results from similar studies performed in rat cortex are mixed. Two out of three studies found no difference in DSD in proestrus compared to other stages (J.-R. Chen et al., 2009; Markham & Juraska, 2002; Prange-Kiel et al., 2008). Taking into account these findings, we explored the possibility that our finding of β4OE-mediated spine loss in female mice could be driven by estrous stage. Vaginal cytology of each female mouse was evaluated, stage of estrous estimated and recorded on P84, day of sacrifice for all (females and males) mice in our study. All animals in the study were sacrificed on P84 by design, since DSD is known to fluctuate over the course of neurodevelopment as a function of age, specifically in A1 and sensory cortex of mice (Moyer, Erickson, et al., 2015; Parker et al., 2020). Each estrous stage was not equally represented on P84 across genotypes by chance, therefore we additionally specifically compared DSD of female CN versus β4OE mice in metestrus/diestrus, the only estrous stage represented in both genotypes of mice. Narrowing our focus to metestrus/diestrus again revealed DSD was significantly reduced in female β4OE relative to CN mice. Importantly, DSD of GFP+ (readout of β4OE) neurons was significantly decreased compared to DSD of GFP- internal control neurons in a β4OE mouse in estrus. The same finding was repeated in two β4OE mice in metestrus/diestrus

and DSD of internal control neurons did not significantly differ based on estrous stage in β4OE mice. So, although proestrus, estrus and metestrus/diestrus were not equally represented among the genotypes in the current study, our data collectively indicate that β4OE-mediated DSD reduction in female mice was not an artifact of estrous stage, consistent with two studies focusing on DSD in rat cortex (Markham & Juraska, 2002; Prange-Kiel et al., 2008) and two mouse studies, the first which found no change in spine density of L5 pyramidal cells across estrous in somatosensory cortex (Alexander et al., 2018), and the second which demonstrated no change in spine density of L5 pyramidal cells in frontal cortex of P27 pre-pubertal hormone-treated or ovariectomized female mice (Boivin, Piekarski, Thomas, & Wilbrecht, 2018). Within the broader context, studies of DSD in rodent hippocampus demonstrate estrous stage modulates DSD (Alexander et al., 2018; A. Kato et al., 2013; Woolley et al., 1990; Woolley & McEwen, 1992), whereas in rodent cortex estrous stage regulation has been primarily demonstrated to be independent from DSD (Alexander et al., 2018; Markham & Juraska, 2002; Prange-Kiel et al., 2008). Moreover, our internal control assessment findings suggest that β4OE does not likely exert a network effect on spines of non-β4OE neurons. However, follow up studies are necessary to reject the possibility that β4OE significantly reduces DSD on cells in the broader network and to substantiate the prediction that β4OE's impact is cell-autonomous.

Among mouse studies reporting decreased DSD due to a Sz-related manipulation, our results are noteworthy due to the volume- and sex-specificity of the observed spine loss. We report here β4OE significantly reduced density of spines of small volumes, in particular, spines with volume equal to or smaller than $0.1\mu m^3$. Our group recently become interested in the possibility that spine loss in A1 in Sz could be specific for loss of spines of a particular size/volume. Volume assessment of spines in deep layer 3 of A1 in Sz revealed small spine loss drives the overall

reduction in spines observed in A1 in Sz (MacDonald et al., 2017). The reason for loss of small spines was proposed to imply roles for impaired new spine formation or stability since genetic studies implicate multiple pathways important for spine formation and stabilization in Sz risk (Purcell et al., 2014; Schizophrenia Working Group of the Psychiatric Genomics Consortium, 2014). Moreover, reduced small spine density was provided as evidence an alternative the classic explanation of Sz pathogenesis first proposed by Irwin Feinberg in 1982, which states that mature spines are excessively eliminated in Sz during adolescence (Feinberg, 1983; Keshavan et al., 1994). A major assumption employed in the argument for this alternative possibility was that new or transient spines are small and mature spines large (Holtmaat et al., 2005; Knott & Holtmaat, 2008).

Spines of small volume ($<0.3\mu m^3$) made up the majority (68.96%) of all spines observed in P84 mice in the spine volume assessment of neurons in CN and β4OE in mice the current study. Studies of PSD-95 and longitudinal imaging of spine dynamics *in vivo* demonstrate that spines are divided into two categories based on synapse maturity, "immature spines" which are new and lack PSD-95 protein and "mature" spines with established excitatory synapses and PSD-95. In adult animals, 20% of all spines are highly dynamic, rarely stabilized and immature, whereas 70-80% are mature and PSD-95 containing (Berry & Nedivi, 2017; Cane, Maco, Knott, & Holtmaat, 2014; Holtmaat et al., 2005; Trachtenberg et al., 2002; Villa et al., 2016). Immature spines tend to be small, however, spines of all sizes can be categorized as immature or mature (Holtmaat et al., 2005). If we assume that all or nearly all immature spines in our study are small, this leaves a pool of up to 48.96% spines in our study that are small mature spines (predicted to contain PSD-95) (Figure 3.5A).Thus, we propose β4OE decreases density of small spines, including both new/immature spines as well as mature PSD-95 containing dendritic spines.

If immature small spines fail to form or stabilize in β4OE mice, like was suggested to occur in Sz in our previous study (MacDonald et al., 2017), impaired spine formation or stabilization could drive loss of a portion of, but not 100% of the small spines decreased in the current study. The remaining small spines decreased in our study are likely mature and could be lost to due to destabilization of the actin cytoskeleton through a cell-autonomous process. Spine head volume positively correlates with postsynaptic density size and number of receptors (Arellano et al., 2007). Mushroom spines are characterized by large head volumes and thin neck diameter. β4OE-mediated spine loss included short mushroom and long mushroom types in females, providing additional evidence for mature spines among the small spines lost due to the β4OE manipulation. Finally, without specifically performing *in vivo* imaging of spine dynamics, we cannot rule out the possibility that a portion of small mature spines are eliminated in β4OE mice during adolescence as Feinberg predicted (Feinberg, 1983; Keshavan et al., 1994). Reexamination of data reported in one of our previous studies (Moyer, Erickson, et al., 2015) revealed that spine loss in L2-4 of A1 in normative mouse adolescence (P28-P84) was selective for spines of the smallest volumes (unpublished finding). If small spines are lost during adolescence synaptic remodeling in wildtype mice and in β4OE mice via a shared mechanism, loss of small spines observed in P84 β4OE mice could be characterized by reduced mature small spine number, due to elimination during circuit remodeling in adolescence in addition to immature small spines loss due presumably to failed spine formation or stability (Figure 3.5B).

In concert, our findings of β4OE-mediated small spine loss support our group's previous prediction that new spine formation and stability could be impaired in Sz and also support the notion that mature spines could be eliminated during adolescence. We specifically highlight the possibility that many of the spines lost due to our Sz-related manipulation, β4OE, are likely small

mature spines. Follow-up studies should stain for PSD-95 in CN and β4OE female mice to confirm. Moreover, proportion of spines added, and eliminated should be longitudinally tracked and evaluated using *in vivo* imaging of spine dynamics in CN and β4OE neurons. Additionally, spine lifetimes could be tracked in spine dynamics experiments to characterize transience/persistence of small spines in future studies.

β4 protein is not thought to directly modulate the actin cytoskeleton or play direct roles in mediating spine dynamics or morphology. Cav3 α1 VGCC subunits on the other hand were recently implicated in new synapse assembly (Zhao et al., 2017). Therefore, β4-mediated Cav3 Ca^{2+} signaling may represent a potential mechanism whereby β4OE mediates small spine loss. However, whether β subunits can directly regulate Cav3 VGCCs remains controversial. β4 is known to significantly impact Ca^{2+} signaling via regulation of the α1 subunit of high voltage-activated VGCCs and Ca^{2+} signaling, in turn, is critical for the structural and functional plasticity of dendritic spines (Higley & Sabatini, 2012; H. Kasai et al., 2003; Yuste et al., 2000). Post-synaptic β4-mediated VGCC Ca^{2+} entry is therefore predicted to initiate signaling cascades that implicate downstream proteins that control actin organization and dynamics in spines. Investigating such proteins, including Rho family GTPases, which have established roles in regulating the actin cytoskeleton (Ethell & Pasquale, 2005), and dendritic microtubule-associated proteins (MAPs), which are of high interest to our group, and have been shown to bundle f-actin (Roger, Al-Bassam, Dehmelt, Milligan, & Halpain, 2004; Selden & Pollard, 1983) could provide key insights into potential mechanisms by which β4OE reduces density of small dendritic spines in a cell-autonomous manner. Our group recently demonstrated that MAP2-immunoreactivity is significantly reduced in A1 and positively correlated with small spine loss in this region in Sz (DeGiosio et al., 2019; Grubisha et al., 2019; McKinney et al., 2019).

Finally, after completing the experiments described in the current study, two major unanswered questions remained and warranted the follow-up study performed in Chapter 4. The first question was: why are female mice more vulnerable to the β4OE manipulation? The second question was: how might β4OE reduce DSD on a mechanistic level? β4 subunits traffick α1 VGCC subunits to the plasma membrane, strongly regulate channel gating, on one hand increasing the voltage-dependent threshold of channel activation and increasing macroscopic Ca^{2+} current density, and on the other hand promoting closed state voltage-dependent inactivation. Additionally, β4 subunits promote channel inhibition by accelerating Gβγ dissociation following Gβγ-mediated inhibition of VGCCs and β4 has also recently been implicated in modulation of transcription machinery in the nuclear compartment (Buraei & Yang, 2010; Dolphin, 2016). Given the diversity of roles played by β4 and lack of literature on β4 sex differences, we designed and performed an exploratory experiment to nominate mechanisms that could mediate the volume- and sex-specific β4OE-mediated spine loss observed in the current study. Co-immunoprecipitation combined with mass spectrometry was utilized to identify sex differences in the "β4 interactome" of P84 mouse cortex (Chapter 4). Importantly, we propose a model in the overall discussion (Chapter 5) of this document to explain volume- and sex-specific β4OE-mediated spine loss observed in P84 mouse sensory cortex.

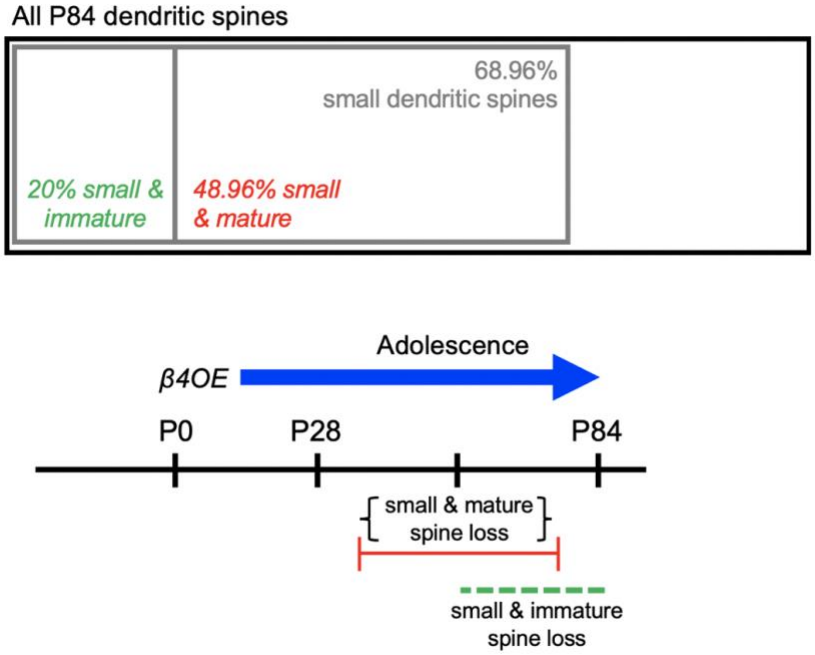

Figure 3.5: β4OE decreased density of small spines, including potentially both new/immature spines and mature PSD-95 containing dendritic spines

(A) Proposed breakdown of immature (non-PSD-95 containing) and mature (PSD-95 positive) dendritic spines in P84 mice. (B) Proposed timeline of small spines loss in β4OE mice. Small and mature spine loss occurs during adolescent synaptic remodeling (red line)(Zuo, Lin, Chang, & Gan, 2005). Small and immature spines fail to form or stabilize during early adulthood (green dashed line).

4.0 Sex Differences in the β4 Interactome

4.1 Introduction

β is the most extensively studied auxiliary subunit of voltage-gated calcium channels (VGCCs) (Zamponi, 2005). β along with two other auxiliarly VGCC subunits, $\alpha_2\delta$ and γ, bind to the α1 (ion permeable channel) VGCC subunit with a 1:1:1:1 reversible stoichiometry (Buraei & Yang, 2010, 2013; Dolphin, 2016). There are four β protein subfamilies, β1-4 (Castellano & Perez-Reyes, 1994). Each β protein subtype is encoded by a separate gene with multiple splice variants, all of which are highly expressed at transcript and protein levels in mouse brain tissue with the exception of β1a, β1d, β2d, and β2e (Buraei & Yang, 2010; Schlick et al., 2010). Evidence of β4a is limited to the cerebellum (Buraei & Yang, 2010). Of the β proteins found in brain, particular subunits predominate in neuronal subcellular compartments depending on the α1 subunits they preferentially bind to and modulate (Buraei & Yang, 2010). β subunits can bind to any high-voltage activated (HVA) α1 VGCC subunit and pair with α1 subunits with a 1:1 stoichiometry. Although the binding affinity of β to α1 is high, ranging from 2–54nM, α1 to β pairing is reversible and α1-β reshuffling may occur either to compensate for loss of β or through competitive replacement (Buraei & Yang, 2013; Burgess et al., 1999; Burgess et al., 1997; Dolphin, 2016; Yeon et al., 2018).

β4 is the focus of the current study and has now five known splice variants (Etemad et al., 2014). β4 variants are generally expressed highly in brain, including in rodents, where transcript and protein levels are altered in several brain regions as a function of age (Buraei & Yang, 2010; Ferrándiz-Huertas et al., 2012; Ludwig et al., 1997). As a general rule, β4 preferentially binds the

presynaptic α1 $Ca_V2.1$ (P/Q-type) VGCC (Tanaka et al., 1995; Wittemann et al., 2000). β4 also has been shown to bind to approximately 40% of α1 Ca_V1 (L-type) VGCCS, in addition to other high-voltage activated (HVA) calcium channels, $Ca_V2.2$ (N-type) and $Ca_V2.3$ (R-type) (Buraei & Yang, 2010; McEnery, Vance, et al., 1998; Scott et al., 1996). Neuronal subcellular distribution of β4 appears diffuse. There is evidence for β4 at the plasma membrane, in intracellular space, in dendrites and dendritic spines and in axons. Electron Microscopy revealed murine cerebellar and hippocampal β4 levels are significantly higher in intracellular space than other compartments (Ferrándiz-Huertas et al., 2012). β4 co-localizes with VGLUT1 in presynaptic terminals of glutamatergic neurons, and is present in synapse preparations for mass spectrometry (Etemad et al., 2014; Klemmer et al., 2009). β4b is the only isoform specifically demonstrated to exibit nuclear targeting (Subramanyam et al., 2009).

β proteins (β1-4) perform similar, but non-identical functions (Buraei & Yang, 2010). It has been argued that β is the most critical auxiliary subunit; Presence of β has long been presumed to be required for trafficking the α1 subunit of HVA VGCCs to the plasma membrane (Giovanni Gonzalez-Gutierrez et al., 2008; Jones et al., 1998; Josephson & Varadi, 1996; Maltez et al., 2005). More recent work has indicated that β is essential for proper function of the α1 channel in a couple of important ways; briefly, β subunits are responsible for α1 channel gating kinetics as well as play critical roles in RGK- and G protein inhibition of VGCC channels (Buraei & Yang, 2010). The β subunit strongly regulates channel gating; relative to native currents, β isoforms generally increase channel activation and enhance the closed state of voltage-dependent inactivation (β3>β1b=β4>>β2a). β2a is the exception to this rule because it inhibits voltage-dependent inactivation (Buraei & Yang, 2010; Patil et al., 1998; T. Yasuda et al., 2004). The RGK subfamily, which include Rad, Rem, Rem2 and Gem/Kir, are GTP-binding proteins with two known

functions, to modulate cytoskeletal dynamics and inhibit HVA VGCCs. Several mechanisms by which RGKs inhibit VGCC have been reported. In all cases β VGCCs subunits are required for this inhibition. Finally, β is required for voltage-dependent current inhibition of Ca_V2 channels by G protein βγ subunits in hormone and neurotransmitter negative feedback of VGCCs (Meir et al., 2000; Yun Zhang et al., 2008).

Given that β subunits are known to be promiscuous, meaning each β1-4 has the capacity to bind to any HVA α1 VGCC subunit, and do so reversibly, it is no surpise that β subunits have been repeatedly demonstrated to stand in for one another, in cases of scientific manipulation, injury or disease (Berggren et al., 2004; Buraei & Yang, 2013; Heyes et al., 2015; Namkung et al., 1998; Neef et al., 2009). A classic and well-known example of this in the VGCC literature is α1-β reshuffling in lethargic (β4-knockout) mice (Burgess et al., 1999; Burgess et al., 1997). These mice result from a naturally occurring null mutation in CACNB4, the gene that encodes β4 (Burgess et al., 1997). Increased pairing of $Ca_V2.1$ and $Ca_V2.2$ with β subunits other than β4, are observed in lethargic mice, particluarly increased pairing of $Ca_V2.2$ and β1b (Burgess et al., 1999). Although α1-β reshuffling occurs in these mice, this reshuffling does not fully compensate for the loss of β4 or reverse the epilepsy-like phenotype of these mice (Buraei & Yang, 2010, 2013; Burgess et al., 1999; Burgess et al., 1997). Lethargic mice display a ~50% upregulation in thalamic Ca_V3 VGCCs, reduced excitatory neurotransmission in thalamus and lower $Ca_V2.2$ VGCC expression in forebrain and cerebellum (Caddick et al., 1999; McEnery, Copeland, et al., 1998; Yi Zhang et al., 2002). This partial compensation, despite β reshuffling in lethargic mice highlights the distinct roles played by β4 among the β subunits, potentially due in part to the unique-to-β4 interactions of the NH_2 and COOH termini of β4 with α1 VGCCs (Brice & Dolphin, 1999; De Waard et al., 1995; Stotz et al., 2004; Walker et al., 1998; Walker et al., 1999; Wittemann et al., 2000).

The purpose of the current study was to identify potential sex differences in the β4 interactome in P84 mouse brain. The ultimate goal of the study was to inform our previous finding that overexpressing β4 in the developing brain significantly reduces dendritic spine density in female but not male mice (see Chapter 3). We used co-immunoprecipitation combined with mass spectrometry (CoIP-MS) to examine protein-protein interactions (Collins et al., 2006). To our knowledge this is the first study to specifically compare the β4 interactome of male to that of female mice. Remarkably, the β1b VGCC subunit was contained within the β4 interactome of male but not female mouse brain. Finally, four peptides included in three neuronal microtubule-associated proteins (MAPs) are differentially distributed among the β4 interactome of male mice and the β4 interactome of female mice.

4.2 Methods

4.2.1 Experimental Animals

Co-immunoprecipitation (CoIP) was combined with mass spectrometry (CoIP-MS) as our group has done previously to characterize the β4 interactome in mouse brain (Grubisha et al., 2019). Four male P84 and four female P84 C57BL/6J mice were sacrificed by lethal CO_2 followed by rapid decapitation. Brains were extracted, rapidly frozen and stored at -80°C until β4 immunoprecipitation. These experiments were approved by the IACUC at the University of Pittsburgh in accordance with the guidelines outlines in the USPHS Guide for Care and Use of Laboratory Animals.

4.2.2 Tissue Preparation and Co-Immunoprecipitation

Tissue samples were prepared and CoIP run in block design (Figure 4.1A-B). Bilateral cerebral cortex and underlying structures from each brain were separated from the olfactory bulb at the optic chiasm, and from tissue posterior to the cerebral cortex-midbrain junction (the cerebellum and majority of the brainstem). Brain tissue samples were homogenized in ice-cold Triton x-100 lysis buffer (Klemmer et al., 2009) (1% Triton x-100, 5M NaCl, 25mM HEPES [ph 8]),1mM EDTA [ph 8] in double distilled H_2O) using a pre-chilled micro-pestle and passing homogenate through a 1mL syringe with a 23G needle ten times. Brain lysate was then incubated on ice for 10m to solubilize proteins and centrifuged for 20m at 14,000g at 4°C to remove the insoluble fraction. Supernatant was then transferred to a new tube and centrifuged for 10m at 12,000g at 4°C. Supernatant was RNAse treated on ice for 30m. Protein concentration was estimated using a Micro BCA Protein Assay Kit (ThermoFisher Scientific #23235)(R^2 values > 0.99 for each sample). 50μL input samples were generated prior to supernatant combination with antibody coupled beads. Antibody coupled beads were prepared by incubating 10μg mouse anti-Ca_Vβ4 (Neuromab #75-054) per mg Dynabeads (Thermo Fisher Scientific) overnight. This antibody has been used previously to immunoprecipitate β4 from synaptosome preparations using a CoIP-MS method similar to the one described in the current study (Klemmer et al., 2009). Additionally, we demonstrate this antibody can be used to immunoprecipitate β4 using with western blot detection with a goat anti-CACNB4 antibody (Everest Biotech #EB06591, 1:1000) and donkey anti-goat 800 secondary antibody (LiCor #926-32214, 1:10,000) (Appendix C Figure 1A-B). Supernatant was precleared in 1.5mg 1xPBS pre-washed Dynabeads (Thermo Fisher Scientific) on a rotator for 1h at 4°C. Precleared supernatant was then incubated with antibody

coupled beads (one "β4-IP" sample per mouse), or pre-washed Dynabeads beads not coupled to antibody (one "CN" per mouse)(total=16 samples overall) on rotator overnight at 4°C. β4-IP and CN samples were washed three times in ice-cold 1xPBS buffer and boiled at 95°C for 5min in 25μL 1 x SDS and 10% mercaptoethanol in 4x protein sample loading buffer (LiCoR #928-40004) to elute protein from beads.

4.2.3 Sample Preparation and Liquid Chromatography Mass Spectrometry (LC-MS/MS)

1μL (1667fmol) $^{13}C_6$ $^{15}N_4$-L-Arginine $^{13}C_6$ $^{15}N_2$-L-Lysine Stable Isotope Labeled (SIL) β4 protein Standard (Origene #PH310440) was added to each sample (total=16 samples overall). Samples were prepared in a randomized block design (Figure 4.1C). Samples were digested with trypsin on S-Trap™ Micro Spin columns (Protifi #C02-micro-80) following manufacture protocol and prepared for Liquid Chromatography Mass Spectrometry using 0.6μL C_{18} resin ZipTips (Millipore Sigma #ZTC18S096). A pooled instrument control (PC) was made by combining 1μL from each sample. 2μL (~1μg) each sample plus three 2μL aliquots of the PC were resolved on an EASY C18 column (1.7μm, 2.1x50cm) at 300 nL/min with an UltiMate™ 3000 RSLCnano HPLC system over a 90-min gradient and analyzed on an Orbitrap Eclipse™ Tribrid™ MS (Thermo Fisher Scientific) operated in MS/MS (Figure 4.1D). Peptide/protein identification, quantification and initial peptide peak area normalization were performed in Skyline Software (MacLean et al., 2010).

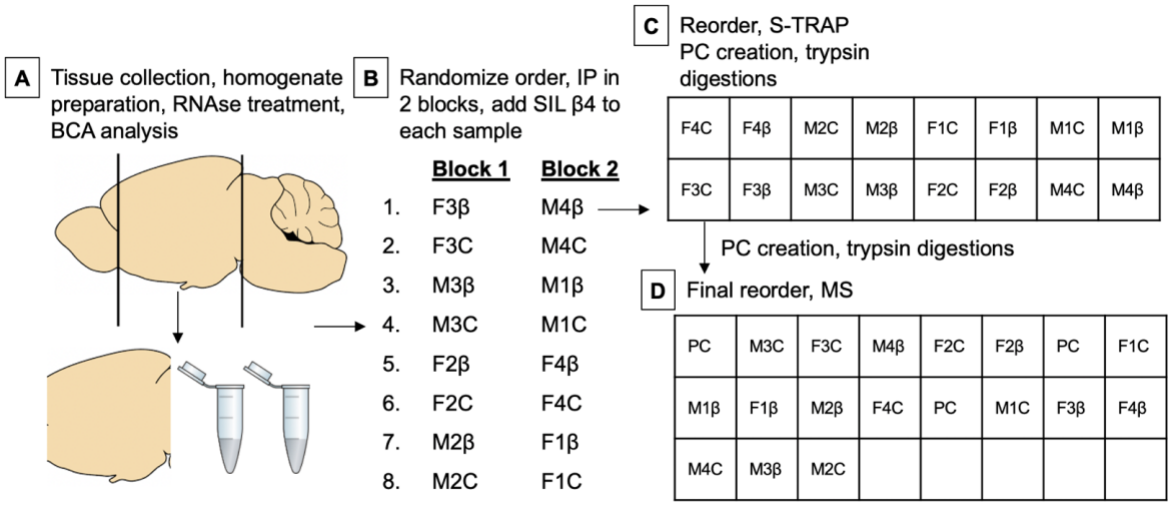

Figure 4.1: Co-Immunoprecipitation Mass spectrometry (CoIP-MS) methods

(A) For each brain, bilateral cerebral cortex and underlying structures were separated from the olfactory bulb at the optic chiasm, and tissue posterior to the cerebral cortex, midbrain junction. Mouse brain tissue was homogenized using Triton x-100 lysis buffer, treated with RNAse and total protein amount determined using BCA. (B) Sample name abbreviations were created e.g. Female mouse # 3 β4-IP (F3β), Male #1 CN (M3C), and immunoprecipitation (IP) run in two blocks with sample pairs in random order. 1µL stable isotope labeled (SIL) β4 protein was added to each sample (samples=16). (C) Samples were reordered, and S-TRAP performed. A pooled instrument control (PC) was created from all samples and each sample digested with trypsin. (D) Samples were reordered a final time and loaded onto the LC-MS for analysis.

4.2.4 Statistical Analysis

β4 interactome data was analyzed similarly to previously described (Grubisha et al., 2019). Briefly, within each sample peptide peak areas were exported from Skyline Software. β4 peptide levels were first normalized to SIL β4 peptide levels to control for differences in efficiency of the IP. Next, within each CoIP, peptide peak areas were divided by the normalized β4 peptide levels to generate normalized peak area ratios. Mean overall (includes samples from male and female mice) β4-IP peak area and mean overall CN peak area ratios were calculated. Log2 fold change

values were calculated using the overall means to detect shifts in distributions of β4-IP enriched protein levels, relative to CN. Peptides with CV<0.3 were compared using paired Student's t-tests of log2-transformed peak ratios. The most significantly enriched peptides in the β4 interactome (males and females combined) are listed in Appendix C Figure 2 and Appendix C Table 1.

Sex differences in the β4 interactome, the group of 13023 peptides with ratio of abundance in β4-IP/Negative CN>1, were the focus of this study. Mean peak area ratio for each sex and log2 fold change (Log2(M)-Log2(F) were calculated and the sexes compared using paired Student's t-test. Significantly altered peptides were defined as those with p value less than 0.05 and log2 fold change>1 (peptides enriched >100% in males) or log2 fold change<-1 (peptides enriched >100% in females).

4.3 Results

To confirm the validity of our CoIP LC-MS approach as a prerequisite to the sex differences assessment, we first identified the 13023 peptides that comprise the β4 interactome in P84 mouse brain homogenate, including a number of expected peptide/proteins consistent with previous reports of proteins associated or predicted to be associated with the β subunit or β4 specifically (guided primarily by this excellent review (Buraei & Yang, 2010)). Included in this list were the VGCC subunits Cav2.1, Cav2.2, Cav2.3 and $\alpha_2\delta 1$, most notably. Furthermore, ryanodine receptors 1 and 2 were identified as were dynamin 1-3, phosphoinositide 3-kinase (PI3K), calcium/calmodulin-dependent kinase II (CaMKII, protein ID label KCC2), members of the synaptic protein family synaptotagmin, zinc transporter 1 (plus zinc transporter 3, 9 and 10), members of the Mitogen-activated protein kinase (MAPK) and MAPK kinase families (protein ID

labels MK and MP2K), members of the Protein Kinase C family of proteins and the relatively recently discovered and described protein VGCC β-anchoring and -regulatory protein (BARP) (Abiria & Colbran, 2010; Béguin et al., 2014; Beharier et al., 2007; Buraei & Yang, 2010; Cheng, Altafaj, Ronjat, & Coronado, 2005; Fitzgerald, 2002; Gonzalez-Gutierrez, Miranda-Laferte, Neely, & Hidalgo, 2007; Grueter, Abiria, Wu, Anderson, & Colbran, 2008; Levy et al., 2009; Nakao et al., 2015; Ohana et al., 2006; Segal et al., 2004; Sheng, Westenbroek, & Catterall, 1998) (Table 4.1).

Among the 13023 peptides in the β4 interactome (Figure 4.2), eighteen were significantly enriched in males mice with log2 fold change greater than 1 and p value less than 0.05. Twenty-four peptides in the β4 interactome were significantly enriched in females with log2 fold change less than -1 and p value less than 0.05 (Table 4.2). Zero peptide/protein ids were shared among the two enrichment lists. Of particular interest was the peptide TMATAALAASPAPVSNLQGPYLASGDQPLDR, which was significantly enriched in the β4 interactome of male relative to female P84 mice (log2 fold change=3.9357, p=0.0201). This peptide is contained in the auxiliary VGCC subunit β1. Amino acid sequence alignment of this peptide alongside the amino acid sequences of each of the four β1 isoforms revealed this peptide is exclusively found in the "neuronal" β1 isoform β1b.

MAPs were represented in both significantly enriched in male and enriched in female lists (Table 4.2). The MAP6 (also known as stable tubule-only polypeptide [STOP protein]) peptide GPMQLSADARDPEGAGGAGVLAAGK was significantly enriched in males (log2 fold change=1.1276, p=0.0254). Two MAP2 (known as MTAP2 in mice) peptides were significantly enriched in females, QDSFPISLEQAVTDAAMTSK (log2 fold change=-1.3215, p=0.01828) and DWFIEMPTESK (log2 fold change=-1.5552, p=0.0355). Furthermore, the MAP1A peptide

AELEEMEEVHPSDEEEEETKAESFYQK was also significantly enriched in females (log2 fold change=-1.2969, p=0.0459).

Table 4.1: Previously reported β-interacting proteins

VGCCs and other previously reported β-interacting proteins identified within the β4 interactome of male and female P84 mice, including CaMKII (KCC2; gray boxes) and MAPKs (MK, MP2K; gray boxes). In nearly all cases, multiple peptides per Protein ID were identified. Peptide with the lowest significant p value per Protein ID is reported in the table.

Peptide	Protein ID	β4-IP Mean	Negative CN Mean	Log2(β4-IP)-Log2(CN)	p value
ILLDAGFTNELVQNYWSK	CA2D1	4679428.52	430883.648	3.44096209	0.0020032
HLNVQIAASEK	CACB1	1972810.91	575075.819	1.7784286	0.000678
EGGDIAFIPSPQR	CACB3	12280054.2	1034063.14	3.56992075	0.00132655
TSLAPIIVHVK	CACB4	220800749	4296093.28	5.68357594	6.6278E-06
GSSAGFLTLHNAFPK	CCG8	26893944.7	2476365.74	3.44098507	2.2347E-05
GPDGEPQPGLESQGR	CAC1B	3660770.58	984309.532	1.89496339	0.07737068
SKTDLLNPEEAEDQLADIASVGSPFAR	CAC1A	7684689.21	1429661.12	2.42631369	0.00037217
SLFIFGEDNIVR	CAC1E	15626148.1	1367039.48	3.51483538	4.2502E-05
HASLDGASPYFK	CBARP	7077283.81	386774.592	4.19363085	0.00011575
LADFGLAIEVEGEQQAWFGFAGTPGYLSPEVLR	KCC2A	16655492.9	4292426.25	1.9561328	0.00029843
NSLVSPAQEPAPLQTAMEPQTTVVHNATDGIK	KCC2G	11039219.1	3554233.61	1.6350277	0.00211111
WQNVHFHCSGAPVAPLQ	KCC2B	48924331.4	8320871.35	2.55574562	0.00031296
VTEQLIEAINNGDFEAYTK	KCC2D	170897637	51071238.1	1.74254951	9.0052E-05
HIFALFNTEQR	DYN1	1337059441	248763365	2.42621766	5.726E-05
NLVDSYVAIINK	DYN2	26011838.4	4424921.46	2.55544462	0.00036523
DFINSELLAQLYSSEDQNTLMEESAEQAQR	DYN3	4692986.01	844595.315	2.47417401	3.1317E-06
GPGPLQER	MATR3	9081529.79	1012921.79	3.16441255	0.00030925
ELIFEETAR	MK01	19980737	5684580.29	1.81348406	0.00049902
YAGLTFPK	MK10	47936716.2	11171215.2	2.10134495	0.0006719
EIQILLR	MK03	26591656.5	5242495.99	2.34264789	0.00012184
NIIGLLNVFTPQK	MK08	18472179	3011726.26	2.61669151	6.4344E-05
KLIHLEIKPAIR	MP2K1	7366876.12	699448.954	3.3967623	0.00061777
LQGTHYSVQSDIWSMGLSLVELAIGR	MP2K2	9130170.09	595500.023	3.93846827	4.9442E-05
SDVWSLGITLYELATGR	MP2K4	14163070.2	1889143.79	2.90632961	5.4254E-05
ILANGQMNEQDIR	MP2K5	1688528.28	158518.721	3.4130412	0.02430607
EAFEQPQTSSTPPR	MP2K6	12080013.4	1895764.2	2.67177063	0.00155127
DVKPSNILLDER	MP2K7	21391015.4	4721868.32	2.17957525	0.0001709
SLLAAQQTFVDR	PK3C3	14133065.9	2561537.4	2.4639926	0.0003328
TLVTGGATPELEALIAEENALR	KCMA1	15441800	4596895.79	1.74810907	0.00029363

Table 4.1 continued

KGTEELYAIK	KPCA	17227148.3	3350753.57	2.36212641	3.603E-05
DIKEHAFFR	KPCB	125821888	30482936.7	2.04530912	0.00024614
SEEEAKFPTMNR	KPCD	3634260.09	746119.948	2.28418219	0.00059478
LAAGAESPQPASGNSPSEDDRSK	KPCE	25555749.4	3750681.52	2.76842323	8.7931E-06
LVLASIDQADFQGFTYVNPDFVHPDAR	KPCG	119358003	34747156.5	1.78032847	8.6122E-05
DVVLMDDDVECTMVEK	KPCT	33955244.7	3786334.84	3.16476053	0.02319497
YFAQEALTVLSLA	2AAA	60900968.3	17238564.7	1.82082551	7.5425E-05
FFEEPEDPSSR	2ABD	13957147.7	3499596.63	1.99574359	0.00284384
INLWHLAITDR	2ABG	7969074.15	1967713.85	2.01789169	7.9454E-05
EAPVPRPTPQVAASGGQS	2A5B	5852125.35	1087748.13	2.42761614	0.00019822
ELFEGAVR	REM2	30209737.4	13006994.4	1.21572601	0.00392079
YVDEAHQYILEFDGGSR	RYR2	11191113.9	2322597.47	2.26854259	7.9859E-05
EINDLAESGAR	RYR3	161878090	1147912.95	7.13975068	8.677E-05
ESALILLQTVPK	ZNT1	4402207.23	1475242.63	1.5772748	0.01102076
SLFTEPSEPLPEEPK	ZNT3	33314252.1	4630270.12	2.84697124	8.3469E-05
LTELLESDPSVR	ZNT9	4013997.57	744806.691	2.43010181	0.06512629
LLTNLGLGEIK	S39AA	8379085.3	1143707.33	2.87307485	0.00157128
NTLNPYYNESFSFEVPFEQIQK	SYT1	126552581	15797161.5	3.00199967	8.6181E-05
VPMNTVDLGQPIEEWR	SYT2	16821234.5	2471263.78	2.76696267	0.00022299
YDYESETLIVR	SYT6	12489316.5	2271135.4	2.4592089	4.5682E-05
IYLLPDKK	SYT7	5776414.96	764432.873	2.91771266	2.751E-05
GELQVSLSYQPVAQR	SYT11	5802165.07	1491297.49	1.96002326	0.003395
VSLLPDEQIVGISR	SYT12	45324978.2	7494428.56	2.59641594	2.6405E-05
TGSVEAQTALK	SYT13	17223089.9	3194783.8	2.43055378	0.00041057
QLLQTDVSQGSDPFVK	SYT17	7371700.44	2053695.22	1.84377535	0.00040559

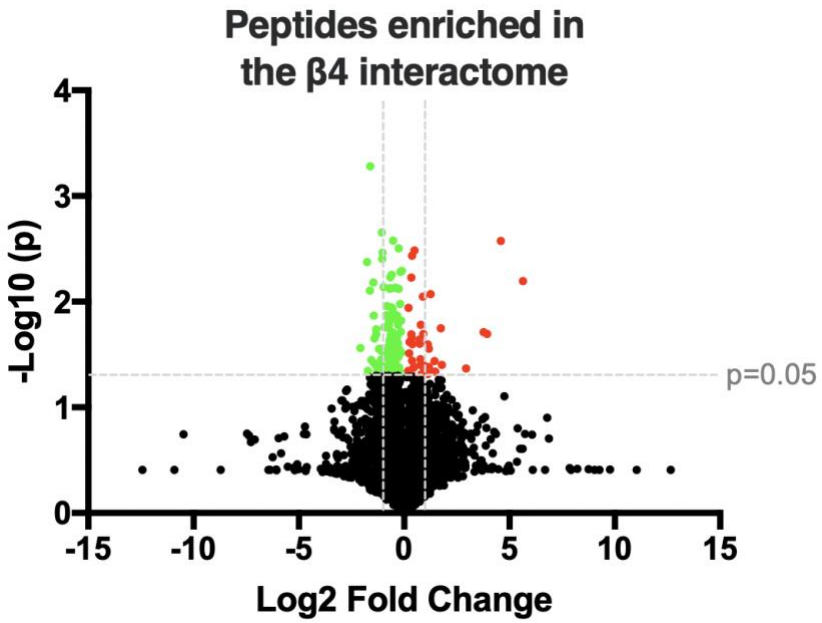

Figure 4.2: Sex differences in the β4 interactome of male relative to female P84 mice

Volcano plot showing 13023 β4-IP enriched peptides that make up the β4 interactome. Significantly enriched peptides with $p<0.05$ are represented either in green (enriched in females) or red (enriched in males). Grey vertical lines (*L*-*R*) located at log2fold change = -1, 1.

Table 4.2: Top significantly enriched peptides in males and in females

Top 18 significantly enriched peptides in males (with log2 fold change>1) and top 24 significantly enriched peptides in females (with log2 fold change<-1). TMATAALAASPAPVSNLQGPYLASGDQPLDR (bolded, italicized) is the primary peptide of interest in these results; this peptide is significantly enriched in the β4 interactome of male relative to female P84 wildtype mice and is contained in the b isoform of the β1b subunit of voltage-gated calcium channels. MAPs (MAP, MTAP; gray boxes) were found among significantly enriched peptides in both male and female lists. Note: murine MAP2 is known as MTAP2.

Peptide	Protein ID	Males Mean	Females Mean	Log2(M)-Log2(F)	p value
FELDTSER	RPN2	17401939.44	349755.8101	5.636756269	0.006358425
TGQPMINLYTDRETGK	FUS	13520868.06	559677.5072	4.594448199	0.002652508
VHLLNAHGLDEAGIDGGGIFR	UBE3C	282880322.8	18484610.09	3.935795309	0.02015541
TMATAALAASPAPVSNLQGPYLASGDQPLDR	CACNB1	4884346.69	355368.8162	3.780776611	0.019350387
ILYIVASDPYSR	HECD1	20640603.37	2693062.309	2.93816563	0.042811489
NGALVNAATAGAQETPLHLVALYSPK	ANFY1	7234761.889	2096272.145	1.787119511	0.039509179
QGLYDRLPPLPVTPGMEGAGVVVAVGEGVGDR	VAT1	1062620.533	315923.6389	1.7499787	0.0178449
VINEPGETEVFMTPQDFVR	MICU1	3799856.889	1361356.38	1.480900295	0.045872859
TPVVQNAASIVQPSPAHVGQQGLSK	P66B	5652815.158	2084359.292	1.439365539	0.036511712
GASSPGILVLTTGLSKPFMR	ARHG7	2969081.438	1241885.049	1.257485023	0.008477129
DYENDEDVNKQLDR	TPPC3	5551099.769	2449276.983	1.180417689	0.041564587
FLSHWDHITR	ECHM	21489877.88	9563472.165	1.168050874	0.027862187
LACGVIGIAQ	SODC	4510940.556	2018943.97	1.159827402	0.042460054
EATTLANGVLASLNLPAAIEDVSGDTVPQSILTK	PDC6I	4808749.769	2192425.326	1.13313415	0.048283119
GPMQLSADARDPEGAGGAGVLAAGK	MAP6	18363830.98	8404465.714	1.127639046	0.025420789
LQEAQVYKEEGNQR	TTC9C	4911194.58	2331085.791	1.075071882	0.041599862
SIIKEPESAAEAVK	CLPX	70453242.07	33510104.26	1.072069922	0.041860253
VPFIHVGNQVVSELGPIVQFVK	MTX2	14428766.34	6950099.022	1.053842517	0.042402935
LEMIAMENPADLKK	UBE3A	3354021.769	10282195.99	-1.61618446	0.000523819
LEDLSYLDGQR	TANC1	1910563.607	3974743.218	-1.05686337	0.002215196
DELHIVEAEAMNYEGSPIK	NPM	4533402.707	9259790.565	-1.03038524	0.003422214
RLATLLGLQAPPTR	EIF3A	8121564.811	16655515.96	-1.03617042	0.003928781
TNADTDGMVK	DLDH	2429127.93	8237318.07	-1.76173623	0.004218089
LHLVESLLNR	ECM29	1562611.761	4307106.636	-1.46275966	0.006566793
HAYSFHQSSEEAGDFLAHADLQR	BTBDH	5824908.639	17973288.27	-1.62554705	0.007873933
TNLIVNYLPQNMTQEELK	ELAV2	1566101.661	4246855.861	-1.43921728	0.013501626

Table 4.2 continued

QDSFPISLEQAVTDAAMTSK	MTAP2	2779823.82	6947918.478	-1.32158738	0.018285735
HNELTGDNVGPLILK	CISD2	13911646.83	34711770.64	-1.31913175	0.020294739
GIPILVGLLDHPK	CTND1	2073947.694	5517484.399	-1.41163114	0.022381052
EAAPDTGAEPSPEDSDPTYSSK	CCAR2	579773.3555	2453604.538	-2.0813418	0.027507595
GSPFPEVAESVQQELESYR	SCFD1	1358195.251	3000238.788	-1.14338644	0.02794903
LQDSSDPDTGSEEEVSSR	ARHG2	615075.9061	1412983.668	-1.19990842	0.027977123
EIMAEDDQVFLMK	DC1L1	5251474.805	10942854.08	-1.05919452	0.029420905
SQQQDDIEELETK	WNK1	1924512.332	4119010.216	-1.09780479	0.03544252
DWFIEMPTESK	MTAP2	939118.3796	2759898.79	-1.55523643	0.035565857
VTNIPQGMVTDQFGMIGLLTFIR	CNOT2	2671970.354	5816826.989	-1.12232839	0.037926659
DYFEQYGK	ROA1	6628176.335	17791406.45	-1.42449667	0.038063991
SIPQEAVQTLSSVR	TTC27	1394579.898	3677389.437	-1.39885138	0.039147056
QPGTSLVDADTFHHQVR	EMD	4233512.137	9560070.331	-1.17516621	0.044448088
RGFASMFSNR	ACO11	592793.6206	1949827.01	-1.71774431	0.045279178
AELEEMEEVHPSDEEEEETKAESFYQK	MAP1A	6847245.177	16824421.08	-1.29696129	0.045925857
DLDELSRYPEDK	MATR3	3679785.205	7465310.481	-1.02058071	0.048815324

4.4 Discussion

We set out to identify potential sex differences in the β4 interactome of mouse brain using CoIP-MS and a pan-β4 antibody previously used for β4 CoIP-MS with triton x-100 in mouse cortex (Klemmer et al., 2009). Our study is the first to date to specifically compare the β4 interactome of male to that of female mice. We were primarily interested in sex differences in β4 interactome constituents, as well as the possibility that our data could provide insight about sex differences in subcellular localization, α1 binding, and β4 involvement in Ca^{2+} signaling pathways. The overarching goal of this study was for the data revealed herein to inform our previous finding that overexpressing β4 in the developing brain significantly reduces dendritic spine density in female but not male mice (Chapter 3). Curiously, the β1b VGCC subunit was contained within the

β4 interactome of male but not female mouse brain homogenate. Moreover, MAPs were represented both in the list of peptides most enriched in the β4 interactome of male mice and in the β4 interactome of female mice, differentially distributed in a sex-specific manner. MAPs are known to play critical roles in cytoskeletal remodeling, and the formation and morphology of dendrites and dendritic spines (Kapitein et al., 2011; Matus, 1990; McKinney et al., 2019; Peris et al., 2018; Shelton et al., 2015).

Peptides in the overall β4 interactome included expected VGCC subunits Cav2.1, Cav2.2, Cav2.3, and $\alpha_2\delta 1$, plus non-VGCC peptide/proteins previously predicted or reported to interact with the β subunit of VGCCs (Buraei & Yang, 2010; McEnery, Vance, et al., 1998; Scott et al., 1996). The auxiliarly γ VGCC subunit was not identified in the β4 interactome and this was not surprising since there is little evidence that neuronal γ subtypes (γ2-γ7) modulate VGCCs. Aptly known as transmembrane AMPA receptor regulatory subunits (TARPs), γ subtypes have instead been shown to regulate AMPA receptors (A. S. Kato et al., 2007; Klugbauer et al., 2000). We also did not identify Cav3 (T-type) low voltage-activated (LVA) α1 VGCC subunits in the β4 interactome, consistent with many previous reports revealing that β subunits are not required for proper function of LVA VGCCs (Perez-Reyes, 2003, 2006). The β4 interactome was characterized explicitly in an earlier study using similar methods described herein: proteomics to analyze β4 immunoprecipitates. This study identified seven peptide/proteins in the synaptic β4 interactome: Cav2.3, the $\alpha_2\delta$ VGCC subunit, Matrin-3, Tubulin β4, Tubulin α6, Actin α, and β4 itself. We similarly identified Cav2.3, the $\alpha_2\delta$ VGCC subunit, and β4 in our study, consistent with separate previous reports (Buraei & Yang, 2010, 2013) as well as Matrin-3 (Klemmer et al., 2009). However, we did not identify Tubulin β4, Tubulin α6, or Actin α in the β4 interactome of male and female mouse homogenate. Although our study and the previous study employed very similar

methods (including the use of Triton x-100, the same pan-β4 antibody, and proteomics to analyze β4 immunoprecipitate), our methods were not identical. The previous assessment characterized the β4 interactome of synaptosome samples from mouse cortex (presumably from 1 male mouse), whereas we describe the β4 interactome in male and female mouse brain homogenates. The previous study's authors discussed the possibility that Tubulin β4 and Tubulin α6 were contaminants in their data (Klemmer et al., 2009).

Eighteen peptides in the β4 interactome were significantly enriched in male mice, and twenty-four peptides in the β4 interactome were significantly enriched in female mice. The most intriguing peptide in these two lists was TMATAALAASPAPVSNLQGPYLASGDQPLDR, which was significantly enriched in the β4 interactome of male relative to female mice and is contained in the β1b isoform of the auxiliary VGCC subunit β1. β1b is considered the neuronal β1 isoform. β4 and β1b are both widely distributed β auxiliary VGCC subunits found in many different tissues, including the cerebral cortex in particular (Buraei & Yang, 2010; McEnery, Vance, et al., 1998; Pichler et al., 1997). Based on transcript level findings, overall β1b protein levels are not likely different in male versus female mice (Takahashi, Mitsuhiro, & Nagasu, 2004). The presence of β1b in the β4 interactome of male but not female mice strongly implies that β4 and β1b are proximally located within single subcellular compartments in male mice. The dual presence of these two β subunits in close proximity, but not in direct contact, implies 1) potential competition among β4 and β1b to bind and regulate specific α1 VGCC subunits (and/or non-VGCC proteins) and 2) possible simultaneous regulation by β4 and β1b of separate proteins, both which are unique to males and could both have functional implications for calcium signaling at the level of single subcellular compartments. Dual presence of β4 and β1b is predicted to exclude axons because unlike β4, β1 has limited targeting to axons, at least in hippocampal cultured

neurons (Obermair et al., 2010), implying additionally that β1 probably also does not couple with $Ca_V2.1$ α1 VGCC subunits as β4 does as a general rule (Tanaka et al., 1995; Wittemann et al., 2000)(although see (Bogdanov et al., 2000)).

β subunits increase calcium currents of HVA VGCCs via four mechanisms: 1) trafficking α1 VGCC subunits to the plasma membrane, 2) facilitating their proper folding, 3) hyperpolarizing the voltage-dependence of activation of α1 VGCC subunits and 4) by increasing the maximum opening probability of α1 VGCC subunits (Dolphin, 2012). β4 and β1b likely perform redundant roles in these four processes. β subunits also promote voltage-dependent inactivation (VDI) which decreases Ca^{2+} influx after depolarization and reduces the number of channels available for activation during subsequent depolarizations (Buraei & Yang, 2010). Competitive replacement of β4 by β1b at $Ca_V2.2$ would result in no change in the rate of "closed-state" VDI (Buraei & Yang, 2010; Patil et al., 1998; T. Yasuda et al., 2004). β subunits are required for voltage-dependent Gβγ inhibition of Ca_V2 channels. This has been studied in great detail in $Ca_V2.2$ channels. Following Gβγ inhibition of $Ca_V2.2$, depolarization relieves the channel from inhibition and β1b would accelerate voltage-dependent dissociation of Gβγ from $Ca_V2.2$. However, β1b acceleration of Gβγ dissociation is not as effective as β4 acceleration of Gβγ dissociation (Feng, Arnot, Doering, & Zamponi, 2001). Thus, since β1b promotes voltage-dependent Gβγ inhibition less effectively than β4 at $Ca_V2.2$ (Buraei & Yang, 2010; Giovanni Gonzalez-Gutierrez et al., 2008) overall, β1b replacement could conceivably lead to decreased Ca^{2+} influx through β1b paired $Ca_V2.2$ VGCCs undergoing voltage-dependent Gβγ inhibition over time. If a modest decrease in VGCC Ca^{2+} influx is sufficient to impact activity-dependent cytoskeletal remodeling, β1b displacement of β4 bound to $Ca_V2.2$ could remove the breaks enough on Gβγ inhibition to mitigate spine loss. Neither β4 nor

β1b has been shown to significantly impact calcium-dependent facilitation of HVA VGCCs (Chaudhuri, Alseikhan, Chang, Soong, & Yue, 2005; Lee, Scheuer, & Catterall, 2000).

If β4 is not competitively replaced by β1b, the latter could in theory bind to a nearby α1 VGCC subunit, where it would provide largely redundant regulation of the second VGCC channel (Buraei & Yang, 2010). One can imagine various complex combinations of β4 and β1b at VGCCs, carrying out various, potentially opposing roles within a shared microdomain. The addition of β1b as a regulator of a second VGCC could have a substantial impact on Ca^{2+} signaling if the predominant direction of regulation replicates the major direction of regulation provided by β4, for example if both β4 and β1b shift the voltage-dependence of channel activation to hyperpolarized voltages the net effect would be increased macroscopic Ca^{2+} current density. Ca^{2+} signaling in spines alter spine dynamics and morphology (Higley & Sabatini, 2012; H. Kasai et al., 2003; Yuste et al., 2000). Increased postsynaptic Ca^{2+} initiates Ca^{2+} signaling cascades in dendritic spines and is required for new synapse formation and dendritic spine assembly (Lohmann & Bonhoeffer, 2008; Lohmann, Myhr, & Wong, 2002; Yuste et al., 2000). On the other hand, if the actions of β1b bound to a nearby VGCC opposes the predominant direction of β4 mediated regulation, presence of β1b may counteract (although unlikely "cancel out") β4-mediated regulation of VGCC gating. This latter possibility is not likely to elicit a substantial impact on Ca^{2+} signaling overall.

Given that β4 and β1b appear to interact with largely the same non-VGCC proteins (Buraei & Yang, 2010), β1b the β4 interactome of male mice may potentially be primarily redundant in terms of interaction with non-VGCC proteins. So far, CaMKII appears to be the exception to this observation. CaMKII was recently shown to both coimmunoprecipitate and associate with β1b but not β4 (Abiria & Colbran, 2010; Grueter et al., 2008). Despite the fact that the physiological

consequence of CaMKII phosphorylation of β subunits has not been identified (Buraei & Yang, 2010), it is reasonable to predict that phosphorylated β1b acting within the β4 interactome of male mice could have significant consequences for signal transduction in neuronal subcompartments, including in dendrites (Ding, Kennedy, & Weinberg, 2013; Lisman, Schulman, & Cline, 2002; Schulman, 2004). Finally, although the presence of β1b in the β4 interactome does not specifically guarantee that the two proteins are directly interacting, we cannot rule out this possibility. Heterodimers comprising β3 and other β subunits, including β1b, have been previously reported (Lao, Kobrinsky, Liu, & Soldatov, 2010). Although β4 and β1b have not been shown to heterodimerize, this has not been specifically tested. If β4 and β1b do directly interact, the association is likely to take place at residues in the guanylate kinase subdomain of the membrane-associated guanylate kinase-like (MAGUK) domain of the β proteins (Lao et al., 2010). β homodimerization was recently implicated in the regulation of dynamin-mediated channel internalization (Gonzalez-Gutierrez et al., 2007; Miranda-Laferte et al., 2011). Potential functional consequences of β heterodimerization remain to be discovered.

Three neuronal MAPs were represented among the peptides significantly enriched in the β4 interactome of males and those significantly enriched in female mice. MAP6 was significantly enriched in males, and MAP2 and MAP1A were significantly enriched in females. The fact that MAPs are represented in *both* sexes seems to imply the existence of MAP signaling in close proximity to or potentially downstream from activity-dependent β4 regulation of VGCCs. β4 and all three MAPs localize to dendrites (Ferrándiz-Huertas et al., 2012; Matus, 1990). MAP6, MAP2, and MAP1A are each implicated in the development and morphology of dendrites and dendritic spines (Gu & Zheng, 2009; Kapitein et al., 2011; Matus, 1990; McKinney et al., 2019; Peris et al., 2018; Shelton et al., 2015; Szebenyi et al., 2005). β4 to MAP signaling may be mediated by two

kinases, CaMKII and MAPK, each of wich were previously demonstrated to associate with β4 and identified in the β4 interactome in the current study (Abiria & Colbran, 2010; Fitzgerald, 2000, 2002; Grueter et al., 2008). Finally, MAPK may significantly alter Ca^{2+} signaling leading to altered spine morphology through a MAP-independent mechanism, regulation of α1 VGCC subunit Ca^{2+} influx, which requires β subunits (Fitzgerald, 2002). MAPK/ERK signaling has been previously implicated in synapse formation and short-term homeostatic plasticity mechanisms (although, note this was via synapsin phosphorylation not direct regulation of α1 VGCC subunit Ca^{2+} influx) (Giachello et al., 2010). An overall model for how β4 overexpression might lead to loss of small spines in female but not male mice is outlined in and discussed in detail in the Chapter 5 of this dissertation.

5.0 General Discussion

5.1 Summary of Findings

This dissertation is a collection of three major studies: 1) a descriptive study of sex differences in dendritic spines in murine sensory cortex over adolescent neurodevelopment (Chapter 2), 2) an assessment of the impact of β4OE on dendritic spines of male and female P84 mice (Sz-related manipulation) (Chapter 3) and 3) a descriptive study of sex differences in the β4 interactome of P84 mouse brain homogenates (Chapter 4). We assessed sex differences in all three studies, at baseline and in the context of our Sz-related manipulation, since sex is an important biological factor and the clinical presentation and expression of psychiatric illnesses, including Sz, differs based on sex (Abel et al., 2010; McCarthy et al., 2012).

In Chapter 2 we characterized the dendritic spines of male and female wildtype mouse in sensory cortex (A1, A2, V1, V2, and TeA) over adolescent neurodevelopment. We assessed dendritic spine density and morphology of GFP positive pyramidal cells in layers 2-6. This study revealed distinctions in DSD based on laminar location of pyramidal cell soma, evidence of synaptic remodeling over adolescence, but no differences based on region within sensory cortex. Importantly, these results established a sex difference in DSD in male versus female mouse sensory cortex (Parker et al., 2020).

In Chapter 3 we assessed the impacts of overexpressing β4 on dendritic spines on L5 pyramidal cells in sensory cortex of male and female mice. β4OE significantly decreased DSD of female but not male mice. Estrous stage shapes dendritic spine dynamics in hippocampus of rat (A. Kato et al., 2013; Woolley et al., 1990; Woolley & McEwen, 1992). We therefore assessed the

impact of estrous stage on DSD of females in our study and concluded that estrous stage did not significantly mediate β4OE-mediated reduced small spines in L5 of sensory cortex consistent with two previous studies investigating spines in mouse cortex (Alexander et al., 2018; Boivin et al., 2018). Reduced DSD in female mice was driven by loss of the smallest spines, like observed in A1 in Sz (MacDonald et al., 2017; McKinney et al., 2019).

The experiments in Chapter 4 were performed in order to aid interpretation of the sex difference revealed in Chapter 3. We performed CoIP-MS to identify potential differences in the β4 interactome of male versus female wildtype mice. We detected both redundant proteins as well as unique proteins significantly enriched in the β4 interactomes of male versus female mice. Surprisingly, β1b was significantly enriched in the β4 interactome of male mice. In this discussion (see below), we propose that enrichment of β1b in the β4 interactome of male mice protects males from β4OE-mediated dendritic spines loss. We discuss potential roles for kinase activity of CaMKII and MAPK on MAPs and small spine loss in female β4OE mice. We additionally discuss a potential role for a MAPK in Ca^{2+} signaling independent from MAP phosphorylation, that could lead to the reduced formation of small spine density observed in female β4OE mice. Finally, we present an overall model to speculate how β4OE may significantly decrease small spine density in female but not male mice in the subsection below.

5.2 Overall Model for Volume- and Sex-Specific β4OE-Mediated Spine Loss

The two major unanswered questions after completing the experiments described in Chapter 3 were: why are spines in male mice resistant to the β4OE manipulation and what mechanism(s) could account for the volume- and sex-specific loss of spines in β4OE mice? We

thus assessed sex differences in the β4 interactome to generate hypotheses for these unanswered questions.

In Chapter 4 we demonstrated that β1b is significantly enriched in the β4 interactome of male mice and MAPs are distributed among the significantly enriched peptides in the β4 interactome of male and of female mice. Since β1b largely does not target to axons (Obermair et al., 2010) and we did not identify Ca_V1 α1 VGCC subunits in our study, we discussed the dual presence of β4 and β1b in somal and dendritic microdomains of neurons bound to Ca_V2 VGCCs (Tanaka et al., 1995; Wittemann et al., 2000). We considered four possible outcomes for presence of β1b in the β4 interactome of male mice, predicting that two of these could potentially lead to substantial changes in Ca^{2+} signaling: 1) competitive replacement of β1b of β4 bound at an α1 VGCC subunit and 2) complementary regulation of β4 and β1b, both bound to separate but nearby Ca_V2 VGCCs. Ca^{2+} signaling in dendritic spines alters spine dynamics and morphology (Higley & Sabatini, 2012; H. Kasai et al., 2003; Yuste et al., 2000). In particular, transient increased postsynaptic Ca^{2+} has been shown to initiate Ca^{2+} signaling cascades in dendritic spines and is required for new synapse formation and dendritic spine assembly (Lohmann & Bonhoeffer, 2008; Lohmann et al., 2002; Yuste et al., 2000). We also discussed the possibility that β1b and β4 heterodimerize (Lao et al., 2010). Since β binding of α1 VGCC subunits is preferential and the affinity of β subunits for α1 VGCC subunits is high, β4-β1b heterodimerization does not actually seem likely in wildtype mice (Dolphin, 2012, 2016).

In addition to identifying β1b in the β4 interactome of male mice, we observed four MAP peptides (3 MAPs) among those significantly enriched in the male and female β4 interactomes. MAP6 was significantly enriched in the β4 interactome of male mice whereas MAP2 and MAP1A were significantly enriched in females. Presence of MAPs in the β4 interactome of both sexes of

mice, in combination with reports implicating neuronal MAPs in cytoskeletal remodeling, and the formation and morphology of dendrites and dendritic spines (Gu & Zheng, 2009; Kapitein et al., 2011; Matus, 1990; McKinney et al., 2019; Peris et al., 2018; Shelton et al., 2015; Szebenyi et al., 2005), plus our finding in that β4OE significantly reduced spine density in female mice (Chapter 3) suggest β4 signaling may occur upstream from MAP-mediated cytoskeletal remodeling in mice. Recent evidence for proposed roles for MAPs in dendrite and dendritic spine remodeling implicate two potential pathways connecting β4-mediated VGCC Ca^{2+} signaling to MAP regulation of cytoskeletal dynamics of spines.

In our proposed Pathway 1 MAP6 mediates stability of mature dendritic spines following CaMKII phosphorylation of MAP6 (Baratier et al., 2006). MAP6 was recently shown to mediate activity-dependent stabilization of f-actin in PSD-95 containing spines (Peris et al., 2018). Moreover, density and maintenance of mature spines was significantly impaired following siRNA MAP6 depletion and in cortical neurons of MAP6 knockout mice (Peris et al., 2018). Interestingly, MAP6 knockout mice have been previously used to model cognitive and synaptic deficits in Sz (Andrieux et al., 2002; Delotterie et al., 2010). In our proposed Pathway 2, MAP2 signals to impact dendritic spine morphology. MAP2 regulates dendritic development and plasticity in an activity-dependent manner (Fontaine-Lenoir et al., 2006; Poplawski et al., 2012) and has been shown to bundle f-actin (Roger et al., 2004; Selden & Pollard, 1983). Our lab has shown in previous studies that MAP2 immunoreactivity (MAP2-IR) is significantly reduced in Sz in various brain regions, including in A1, where spine loss is driven by loss of the smallest spines (DeGiosio et al., 2019; McKinney et al., 2019). MAP2-IR positively correlated with DSD in A1 in Sz, suggesting a role for MAP2 in formation or maintenance of small spines, at least in the context of pathology (Grubisha et al., 2019). MAP2-IR but not MAP2 protein levels is significantly reduced in Sz,

raising the possibility that reduced small spine density in Sz could represent a downstream effect of altered phosphorylation status of MAP2 (DeGiosio et al., 2019; Grubisha et al., 2019; McKinney et al., 2019). In our proposed Pathway 3, Ca^{2+} current is upregulated via β subunit-requisite MAPK-dependent channel modulation. Altered Ca^{2+} current signals down to intracellular pathways that alter spine morphology.

We established in Chapter 3 that small-volume spines ($<0.3\mu m^3$) made up the majority (68.96%) of all spines observed in adult CN and β4OE mice. *In vivo* imaging of spine dynamics demonstrate spines are partitioned in two categories based on synapse maturity: 1) "immature" spines that lack PSD-95 and are highly dynamic and rarely stabilized and 2) "mature" spines with established excitatory synapses and PSD-95. Among all spines in adult animals, 20% are immature and 70-80% mature (Berry & Nedivi, 2017; Cane et al., 2014; Holtmaat et al., 2005; Trachtenberg et al., 2002; Villa et al., 2016). Assuming that all immature spines in experiments described in Chapter 3 are small, up to 48.96% of the small spines we observed are presumed to be small *and* mature. Thus, we proposed that β4OE decreases density of small spines, including both new immature spines and mature small spines (Figure 3.5A).

Here we propose in an overall model whereby in male and female C57Bl/6J mice, post-synaptic β4 VGCC-mediated Ca^{2+} entry leads to the stability of mature spines (some of which are small) via MAP6 signaling in spines (Pathway 1). Post-synaptic β4 VGCC-mediated Ca^{2+} entry also leads to remodeling of small, including presumably immature spines through MAP2 regulation of postsynaptic cytoskeletal dynamics in male and female wildtype mice (Pathway 2). Finally, normal β4 protein levels facilitate MAPK-modulation of Ca^{2+} currents, which may be associated with spine formation (Pathway 3) (Figure 5.1A). In female β4OE mice, overexpressed β4 disrupts Ca^{2+} signaling, reducing DSD of spines of small volumes, mirroring small spine loss

observed in A1 in Sz (MacDonald et al., 2017; McKinney et al., 2019). How this is achieved in unclear. One possibility is that β4OE-mediated Ca^{2+} signaling may fail to give rise to CaMKII phosphorylation of MAP6, leading to destabilization and potential collapse of mature small spines (Pathway 1). CaMKII was previously demonstrated to interact with β4 (Grueter et al., 2008) (although see (Abiria & Colbran, 2010)) and was specifically identified in the β4 interactome of male and female mice in our study. In addition, soluble β4 may recruit proteins in the pathway of the serine/threonine-specific protein kinase MAPK, a known interactor of β4 (Fitzgerald, 2000, 2002), which was identified in the β4 interactome of male and female mice in our study. MAP2 is a substrate of and has been previously shown to be phosphorylated by MAPK, which resulted in impairment in the ability of MAP2 to polymerize tubulin (Hoshi et al., 1992). MAP2 has been shown to bundle f-actin (Roger et al., 2004; Selden & Pollard, 1983). MAPK phosphorylation of MAP2 is predicted to similarly impair MAP2-mediated regulation of actin and or microtubule cytoskeletal dynamics in dendrites and lead to spine loss, including small spines, mirroring MAP2-mediated spine loss in A1 in Sz (Pathway 2) (Grubisha et al., 2019; McKinney et al., 2019). Finally, β4OE could dysregulate MAPK-mediated upregulation of Ca^{2+} current density and fail to form new spines (Pathway 3) (Figure 5.1B).

In male β4OE mice, animals that are protected from β4OE-mediated small spine loss, β4OE inhibition of Pathway 1 and/or disruption of Pathway 2 and/or Pathway 3 is blocked by β1b, which is poised in the β4 interactome of male mice to mediate the effects of or compensate for dysregulation of β subunits. Either β1b binds directly to soluble β4, sequestering it (simplest explanation) and therefore protecting male spines from the β4OE manipulation, or β1b counteracts the effects of β4OE by providing a compensatory effect on Ca^{2+} signaling coupled to spine remodeling without directly associating with overexpressed β4, potentially as a result of α1-β

reshuffling. Presence of β1b in the β4 interactome does not guarantee that the two proteins directly interact. However, β subunits have been previously reported to heterodimerize, including β1b specifically (Lao et al., 2010). Although β4 and β1b have not yet been shown to heterodimerize, and oligomerization of these β subunits is unlikely in the presence of an α1 VGCC subunit, heterodimerization of soluble β4 to unbound β1b is within the realm of possibility in the context of β4OE due to higher-than-normal β4 levels. If soluble β4 and β1b form heterodimers in males, the two β subunits are likely to associate at residues in the guanylate kinase subdomain of the membrane-associated guanylate kinase-like (MAGUK) domain of the β proteins (Lao et al., 2010)(Figure 5.1C).

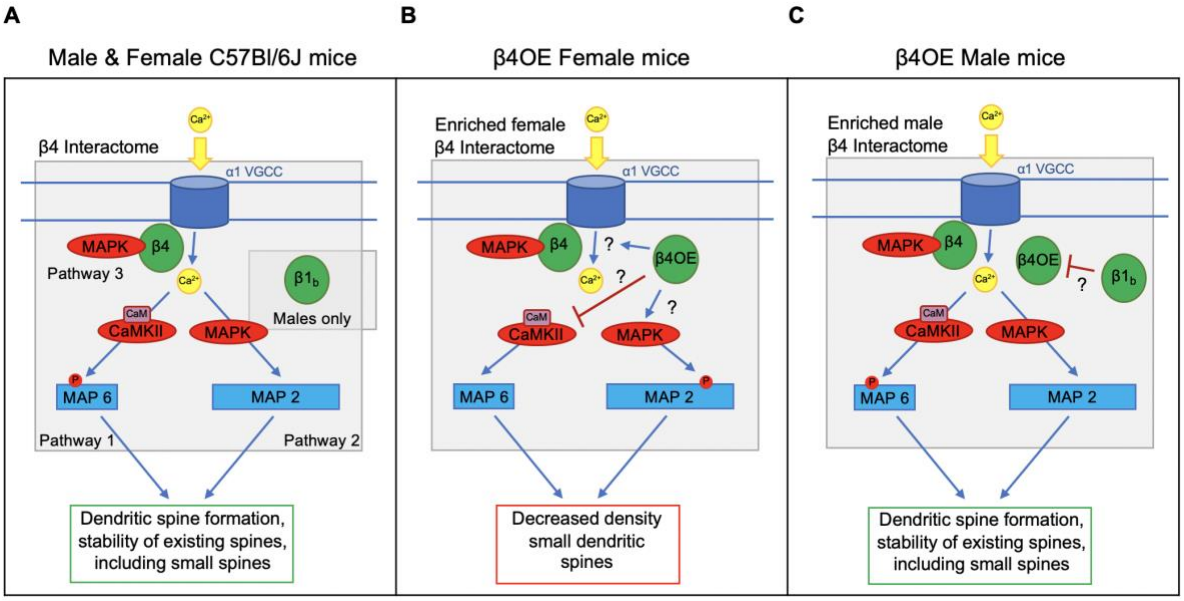

Figure 5.1: Proposed overall model to account for volume- and sex-specific loss of spines in β4OE mice

(A) In male and female wildtype mice, β4-mediated activity-dependent VGCC Ca^{2+} signaling increases intracellular Ca^{2+} and leads to dendritic spine formation and stability of existing spines via three proposed cell-autonomous MAP and/or MAPK pathways. In Pathway 1, mature spines, some of which are presumably small, are stabilized as a result of activity-dependent MAP6 signaling in spines. In Pathway 2, small spines, including those that are immature, are formed or stabilized as a result of activity-dependent MAP2 signaling. In Pathway 3, new spines are formed due to MAPK-dependent upregulation of channel current. (B) In β4OE female mice, β4OE disrupts postsynaptic Ca^{2+} signaling and leads to small spine loss potentially via β4OE inhibition of CaMKII phosphorylation of MAP6 (Pathway 1) and/or β4OE activation of the MAPK phosphorylation of MAP2 (Pathway 2) and/or β4OE-mediated dysregulation of MAPK-dependent Ca^{2+} current upregulation, reducing spine formation (Pathway 3). (C) In β4OE male mice, β1b is proposed to heterodimerize with soluble β4 and sequester it, preventing MAPK activation and inhibition of CaMKII signaling, or recover MAPK-mediated Ca^{2+} influx, potentially via β subunit reshuffling, resulting in protection from β4OE-mediated small spine loss downstream.

5.3 Relevance to Feinberg Hypothesis of Sz Pathogenesis

Sz onset typically occurs during late adolescence/early adulthood, concomitant with a period of substantial circuit rewiring and synapse remodeling in neurodevelopment (A. Wong & H. Van Tol, 2003). In 1982 Irwin Feinberg proposed a theory for Sz pathogenesis in order to account for Sz emerging during adolescence in some cases following a childhood characterized by premorbid neurodevelopmental abnormalities (e.g. impaired cognitive functioning) and in other cases following seemingly intact childhood neurodevelopment (Feinberg, 1983; Keshavan et al., 1994). This theory has now been come to be known as the "overpruning" hypothesis of Sz. According to this hypothesis, Sz results from increased elimination of mature synapses during adolescence in brain regions involved in cognitive development (Feinberg, 1983; Keshavan et al., 1994). Others later suggested refinements to this model, proposing for example that axon collaterals are hyper-pruned in prefrontal cortex of individuals with Sz (Keshavan et al., 1994). In the 1990s and 2000s, a number of influential magnetic resonance imaging and postmortem studies demonstrated progressive cortical gray matter reductions and significantly reduced DSD in frontal and temporal cortices of Sz subjects (Moyer, Shelton, et al., 2015; Vita et al., 2012). For some time, Feinberg's theory was used in conjunction with the studies reporting gray matter and synapse reductions reported in Sz adults to explain Sz pathogenesis.

Our group recently demonstrated that reduced DSD in deep layer 3 of A1 in Sz is selective for and driven by loss of the spines with the smallest volumes (MacDonald et al., 2017; McKinney et al., 2019). Since spines of the smallest volumes were significantly lost, our group suggested a rethinking of the Feinberg hypothesis on the grounds that genetic studies implicate spine formation and stabilization in Sz risk and new or transient dendritic spines are small and mature or stable spines large (Holtmaat et al., 2005; Knott & Holtmaat, 2008; Purcell et al., 2014; Schizophrenia

Working Group of the Psychiatric Genomics Consortium, 2014). DSD of small but not large spine objects was negatively correlated with levels of the tryptic peptide ALFDFLK, which is found in the β subunit of VGCCs (MacDonald et al., 2017). β4 was then nominated as a protein that could potentially drive small spine loss and β4OE demonstrated to significantly reduce small spines in primary cortical neuronal culture (MacDonald et al., 2017).

β4OE similarly significantly decreased small spine density of L5 pyramidal cells in sensory cortex of female mice (Chapter 3). Small <0.3μm^3 volume spines comprised 68.96% of all spines observed in adult (P84) CN and β4OE mice. We propose in Chapter 3 and reiterate in this discussion that both immature *and* mature dendritic spines were lost as a consequence of the β4OE manipulation. Since small spines were significantly reduced in A1 in normal murine adolescent development (unpublished data), we developed the hypothesis that small spine loss observed in female P84 β4OE mice could be due to the combined loss of reduced mature small spines, due to excessive reduced net spine number during adolescence plus reduced immature small DSD due to failed spine addition or stability during adulthood. β4OE-mediated small spine loss is a model for the small spine loss observed in A1 in Sz. If the spine dynamics mechanisms proposed to lead to small spine loss in β4OE mice translate to small spine loss observed in A1 in Sz, this could mean that decreased number of small mature spines are eliminated, excessively, during programmed synapse remodeling in adolescence in addition to failure of immature small spines to form or stabilize in adulthood of Sz subjects. Moreover, if our findings translate to A1 in Sz, our data support both the important argument for the possibility for new small spines loss in A1 in Sz and the classic explanation of excess mature spines elimination during adolescence in Sz, as was first proposed by Irwin Feinberg in 1982 (Feinberg, 1983; Keshavan et al., 1994).

5.4 Limitations and Considerations

All of the experiments described herein were carefully designed and executed with strong scientific promise. Despite this, we consider several overarching limitations of our studies that warrant discussion.

First, the dendritic spine studies described in Chapter 2 and Chapter 3 of this document evaluated dendritic spine morphology and density in mice, postmortem. The methods employed to harvest and preserve mouse brain tissue were careful to avoid disrupting neuron and spine morphology and were largely based on those developed in and honed for many years by the of laboratory of collaborator David Lewis, MD, who has been evaluating dendritic spines in postmortem tissues for now over three decades (Glantz & Lewis, 2000; Glausier & Lewis, 2013). For example, mice were euthanized with Nembutal, rather than Isoflurane, which has been shown to impact spine density (Lemkuil et al., 2011; Platholi, Herold, Hemmings Jr, & Halpain, 2014), fixed with ice-cold PBS followed by 4% PFA, a preferred method for preserving neuronal cytoarchitecture in rodents, and carefully stored in cryoprotectant prior to cryostat sectioning. We should note that it is possible that the procedures we employed, although designed to preserve dendritic spines, could have altered spine morphology or size. Mouse brain tissue was harvested and preserved identically in all mice, regardless of group in each study, as carefully and swiftly as possible in order to mitigate risk of altered spine morphology during tissue harvesting and preparation. Spine morphology of new small spines in particular has been demonstrated to rapidly change via activity-dependent and activity-independent mechanisms (Rochefort & Konnerth, 2012), changes that our assessments are not equipped to capture. Finally, since spines were assessed in mice after death, it was clearly not possible for us evaluate spine dynamics or spine lifetime transience/persistence in mice in our studies, therefore, our prediction that small spines in

β4OE mice could be due to faulty spine addition, and/or stabilization of immature spines on a background of excessively eliminated mature spines during adolescence (Figure 3.5B) is purely speculative. Longitudinal *in vivo* imaging of spine dynamics over the murine life course is required to specifically test this hypothesis.

Moreover, the mouse model of small spine loss we developed for use in Chapter 3, and all other animal models of psychiatric illness are limited due to the fact that psychiatric illness is distinctively human. Sz is particularly difficult to model using non-human animals due to the fact that in most cases of Sz is proposed to result from polygenic inheritance interacting with a non-genetic environmental insult (Insel, 2010; Purcell et al., 2014). Symptoms and associated deficits in Sz are still incompletely understood. Additionally, prefrontal cortical neuroanatomy and executive functions are unique to humans (Insel, 2010). Unlike prefrontal cortex, A1, and V1 in what we refer to as sensory cortex, and regions in the ascending sensory pathways do have comparatively similar neuroanatomy in mice and humans. With that said, the β4OE manipulation is specifically utilized herein to model a single anatomical phenotype of Sz, small dendritic spine loss in A1. It does not attempt to model Sz. β4OE is achieved via viral mediated gene delivery to the cortex of neonate mice. This approach provides spatial and temporal control over genetic change, focusing on a single anatomical phenotype, but it does not have the ability to model or capture the complexity of the etiology of Sz (Nestler & Hyman, 2010).

Given dendritic spines are necessary for signal processing, spine loss could contribute to Sz symptoms and associated deficits, including, most notably in the case of spine loss in deep layer 3 of A1 in Sz, impairment in auditory tone discrimination (Javitt & Sweet, 2015). It is unclear if β4OE mice would exhibit deficits on auditory tone discrimination or modified MMN tasks. Such follow-up studies are appealing however because if such deficits are detected in β4OE mice, this

would increase face validity of this model (Chadman, Yang, & Crawley, 2009). Substantial fine-tuning of the degree of β4OE in A1 would need to be performed before β4OE mice are ready for auditory behavioral assessment. β4OE in the mice generated for the experiments in Chapter 3 is sparse by design. Increasing the viral load delivered neonatal mice cortex using the BREVI method described in Chapter 2 and Chapter 3 or developing a classic transgenic mouse are two potential strategies whereby β4OE mice may be made and utilized for auditory behavioral testing.

Finally, although sex differences in the clinical presentation, incidence, and illness course in Sz (Abel et al., 2010; Aleman et al., 2003), small spines are significantly decreased in A1 in Sz in both sexes (McKinney et al., 2019). β4OE did not significantly reduce small spine density in male mice, which is a major limitation of the β4OE model for the intermediate phenotype of small spine loss in Sz. The data generated in Chapter 4 provided evidence for possible compensation for β4OE by β1b in male mice. Rather than focusing on the fact that β4OE does not significantly reduce small spines in male mice as a limitation of the model, given that male β4OE are *protected* against β4OE-mediated spine loss, these mice can be used to understand relationships between susceptibility and spine morphology/dynamics in the spine intermediate phenotype of Sz. Further, information gathered from future studies comparing spine dynamics in female and male β4OE mice might be used to develop pharmacological strategies that have high target validity, for mitigating spine loss in Sz.

5.5 Final Conclusions

In summation, this dissertation comprises a descriptive study of sex differences in dendritic spines in sensory cortex over neurodevelopment (Chapter 2), an assessment of the impact of β4OE

on dendritic spines of male and female P84 mice (Sz-related manipulation) (Chapter 3) and a final descriptive study of sex differences in the β4 interactome in P84 mouse brain homogenates (Chapter 4). We deliberately assessed sex differences at baseline and in the context of our Sz-related manipulation since sex is an important biological factor and the clinical presentation and expression of psychiatric illnesses, including Sz, differ based on sex (Abel et al., 2010; McCarthy et al., 2012). Overall our findings provide insight about dendritic spines and β4 at baseline and provide a model for the intermediate phenotype of small spine loss in Sz. Surprisingly, our data revealed that our Sz-related manipulation, β4OE, reduced spines in both volume- *and* sex-specific manners. We interpret our findings in β4OE mice to suggest spine loss includes immature small and mature small spines. If these data translate to Sz, our data supports both our group's previous suggestion to rethink the Feinberg hypothesis, but it also cannot refute the possibility that small mature spines are eliminated in Sz during adolescence, as Feinberg predicted. The data we collected in the experiment detailed in Chapter 4, particularly the discovery of enriched β1b in the β4 interactome of male mice shed light on our major unanswered questions posed in the discussion of Chapter 3. β1b is predicted to confer protection for males from the effects of β4OE. Finally, we detail three pathways through which β4OE could reduce small spine density in females. These proposed pathways nominate MAPs, CaMKII and MAPK in β4-related spine alterations, which future studies should interrogate. We strongly urge other groups to follow in our footsteps and evaluate male and females at baseline and in Sz-related manipulation studies. Finally, we hope the hypotheses generated by the data collected herein may be used for future studies interrogating dendritic spine pathologies in psychiatric illness.

Appendix A

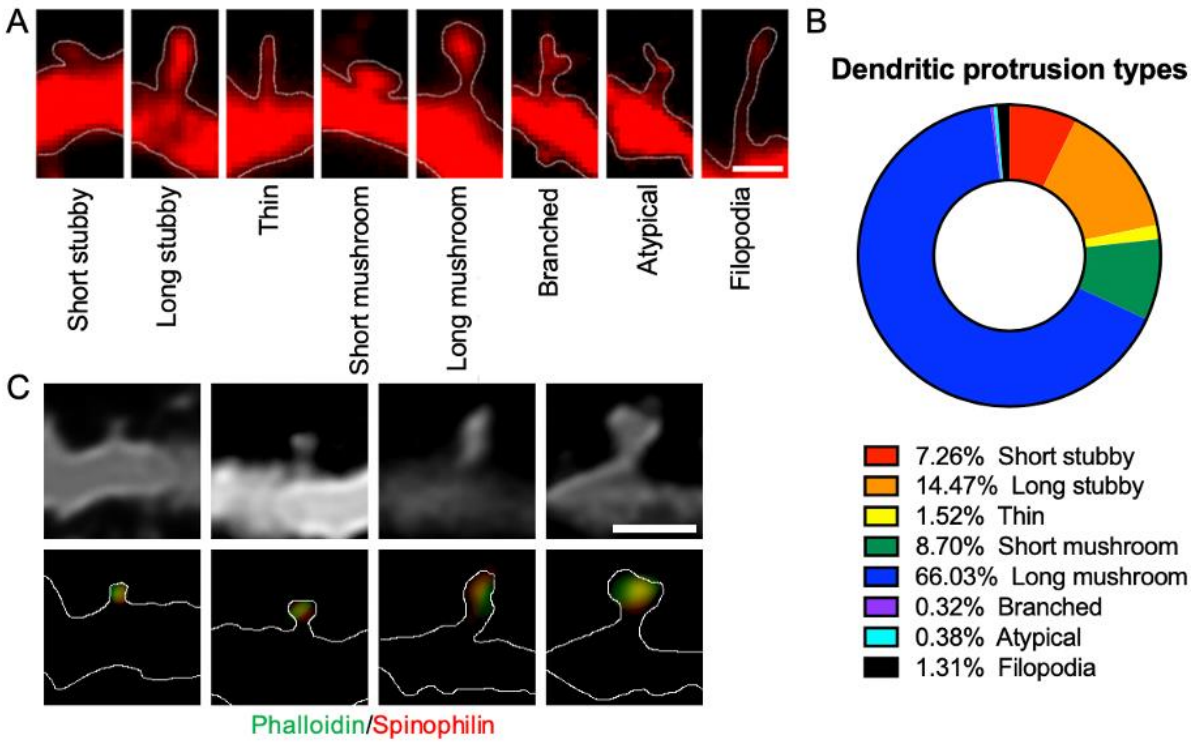

Appendix A Figure 1: Dendritic Protrusions

(A) Depictions of each dendritic protrusion type. Scalebar = 1μm. (B) All dendritic protrusions (n = 6241) were classified into 1 of the 8 morphological types shown in A. (C) GFP filled dendrite (shown in white) from pyramidal cell in mouse cortex. Immunohistochemical strategy used in our previously published study (Moyer, Erickson, et al., 2015), which utilized phalloidin and spinophilin co-localization to identify putative spine objects, identifies GFP-filled spines in the tissue used in the current study. Scalebar = 1μm.

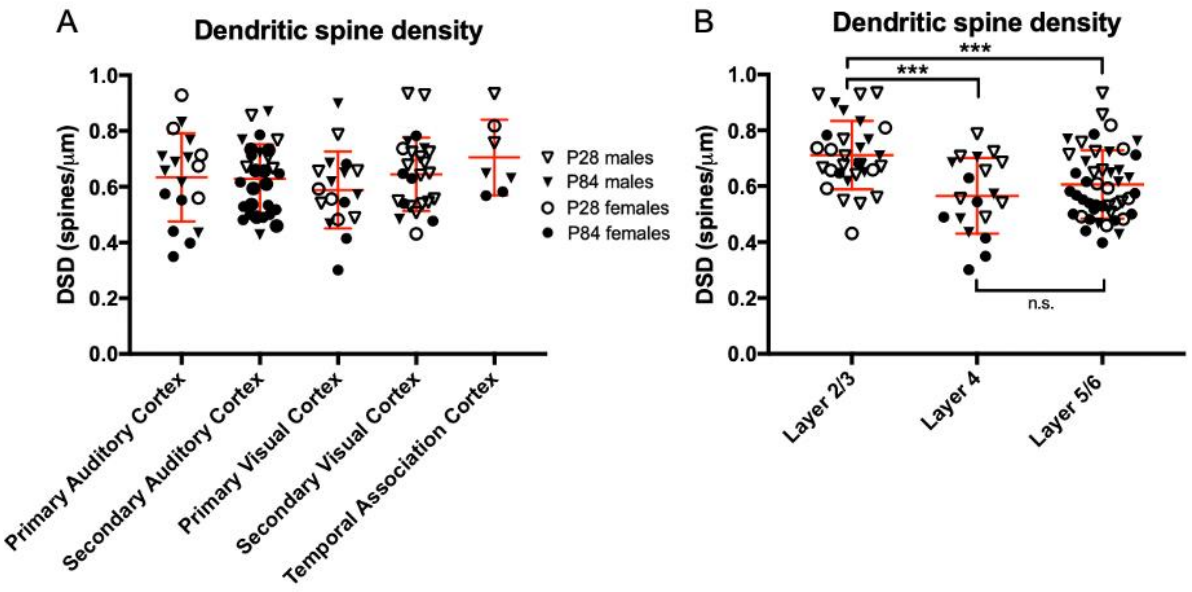

Appendix A Figure 2: Regional and laminar DSD

(A) DSD is not significantly different across primary auditory, secondary auditory, primary visual, secondary visual and temporal association cortices ($F=1.829$, $DF=4$, $p=0.131$), with no significant region by sex nor region by age interactions. Mean DSD and SD represented by red lines. (B) DSD is significantly increased in L2/3 compared to in L4 ($p<0.001$) and to in L5/6 ($p<0.001$). DSD in L4 and L5/6 are not significantly different ($p=0.707$).

Appendix B

Appendix B.1 Methods

Appendix B.1.1 Western Blot: β4OE verification

Two P0 C57BL/6J mouse pups were exposed to AAV using the BREVI method (see Chapter 3 Methods for details). One pup was exposed to AAV2-CaMKII-B4-eGFP-WPRE and the second injected with control GFP virus. On P21 these two female mice plus one injection naïve female C57BL/6J were anesthetized with Nembutol (150mg/kg) and transcardially perfused with ice-cold normal saline. Brains were extracted and rapidly frozen. Bilateral cortical tissue from each brain was separated from the cerebellum and cortex anterior to A1. This tissue was then combined with ice-cold Tris-HCl (pH 7.4) and homogenized in lysing tubes in a bead mill. The samples were transferred to new tubes, combined with 2% SDS, probe sonicated, vortexed for 10m at RT at 1400RPM followed by centrifugation for 10m at 14,000g. Protein concentration was estimated using a Micro BCA Protein Assay Kit (ThermoFisher Scientific #23235) (R^2 values > 0.99 for each sample) and protein levels resolved by SDS-PAGE, using the method described above. The membrane was incubated overnight in Pierce SuperBlock Blocking Buffer (Pierce #37353) with 0.1% Tween 20 (Sigma #P7949) and validated primary antibodies: mouse anti-Ca_Vβ4 (Neuromab #75-054, 1:1000) and rabbit anti-β-tubulin (Abcam #ab6046, 1:600,000). The membrane was then incubated in LiCor Blocking Buffer (LiCor #927-4000) diluted 1:1 with TBS (0.1% Tween 20 and 0.02% SDS) and LiCor IRDye secondary antibodies: goat anti-mouse 800 (#926-32210, 1:10,000) and goat anti-rabbit 680nm (#926-68071, 1:10,000). β4 isoforms are present at bands ~37.5-

59kDa. Signal intensity was calculated by normalizing the optical density of β4 to β-tubulin for each technical replicate and then averaging the normalized optical density of the technical replicates. Mean optical density β4OE versus AAV Naïve was evaluated via t-test, as was mean optical density of β4OE versus CN.

Appendix B.2 Figures

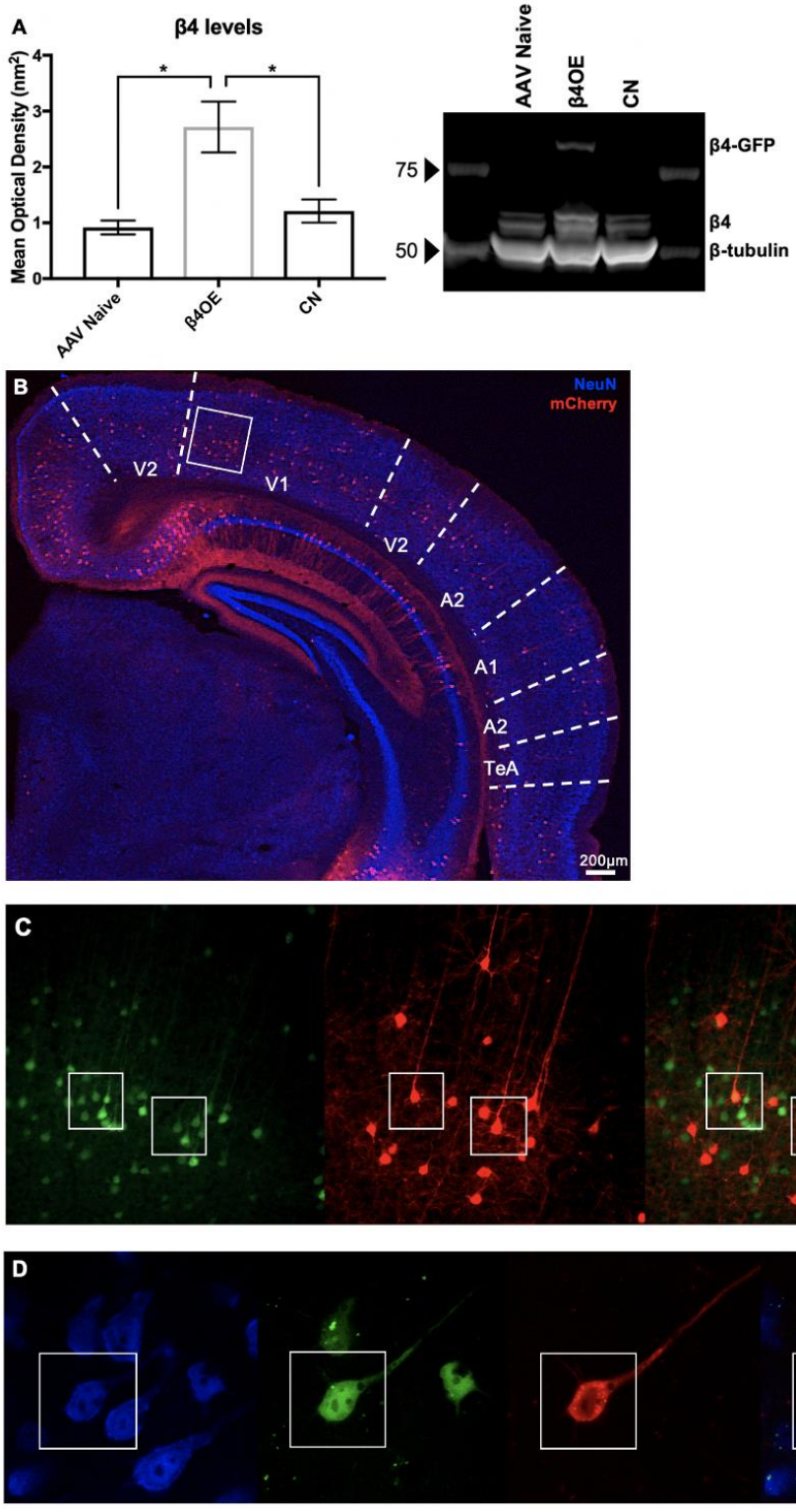

Appendix B Figure 1: Western blot confirming β4 overexpression and image processing sampling methods

(A) (Left) Mean optical density (nm^2) of β4 was significantly increased in β4OE compared to AAV Naïve (t=3.818, DF=2, p=0.0311) as well as to CN (t=3.016, DF=2, p=0.0473). Error bars = SEM. (Right) Western blot showing β4 bands at ~51-55kDa as well as band at ~82kDa in β4OE tissue, which is the predicted molecular weight of a β4-GFP fusion protein (GFP molecular weight = 27kDa). Mean optical density of β4-GFP fusion protein band was not included in assessment of overall β4 overexpression. (B) 1.25x image of ROI including five regions of sensory cortex of male CN mouse Ms8-164. NeuN (blue) and mCherry but not GFP fluorescence visible at 1.25x. Dashed lines designate region boundaries and white box in V1 outlines 10x image of L5 pyramidal cells in shown C. Scalebar = 200 μm. (C) 10x image of L5 pyramidal cells with GFP+mCherry+ fluorescence. Two L5 pyramidal cells with the highest total GFP and mCherry combined fluorescent intensity outlined by white boxes. Scalebar = 50 μm. (D) 60x 2-D image of GFP+mCherry+ pyramidal cell from Ms8-164. White box outlines the cell body of the L5 pyramidal cell of interest. Scalebar = 10 μm.

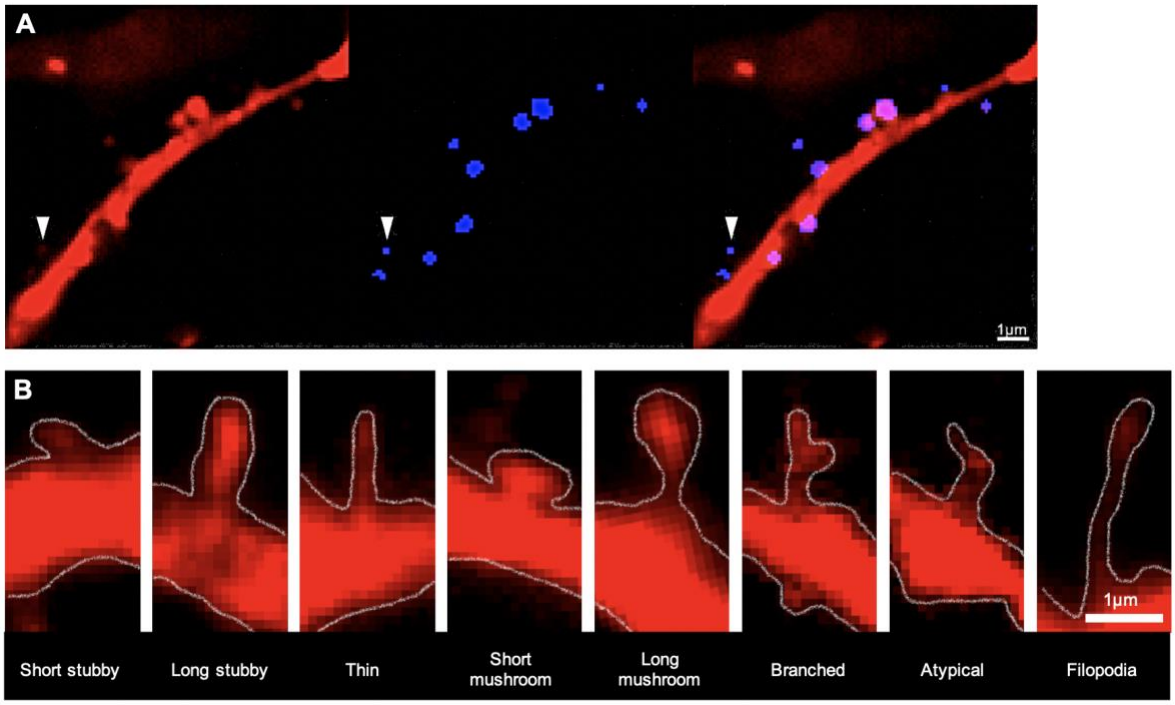

Appendix B Figure 2: Spine Masking and dendrite protrusion categorization methods

(A) Masking strategy used to calculate dendritic spine object volume. For two neurons per mouse, each spine included in neuron DSD was manually marked in Slidebook6. Then, each marked spine object was manually masked using the brush tool in Slidebook6 in the 3D planes in which it occurred. Far left panel shows a 2D image of an unmasked dendritic segment from Neuron18 (DSD=0.7307spines/µm) of Ms9-167 (female CN in proestrus). Middle panel shows the mask only for this dendritic segment. Far right panel shows the merge. White triangle in each panel points to a masked spine with < 0.1µm^3 volume. Scalebar = 1 µm. (B) Dendrite protrusion category examples. Scalebar = 1 µm.

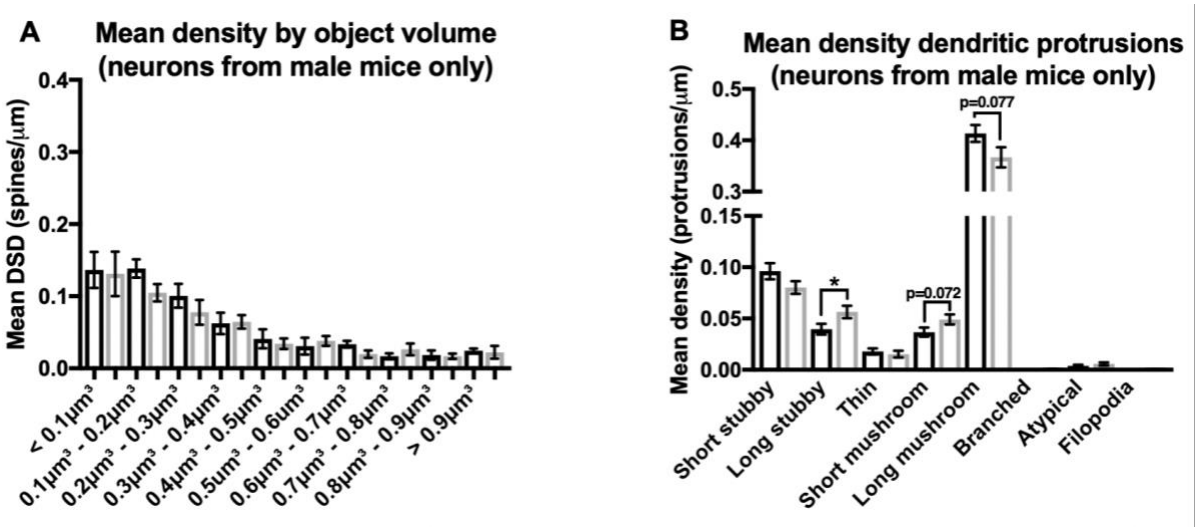

Appendix B Figure 3: Impact of β4OE on dendritic spines of male mice

(A) Unlike in females, in male mice β4OE did not significantly reduce mean DSD of masked objects with small < 0.1μm^3 volume (F=0.017, DF=1, p=0.900). Genotype also did not significantly alter mean DSD of masked objects of 0.1μm^3 - 0.2μm^3 volume in male mice (F=3.620, DF=1, p=0.81). Error bars = SEM. (B) β4OE significantly increased mean density of long stubby spines in male mice (F=4.202, DF=1, p=0.044).There was a trend level increase in mean density of short mushroom (F=3.332, DF=1, p=0.072) and a trend level decrease in mean density of long mushroom (F=3.215, DF=1, p=0.077) spines in male β4OE mice. Error bars = SEM.

Appendix C

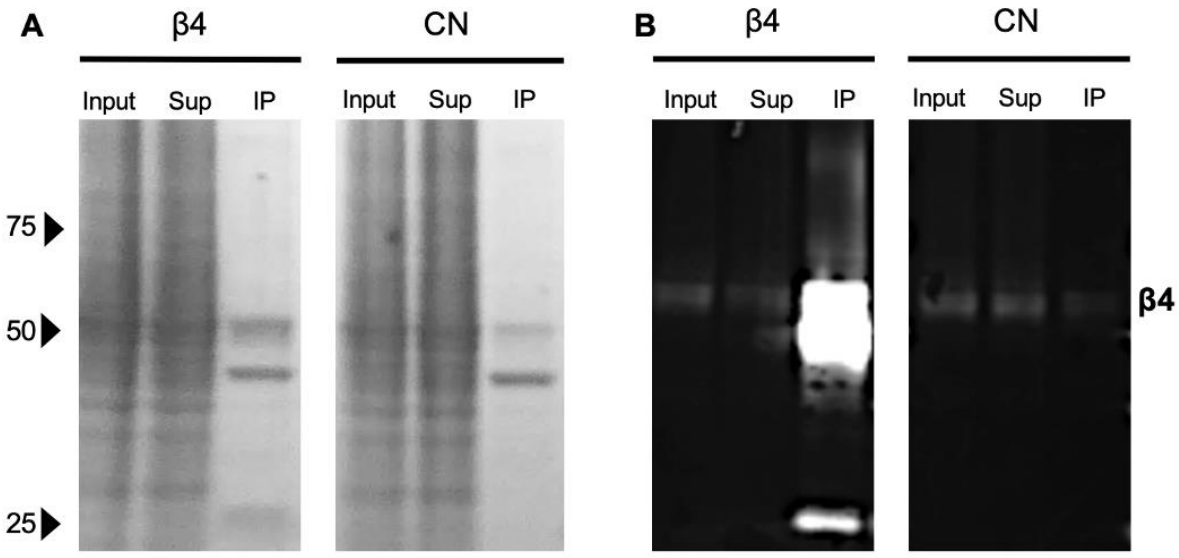

Appendix C Figure 1: β4 immunoprecipitation (β4-IP) proof-of-concept using western blot

(A) β4 was immunoprecipitated from RNAse treated mouse brain lysate (n=1 adult female C57Bl/6J mouse) using 10µg mouse anti-CaVβ4 antibody (Neuromab #75-054) per 1mg beads (Input=lysate prior to antibody coupling, Sup=supernatant, IP=immunoprecipitant) run out on a gel. Non-antibody coupled beads were used as negative control (CN). β4 isoforms are present at 37.5-59kD (predominant isoforms at ~55kD). (B) β4 and β4-IP proteins using western blot and detection with a goat anti-CACNB4 antibody (Everest Biotech #EB06591, 1:1000) and donkey anti-goat 800 secondary antibody (LiCor #926-32214, 1:10,000).

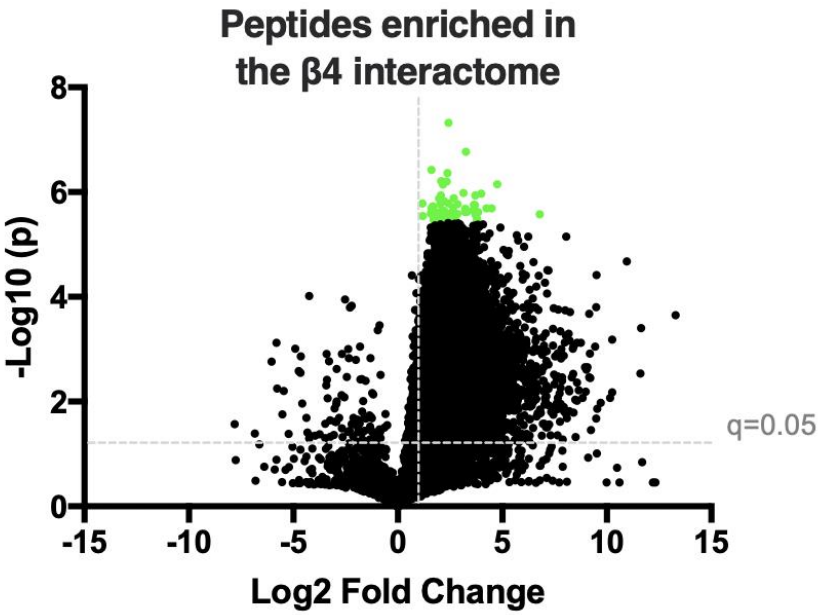

Appendix C Figure 2: The most significantly enriched peptides in the β4 interactome

Volcano plot showing all peptides with CV<0.3. 11315 peptides (grey line with q=0.05) were identified as significantly enriched using a false discovery rate of 0.05 and 63 peptides (green) were identified after Bonferroni correction (α=0.05).

Appendix C Table 1: The most significantly enriched peptides in the β4 interactome

Table listing the peptides identified as the most significantly enriched peptides in the β4 interactome after Bonferroni correction.

Peptide	Protein ID	β4-IP Mean	Negative CN Mean	Log2(β4-IP)-Log2(CN)	p value	q value
HLLIGLPSGAILSLPK	EMC1	6168870.582	1152938.263	2.419691118	4.72862E-08	3.83936E-06
SGFLSYLLLLSR	BAIP3	7162459.648	744564.6575	3.265986064	1.69086E-07	7.67872E-06
SFDSLGSQSSHSR	ARHG7	7693670.727	2508974.177	1.616574465	3.79996E-07	1.15181E-05
GTGLQPGEEELPDIAPPLVTPDEPK	UBP5	3308799.823	639496.778	2.371299018	4.35749E-07	1.53574E-05
VAPPPPAPKPFK	AGAP2	54852486.2	13035987.09	2.073057185	6.11966E-07	1.91968E-05
ILAGALTQHNGDAAASLTVAEQYVSAFSK	STML2	4474020.422	886882.1885	2.334757464	6.25643E-07	2.30362E-05
FRPLNESEVNRGDK	KINH	7056191.02	260874.0556	4.757464239	7.0358E-07	2.68755E-05
IGQLQGEIIPTSFYHQGR	ADA23	82497479.42	18538488.14	2.153826447	7.17335E-07	3.07149E-05
ILEPTTFQEPPPKPSRPK	FAK2	81436942.4	9244520.615	3.139012981	1.03755E-06	3.45543E-05
LLMHETQPPSHFSVSTITR	HD	13556014.65	852223.733	3.991557062	1.06713E-06	3.83936E-05
QLGVPLEPVNFPSHFLLR	FBX21	17075422.85	1312563.067	3.701462655	1.15379E-06	4.2233E-05
FVDGLMIHSGDPVNYYVDTAVR	RS3	16860006.01	4062404.761	2.053199154	1.15527E-06	4.60723E-05
YNEVMATYLLLGYK	MARK2	13583558.76	2135736.537	2.669055908	1.29818E-06	4.99117E-05
TALAEAELEYNPEHVSR	SYIM	45311944.9	11561516.87	1.970560725	1.31919E-06	5.37511E-05
HLSLPAGQVVPK	F126B	8805235.179	1874703.201	2.231699329	1.49769E-06	5.75904E-05
GIAFEDVR	ACADM	25568110.41	11307895.52	1.177015084	1.63535E-06	6.14298E-05
AFLVGIVVPDPEVMPSWAQK	ACSL6	3395971.655	631026.2641	2.428052459	1.65878E-06	6.52691E-05
DFLAGGIAAAVSKTAVAPIER	ADT1	7397797.41	1017191.248	2.862504838	1.68738E-06	6.91085E-05
EFATLIIDILSEAK	GIT1	31992280.51	7888816.419	2.019843066	1.72951E-06	7.29479E-05
SSSSSQESLNRPLSAK	CLAP1	2728111.703	219565.4018	3.635180074	1.74195E-06	7.67872E-05
SIFLNQVLAEINKEIEGVTK	EXOC4	9655917.483	749808.4295	3.686819397	1.77019E-06	8.06266E-05
LLNASAYR	GIT1	35380525.06	11057416.38	1.677941126	1.87027E-06	8.44659E-05
KVYFHTDAAQAVGK	NFS1	24715656.26	3974459.31	2.636594701	1.98312E-06	8.83053E-05
HPGVTEQNEELSILYPAAIVTIDGFSLFQSLR	RBGPR	7517353.029	399263.6444	4.234811141	2.04578E-06	9.21447E-05
KGEFVPGTR	NOVA1	11486809.36	509698.1388	4.494191227	2.04619E-06	9.5984E-05
IGYNPDTVAFVPISGWNGDNMLEPSANMPWFK	EF1A1	10819940.74	3534953.96	1.613929267	2.05658E-06	9.98234E-05
ILGNLLQPPNERPELPSGLYVLGLTGISGSGK	COASY	22375087.58	2389676.569	3.227006055	2.0649E-06	0.000103663
GAYIYNTLMEFIR	SYTC	11261568.82	933037.3671	3.593329149	2.22855E-06	0.000107502

Appendix C Table 1 continued

YGFTHLSTGELLR	KAD5	58076023.53	12773355.01	2.184805167	2.26671E-06	0.000111341
VAEVLNDPESMEK	KLC1	4960194.193	1051185.481	2.23837935	2.32913E-06	0.000115181
QAEVALSVPWDPSNQVYLSYYNVSSLK	ACO11	10099431.12	1022363.14	3.304294398	2.36529E-06	0.00011902
LLVELNKVPAVR	PREX1	6697787.446	722581.7185	3.212451933	2.39502E-06	0.00012286
VLLDFLDQHPISFTPLIQR	IPO11	6817529.238	473505.434	3.847796095	2.41302E-06	0.000126699
QVIYSVQR	LMBD2	4380955.619	1232439.221	1.829729099	2.42578E-06	0.000130538
GLPGSGKSTLAR	CN37	2169987.577	543462.5804	1.997434175	2.49533E-06	0.000134378
FLSDFRDLMSWINGIR	SPTN1	17068167.07	2874331.156	2.570009946	2.546E-06	0.000138217
DVIEPLFLLAEVEIPNIQK	RHG44	14431162.77	2516214.519	2.519860719	2.55756E-06	0.000142056
QASQLEFR	SESD1	5525290.814	1856430.946	1.573518748	2.5597E-06	0.000145896
FQDNFEFIQWFK	MARE3	48658650.8	7762151.518	2.648167818	2.5737E-06	0.000149735
AFGPGLQGGNAGSPAR	FLNA	11150855.27	2724905.421	2.032876308	2.57708E-06	0.000153574
APTGEVATFK	DIP2A	4286718.123	1060752.243	2.014785826	2.58049E-06	0.000157414
NKLPGLITSMETIGAK	EXOC7	20192519.07	2822397.548	2.838827784	2.59073E-06	0.000161253
VDGTPVTQGMETTQPSK	LAC1	4138507.205	37300.36571	6.793776884	2.64856E-06	0.000165093
GVQSLWGSLKPK	APBB1	2975148.921	434364.5418	2.775983642	2.69374E-06	0.000168932
ESSIENEIAVLR	KCC1D	30035331.85	5482401.679	2.453780665	2.73727E-06	0.000172771
ATFAFTLGSAHTPGRPPR	MTMR5	28783217.39	2169810.534	3.729586887	2.74443E-06	0.000176611
VVKQASEGPLK	G3P	16699250.34	7298595.734	1.194092521	2.84487E-06	0.00018045
AVAHHTTAAFIR	PRS6B	27193411.04	5085938.478	2.418671213	2.94807E-06	0.000184289
KNQMDIATSLLEYGADANAVTR	ANK3	19463397	5802537.251	1.746007745	2.98163E-06	0.000188129
KMDETDASSAVK	TADBP	4062054.784	1074228.396	1.918908934	2.98461E-06	0.000191968
DFINSELLAQLYSSEDQNTLMEESAEQAQR	DYN3	4692986.011	844595.3154	2.47417401	3.13165E-06	0.000195807
ENAPAIIFIDEIDAIATK	PRS6B	22932554.66	5006194.2	2.195610917	3.15997E-06	0.000199647
SLQVKPSPVLSDGVVR	GRSF1	7881400.528	1970624.267	1.999799292	3.16447E-06	0.000203486
RLEEFPAFPR	SNX15	6975107.132	501986.2212	3.796495706	3.22052E-06	0.000207326
SFAQAAIEK	SYIM	18589178.59	4911532.73	1.920217804	3.26683E-06	0.000211165
VNAQFLELYNEEVLDLFDTTR	KI21A	21852354.65	4481882.739	2.285611934	3.29098E-06	0.000215004
LHTTGDLTMDTDLTAANGK	HS12A	9214281.432	2827344.505	1.70442398	3.37398E-06	0.000218844
NGDENYMEFLEVLTEQLDR	S12A5	17459060.71	1267302.857	3.784142702	3.43558E-06	0.000222683
FLESVEGNQNYPLLLLTLLEK	XPO2	22968264.59	5176083.688	2.149709007	3.45104E-06	0.000226522
VLALASGPELGQLTFLGLVGIIDPPR	AT2C1	3724649.704	546207.5375	2.769583621	3.53555E-06	0.000230362
NVIALAFDYR	LRP1	7199349.195	1914637.55	1.910795187	3.56052E-06	0.000234201

Appendix C Table 1 continued

YTAVGQLVQDLLTQVR	RIN1	7228678.76	1221889.633	2.564617999	3.60848E-06	0.00023804
YGAVEETAWK	MERB1	6333989.492	1246946.59	2.344714801	3.70613E-06	0.00024188

Bibliography

Abel, K. M., Drake, R., & Goldstein, J. M. (2010). Sex differences in schizophrenia. *International Review of Psychiatry, 22*(5), 417-428.

Abiria, S. A., & Colbran, R. J. (2010). CaMKII associates with CaV1. 2 L-type calcium channels via selected β subunits to enhance regulatory phosphorylation. *Journal of Neurochemistry, 112*(1), 150-161.

Aleman, A., Kahn, R. S., & Selten, J.-P. (2003). Sex differences in the risk of schizophrenia: evidence from meta-analysis. *Archives of General Psychiatry, 60*(6), 565-571.

Alexander, B. H., Barnes, H. M., Trimmer, E., Davidson, A. M., Ogola, B. O., Lindsey, S. H., & Mostany, R. (2018). Stable density and dynamics of dendritic spines of cortical neurons across the estrous cycle while expressing differential levels of sensory-evoked plasticity. *Frontiers in Molecular Neuroscience, 11*, 83. doi:10.3389/fnmol.2018.00083

Allen, P. B., Ouimet, C. C., & Greengard, P. (1997). Spinophilin, a novel protein phosphatase 1 binding protein localized to dendritic spines. *Proceedings of the National Academy of Sciences, 94*(18), 9956-9961.

Alvarez, V. A., Sabatini, Bernardo L. (2007). Anatomical and physiological plasticity of dendritic spines. *Annual Review of Neuroscience, 30*, 79-97.

Amatrudo, J. M., Weaver, C. M., Crimins, J. L., Hof, P. R., Rosene, D. L., & Luebke, J. I. (2012). Influence of highly distinctive structural properties on the excitability of pyramidal neurons in monkey visual and prefrontal cortices. *Journal of Neuroscience, 32*(40), 13644-13660.

American Psychiatric Association. (2013). *Diagnostic and statistical manual of mental disorders (DSM-5®)*: American Psychiatric Pub.

Andreasen, N. C. (1995). Symptoms, signs, and diagnosis of schizophrenia. *The Lancet, 346*(8973), 477-481.

Andrieux, A., Salin, P. A., Vernet, M., Kujala, P., Baratier, J., Gory-Fauré, S., . . . Schweitzer, A. (2002). The suppression of brain cold-stable microtubules in mice induces synaptic defects associated with neuroleptic-sensitive behavioral disorders. *Genes and Development, 16*(18), 2350-2364.

Arellano, J., Benavides-Piccione, R., DeFelipe, J., & Yuste, R. (2007). Ultrastructure of dendritic spines: correlation between synaptic and spine morphologies. *Frontiers in Neuroscience, 1*(10). doi:10.3389/neuro.01.1.1.010.2007

Baratier, J., Peris, L., Brocard, J., Gory-Fauré, S., Dufour, F., Bosc, C., . . . Job, D. (2006). Phosphorylation of microtubule-associated protein STOP by calmodulin kinase II. *Journal of Biological Chemistry, 281*(28), 19561-19569.

Barta, P. E., Pearlson, G. D., Brill, L. B., Royall, R., McGilchrist, I. K., Pulver, A. E., . . . Frangou, S. (1997). Planum temporale asymmetry reversal in schizophrenia: replication and relationship to gray matter abnormalities. *American Journal of Psychiatry, 154*(5), 661-667.

Basu, S., Saha, P. K., Roszkowska, M., Magnowska, M., Baczynska, E., Das, N., . . . Wlodarczyk, J. (2018). Quantitative 3-D morphometric analysis of individual dendritic spines. *Scientific Reports, 8*, 345. doi:10.1038/s41598-018-21753-8

Bayne, K. (2018). Environmental enrichment and mouse models: Current perspectives. *Animal Models and Experimental Medicine, 1*(2), 82-90.

Béguin, P., Nagashima, K., Mahalakshmi, R. N., Vigot, R., Matsunaga, A., Miki, T., . . . Tay, H. S. (2014). BARP suppresses voltage-gated calcium channel activity and Ca2+-evoked exocytosis. *Journal of Cell Biology, 205*(2), 233-249.

Beharier, O., Etzion, Y., Katz, A., Friedman, H., Tenbosh, N., Zacharish, S., . . . Moran, A. (2007). Crosstalk between L-type calcium channels and ZnT-1, a new player in rate-dependent cardiac electrical remodeling. *Cell Calcium, 42*(1), 71-82.

Benavides-Piccione, R., Ballesteros-Yáñez, I., DeFelipe, J., & Yuste, R. (2002). Cortical area and species differences in dendritic spine morphology. *Journal of Neurocytology, 31*(3-5), 337-346.

Berggren, P.-O., Yang, S.-N., Murakami, M., Efanov, A. M., Uhles, S., Köhler, M., . . . Aspinwall, C. A. (2004). Removal of Ca2+ channel β3 subunit enhances Ca2+ oscillation frequency and insulin exocytosis. *Cell, 119*(2), 273-284.

Berry, K. P., & Nedivi, E. (2017). Spine Dynamics: Are They All the Same? *Neuron, 96*(1), 43-55.

Bogdanov, Y., Brice, N. L., Canti, C., Page, K. M., Li, M., Volsen, S. G., & Dolphin, A. C. (2000). Acidic motif responsible for plasma membrane association of the voltage-dependent calcium channel β1b subunit. *European Journal of Neuroscience, 12*, 894-902.

Boivin, J. R., Piekarski, D. J., Thomas, A. W., & Wilbrecht, L. (2018). Adolescent pruning and stabilization of dendritic spines on cortical layer 5 pyramidal neurons do not depend on gonadal hormones. *Developmental Cognitive Neuroscience, 30*, 100-107.

Bopp, R., Holler-Rickauer, S., Martin, K. A. C., & Schuhknecht, G. F. P. (2017). An ultrastructural study of the thalamic input to layer 4 of primary motor and primary somatosensory cortex in the mouse. *Journal of Neuroscience, 37*(9), 2435-2448.

Bowman, R. E., Luine, V., Weinstein, S. D., Khandaker, H., DeWolf, S., & Frankfurt, M. (2018). Bisphenol-A exposure during adolescence leads to enduring alterations in cognition and dendritic spine density in adult male and female rats. *Hormones and Behavior, 69*, 89-97.

Brenner, C. A., Krishnan, G. P., Vohs, J. L., Ahn, W.-Y., Hetrick, W. P., Morzorati, S. L., & O'donnell, B. F. (2009). Steady state responses: electrophysiological assessment of sensory function in schizophrenia. *Schizophrenia Bulletin, 35*(6), 1065-1077.

Brice, N. L., & Dolphin, A. C. (1999). Differential plasma membrane targeting of voltage-dependent calcium channel subunits expressed in a polarized epithelial cell line. *The Journal of Physiology, 515*(Pt 3), 685-694.

Brusco, J., Merlo, S., Ikeda, É. T., Petralia, R. S., Kachar, B., Rasia-Filho, A. A., & Moreira, J. E. (2014). Inhibitory and multisynaptic spines, and hemispherical synaptic specialization in the posterodorsal medial amygdala of male and female rats. *Journal of Comparative Neurology, 522*(9), 2075-2088.

Buraei, Z., & Yang, J. (2010). The β subunit of voltage-gated Ca 2+ channels. *Physiological Reviews, 90*(4), 1461-1506.

Buraei, Z., & Yang, J. (2013). Structure and function of the β subunit of voltage-gated Ca2+ channels. *Biochimica Et Biophysica Acta (BBA)-Biomembranes, 1828*(7), 1530-1540.

Burgess, D. L., Biddlecome, G. H., McDonough, S. I., Diaz, M. E., Zilinski, C. A., Bean, B. P., . . . Noebels, J. L. (1999). β subunit reshuffling modifies N-and P/Q-type Ca 2+ channel subunit compositions in lethargic mouse brain. *Molecular and Cellular Neuroscience, 13*(4), 293-311.

Burgess, D. L., Jones, J. M., Meisler, M. H., & Noebels, J. L. (1997). Mutation of the Ca2+ channel β subunit gene Cchb4 is associated with ataxia and seizures in the lethargic (lh) mouse. *Cell, 88*(3), 385-392.

Byers, S. L., Wiles, M. V., Dunn, S. L., & Taft, R. A. (2012). Mouse estrous cycle identification tool and images. *PloS One, 7*(4), e35538. doi:10.1371/journal.pone.0035538

Caddick, S. J., Wang, C., Fletcher, C. F., Jenkins, N. A., Copeland, N. G., & Hosford, D. A. (1999). Excitatory but not inhibitory synaptic transmission is reduced in lethargic (Cacnb4 lh) and tottering (Cacna1a tg) mouse thalami. *Journal of Neurophysiology, 81*(5), 2066-2074.

Calizo, L. H., & Flanagan-Cato, L. M. (2000). Estrogen selectively regulates spine density within the dendritic arbor of rat ventromedial hypothalamic neurons. *Journal of Neuroscience, 20*(4), 1589-1596.

Cane, M., Maco, B., Knott, G., & Holtmaat, A. (2014). The relationship between PSD-95 clustering and spine stability in vivo. *Journal of Neuroscience, 34*(6), 2075-2086.

Capani, F., Ellisman, M. H., & Martone, M. E. (2001). Filamentous actin is concentrated in specific subpopulations of neuronal and glial structures in rat central nervous system. *Brain Research, 923*(1-2), 1-11.

Castellano, A., & Perez-Reyes, E. (1994). Molecular diversity of Ca2+ channel β subunits. *Biochemical Society Transations, 22*(2), 483-488.

Chadman, K. K., Yang, M., & Crawley, J. N. (2009). Criteria for validating mouse models of psychiatric diseases. *American Journal of Medical Genetics Part B: Neuropsychiatric Genetics, 150*(1), 1-11.

Chaudhuri, D., Alseikhan, B. A., Chang, S. Y., Soong, T. W., & Yue, D. T. (2005). Developmental activation of calmodulin-dependent facilitation of cerebellar P-type Ca2+ current. *Journal of Neuroscience, 25*(36), 8282-8294.

Cheetham, C. E. J., Grier, B. D., & Belluscio, L. (2015). Bulk regional viral injection in neonatal mice enables structural and functional interrogation of defined neuronal populations throughout targeted brain areas. *Frontiers in Neural Circuits, 9*(72). doi:10.3389/fncir.2015.00072

Chen, J.-R., Yan, Y.-T., Wang, T.-J., Chen, L.-J., Wang, Y.-J., & Tseng, G.-F. (2009). Gonadal hormones modulate the dendritic spine densities of primary cortical pyramidal neurons in adult female rat. *Cerebral Cortex, 19*(11), 2719-2727.

Chen, J. L., Villa, K. L., Cha, J. W., So, P. T. C., Kubota, Y., & Nedivi, E. (2012). Clustered dynamics of inhibitory synapses and dendritic spines in the adult neocortex. *Neuron, 74*(2), 361-373.

Chen, X., Leischner, U., Rochefort, N. L., Nelken, I., & Konnerth, A. (2011). Functional mapping of single spines in cortical neurons in vivo. *Nature, 475*(7357), 501-507.

Cheng, W., Altafaj, X., Ronjat, M., & Coronado, R. (2005). Interaction between the dihydropyridine receptor Ca2+ channel β-subunit and ryanodine receptor type 1 strengthens excitation-contraction coupling. *Proceedings of the National Academy of Sciences, 102*(52), 19225-19230.

Clemo, R. H., & Meredith, A. M. (2012). Dendritic Spine Density in Multisensory Versus Primary Sensory Cortex. *Synapse, 66*(8), 714-724.

Cohen, L., Rothschild, G., & Mizrahi, A. (2011). Multisensory integration of natural odors and sounds in the auditory cortex. *Neuron, 72*(2), 357-369.

Collins, M. O., Husi, H., Yu, L., Brandon, J. M., Anderson, C. N. G., Blackstock, W. P., . . . Grant, S. G. N. (2006). Molecular characterization and comparison of the components and multiprotein complexes in the postsynaptic proteome. *Journal of Neurochemistry, 97*, 16-23.

de Castilhos, J., Forti, C. D., Achaval, M., & Rasia-Filho, A. A. (2008). Dendritic spine density of posterodorsal medial amygdala neurons can be affected by gonadectomy and sex steroid manipulations in adult rats: a Golgi study. *Brain Research 1240*, 73-81.

De Roo, M., Klauser, P., Mendez, P., Poglia, L., & Muller, D. (2008). Activity-dependent PSD formation and stabilization of newly formed spines in hippocampal slice cultures. *Cerebral Cortex, 18*(1), 151-161.

De Waard, M., Witcher, D. R., Pragnell, M., Liu, H., & Campbell, K. P. (1995). Properties of the-Anchoring Site in Voltage-dependent Ca Channels. *Journal of Biological Chemistry, 270*(20), 12056-12064.

DeFelipe, J. (2015). The dendritic spine story: an intriguing process of discovery. *Frontiers in Neuroanatomy, 9*(14). doi:10.3389/fnana.2015.00014

DeFelipe, J., Hendry, S. H. C., & Jones, E. G. (1989). Synapses of double bouquet cells in monkey cerebral cortex visualized by calbindin immunoreactivity. *Brain Research, 503*(1), 49-54.

DeGiosio, R., Kelly, R. M., DeDionisio, A. M., Newman, J. T., Fish, K. N., Sampson, A. R., . . . Sweet, R. A. (2019). MAP2 immunoreactivity deficit is conserved across the cerebral cortex within individuals with schizophrenia. *npj Schizophrenia, 5*(1), 1-9.

Delevich, K., Okada, N. J., Rahane, A., Zhang, Z., Hall, C. D., & Wilbrecht, L. (2019). Sex and pubertal status influence dendritic spine density onto frontal corticostriatal projection neurons. *bioRxiv*, 787408.

Delotterie, D., Ruiz, G., Brocard, J., Schweitzer, A., Roucard, C., Roche, Y., . . . Andrieux, A. (2010). Chronic administration of atypical antipsychotics improves behavioral and synaptic defects of STOP null mice. *Psychopharmacology, 208*(1), 131-141.

Ding, J. D., Kennedy, M. B., & Weinberg, R. J. (2013). Subcellular organization of camkii in rat hippocampal pyramidal neurons. *Journal of Comparative Neurology, 521*(15), 3570-3583.

Dolphin, A. C. (2012). Calcium channel auxiliary α2δ and β subunits: trafficking and one step beyond. *Nature Reviews Neuroscience, 13*(8), 542-555.

Dolphin, A. C. (2016). Voltage-gated calcium channels and their auxiliary subunits: physiology and pathophysiology and pharmacology. *The Journal of Physiology, 594*(19), 5369-5390.

Dorph-Petersen, K.-A., Delevich, K. M., Marcsisin, M. J., Zhang, W., Sampson, A. R., Gundersen, H. J. G., . . . Sweet, R. A. (2009). Pyramidal neuron number in layer 3 of primary auditory cortex of subjects with schizophrenia. *Brain Research, 1285*, 42-57.

Dunaevsky, A., Tashiro, A., Majewska, A., Mason, C., & Yuste, R. (1999). Developmental regulation of spine motility in the mammalian central nervous system. *Proceedings of the National Academy of Sciences, 96*(23), 13438-13443.

Ehrlich, I., Klein, M., Rumpel, S., & Malinow, R. (2007). PSD-95 is required for activity-driven synapse stabilization. *Proceedings of the National Academy of Sciences, 104*(10), 4176-4181.

Etemad, S., Obermair, G. J., Bindreither, D., Benedetti, A., Stanika, R., Di Biase, V., . . . Geley, S. (2014). Differential neuronal targeting of a new and two known calcium channel β4 subunit splice variants correlates with their regulation of gene expression. *Journal of Neuroscience, 34*(4), 1446-1461.

Ethell, I. M., & Pasquale, E. B. (2005). Molecular mechanisms of dendritic spine development and remodeling. *Progress in Neurobiology, 75*(3), 161-205.

Feinberg, I. (1983). Schizophrenia: caused by a fault in programmed synaptic elimination during adolescence? *Journal of Psychiatric Research, 17*(4), 319-334.

Feldmeyer, D. (2012). Excitatory neuronal connectivity in the barrel cortex. *Frontiers in Neuroanatomy, 6*, 24. doi:10.3389/fnana.2012.00024

Feng, Z.-P., Arnot, M. I., Doering, C. J., & Zamponi, G. W. (2001). Calcium channel β subunits differentially regulate the inhibition of N-type channels by individual Gβ isoforms. *Journal of Biological Chemistry, 276*(48), 45051-45058.

Ferrándiz-Huertas, C., Gil-Mínguez, M., & Luján, R. (2012). Regional expression and subcellular localization of the voltage-gated calcium channel β subunits in the developing mouse brain. *Journal of Neurochemistry, 122*(6), 1095-1107.

Fett, A.-K. J., Viechtbauer, W., Penn, D. L., van Os, J., & Krabbendam, L. (2011). The relationship between neurocognition and social cognition with functional outcomes in schizophrenia: a meta-analysis. *Neuroscience and Biobehavioral Reviews, 35*(3), 573-588.

Fischer, M., Kaech, S., Knutti, D., & Matus, A. (1998). Rapid actin-based plasticity in dendritic spines. *Neuron, 20*(5), 847-854.

Fitzgerald, E. M. (2000). Regulation of voltage-dependent calcium channels in rat sensory neurones involves a Ras-mitogen-activated protein kinase pathway. *The Journal of Physiology, 527*(3), 433-444.

Fitzgerald, E. M. (2002). The presence of ca2+ channel β subunit is required for mitogen-activated protein kinase (mapk)-dependent modulation of α1b ca2+ channels in cos-7 cells. *The Journal of Physiology, 543*(2), 425-437.

Fontaine-Lenoir, V., Chambraud, B., Fellous, A., David, S., Duchossoy, Y., Baulieu, E.-E., & Robel, P. (2006). Microtubule-associated protein 2 (MAP2) is a neurosteroid receptor. *Proceedings of the National Academy of Sciences, 103*(12), 4711-4716.

Forlano, P. M., & Woolley, C. S. (2010). Quantitative analysis of pre-and postsynaptic sex differences in the nucleus accumbens. *Journal of Comparative Neurology, 518*(8), 1330-1348.

Frankfurt, M., Gould, E., Woolley, C. S., & McEwen, B. S. (1990). Gonadal steroids modify dendritic spine density in ventromedial hypothalamic neurons: a Golgi study in the adult rat. *Neuroendocrinology, 51*(5), 530-535.

Franklin, K. B. J., & Paxinos, G. (2004). *The mouse brain in stereotaxic coordinates*: Gulf Professional Publishing.

Galindo-Leon, E. E., Lin, F. G., & Liu, R. C. (2009). Inhibitory plasticity in a lateral band improves cortical detection of natural vocalizations. *Neuron, 62*(5), 705-716.

Gholizadeh, S., Tharmalingam, S., MacAldaz, M. E., & Hampson, D. R. (2013). Transduction of the central nervous system after intracerebroventricular injection of adeno-associated viral vectors in neonatal and juvenile mice. *Human Gene Therapy Methods, 24*(4), 205-213.

Giachello, C. N. G., Fiumara, F., Giacomini, C., Corradi, A., Milanese, C., Ghirardi, M., . . . Montarolo, P. G. (2010). MAPK/Erk-dependent phosphorylation of synapsin mediates formation of functional synapses and short-term homosynaptic plasticity. *Journal of Cell Science, 123*(6), 881-893.

Gilman, J. P., Medalla, M., & Luebke, J. I. (2016). Area-specific features of pyramidal neurons—a comparative study in mouse and rhesus monkey. *Cerebral Cortex, 27*(3), 2078-2094.

Glantz, L. A., & Lewis, D. A. (2000). Decreased dendritic spine density on prefrontal cortical pyramidal neurons in schizophrenia. *Archives of General Psychiatry, 57*(1), 65-73.

Glausier, J. R., & Lewis, D. A. (2013). Dendritic spine pathology in schizophrenia. *Neuroscience, 251*, 90-107.

Goff, D. C. (2013). Future perspectives on the treatment of cognitive deficits and negative symptoms in schizophrenia. *World Psychiatry, 12*(2), 99-107.

Gold, R., Butler, P., Revheim, N., Leitman, D. I., Hansen, J. A., Gur, R. C., . . . Silipo, G. S. (2012). Auditory emotion recognition impairments in schizophrenia: relationship to acoustic features and cognition. *American Journal of Psychiatry, 169*(4), 424-432.

Gonzalez-Gutierrez, G., Miranda-Laferte, E., Naranjo, D., Hidalgo, P., & Neely, A. (2008). Mutations of nonconserved residues within the calcium channel α1-interaction domain inhibit β-subunit potentiation. *Journal of General Physiology, 132*(3), 383-395.

Gonzalez-Gutierrez, G., Miranda-Laferte, E., Neely, A., & Hidalgo, P. (2007). The Src homology 3 domain of the β-subunit of voltage-gated calcium channels promotes endocytosis via dynamin interaction. *Journal of Biological Chemistry, 282*(4), 2156-2162.

Gonzalez-Gutierrez, G., Miranda-Laferte, E., Nothmann, D., Schmidt, S., Neely, A., & Hidalgo, P. (2008). The guanylate kinase domain of the β-subunit of voltage-gated calcium channels suffices to modulate gating. *Proceedings of the National Academy of Sciences, 105*, 14198-14203.

Gottesman, I. I. (1991). *Schizophrenia genesis: The origins of madness*: WH Freeman/Times Books/Henry Holt & Co.

Gray, E. G. (1959). Electron microscopy of synaptic contacts on dendrite spines of the cerebral cortex. *Nature, 183*, 1592-1593.

Green, M. F., Horan, W. P., & Lee, J. (2015). Social cognition in schizophrenia. *Nature Reviews Neuroscience, 16*(10), 620-631.

Green, M. F., Kern, R. S., & Heaton, R. K. (2004). Longitudinal studies of cognition and functional outcome in schizophrenia: implications for MATRICS. *Schizophrenia Research, 72*(1), 41-51.

Green, M. F., & Leitman, D. I. (2008). Social cognition in schizophrenia. *Schizophrenia Bulletin, 34*(4), 670-672.

Grienberger, C., Chen, X., & Konnerth, A. (2015). Dendritic function in vivo. *Trends in Neurosciences, 38*(1), 45-54.

Grubisha, M. J., Sun, X., MacDonald, M. L., Garver, M., Sun, Z., DeGiosio, R. A., . . . Sweet, R. A. (2019). MAP2 is Hyperphosphorylated in Schizophrenia and Alters its Function. *bioRxiv*, 683912.

Grueter, C. E., Abiria, S. A., Wu, Y., Anderson, M. E., & Colbran, R. J. (2008). Differential regulated interactions of calcium/calmodulin-dependent protein kinase II with isoforms of voltage-gated calcium channel β subunits. *Biochemistry, 47*(6), 1760-1767.

Gu, J., & Zheng, J. Q. (2009). Microtubules in dendritic spine development and plasticity. *The Open Neuroscience Journal, 3*, 128-133.

Hackett, T. A. (2008). Anatomical organization of the auditory cortex. *Journal of the American Academy of Audiology, 19*(10), 774-779.

Hamm, J. P., Bobilev, A. M., Hayrynen, L. K., Hudgens-Haney, M. E., Oliver, W. T., Parker, D. A., . . . Clementz, B. A. (2015). Stimulus train duration but not attention moderates γ-band entrainment abnormalities in schizophrenia. *Schizophrenia Research, 165*(1), 97-102.

Hamm, J. P., Gilmore, C. S., Picchetti, N. A., Sponheim, S. R., & Clementz, B. A. (2011). Abnormalities of neuronal oscillations and temporal integration to low-and high-frequency auditory stimulation in schizophrenia. *Biological Psychiatry, 69*(10), 989-996.

Harris, K. D., & Shepherd, G. M. G. (2015). The neocortical circuit: themes and variations *Nature Neuroscience, 18*(2), 170-181.

Heyes, S., Pratt, W. S., Rees, E., Dahimene, S., Ferron, L., Owen, M. J., & Dolphin, A. C. (2015). Genetic disruption of voltage-gated calcium channels in psychiatric and neurological disorders. *Progress in Neurobiology, 134*, 36-54.

Hickmott, P. W., & Ethell, I. M. (2006). Dendritic Plasticity in the adult neocortex. *The Neuroscientist, 12*(1), 16-28.

Higley, M. J., & Sabatini, B. L. (2012). Calcium signaling in dendritic spines. *Cold Spring Harbor Perspectives in Biology, 4*(4), a005686.

Hirayasu, Y., McCarley, R. W., Salisbury, D. F., Tanaka, S., Kwon, J. S., Frumin, M., . . . Jolesz, F. A. (2000). Planum temporale and Heschl gyrus volume reduction in schizophrenia: a magnetic resonance imaging study of first-episode patients. *Archives of General Psychiatry, 57*(7), 692-699.

Hirayasu, Y., Shenton, M. E., Salisbury, D. F., Dickey, C. C., Fischer, I. A., Mazzoni, P., . . . Anderson, J. E. (1998). Lower left temporal lobe MRI volumes in patients with first-episode schizophrenia compared with psychotic patients with first-episode affective disorder and normal subjects. *American Journal of Psychiatry, 155*(10), 1384-1391.

Holtmaat, A. J., Trachtenberg, J. T., Wilbrecht, L., Shepherd, G. M., Zhang, X., Knott, G. W., & Svoboda, K. (2005). Transient and persistent dendritic spines in the neocortex in vivo. *Neuron, 45*(2), 279-291.

Homman-Ludiye, J., & Bourne, J. A. (2014). Mapping arealisation of the visual cortex of non-primate species: lessons for development and evolution. *Frontiers in Neural Circuits, 8*(79). doi:10.3389/fncir.2014.00079

Honea, R., Crow, T. J., Passingham, D., & Mackay, C. E. (2005). Regional deficits in brain volume in schizophrenia: a meta-analysis of voxel-based morphometry studies. *American Journal of Psychiatry, 162*(12), 2233-2245.

Hoshi, M., Ohta, K., Gotoh, Y., Mori, A., Murofushi, H., Sakai, H., & Nishida, E. (1992). Mitogen-activated-protein-kinase-catalyzed phosphorylation of microtubule-associated proteins, microtubule-associated protein 2 and microtubule-associated protein 4, induces an alteration in their function. *European Journal of Biochemistry, 203*(1-2), 43-52.

Hsu, A., Luebke, J. I., & Medalla, M. (2017). Comparative ultrastructural features of excitatory synapses in the visual and frontal cortices of the adult mouse and monkey. *Journal of Comparative Neurology, 525*(9), 2175-2191.

Insel, T. R. (2010). Rethinking schizophrenia. *Nature, 468*(7321), 187-193.

Jacobs, B., Schall, M., Prather, M., Kapler, E., Driscoll, L., Baca, S., . . . Treml, M. (2001). Regional Dendritic and Spine Variation in Human Cerebral Cortex: a Quantitative Golgi Study. *Cerebral Cortex, 11*(6), 558-571.

Javitt, D. C. (1993). Neurophysiological approaches to analyzing brain dysfunction in schizophrenia. *Psychiatric Annals, 23*(3), 144-150.

Javitt, D. C. (2009). Sensory processing in schizophrenia: neither simple nor intact. *Schizophrenia Bulletin, 35*(6), 1059-1064.

Javitt, D. C., & Freedman, R. (2015). Sensory processing dysfunction in the personal experience and neuronal machinery of schizophrenia. *American Journal of Psychiatry, 172*(1), 17-31.

Javitt, D. C., Shelley, A.-M., & Ritter, W. (2000). Associated deficits in mismatch negativity generation and tone matching in schizophrenia. *Clinical Neurophysiology, 111*(10), 1733-1737.

Javitt, D. C., Steinschneider, M., Schroeder, C. E., & Arezzo, J. C. (1996). Role of cortical N-methyl-D-aspartate receptors in auditory sensory memory and mismatch negativity generation: implications for schizophrenia. *Proceedings of the National Academy of Sciences, 93*(21), 11962-11967.

Javitt, D. C., Steinschneider, M., Schroeder, C. E., Vaughan, H. G., & Arezzo, J. C. (1994). Detection of stimulus deviance within primate primary auditory cortex: intracortical mechanisms of mismatch negativity (MMN) generation. *Brain Research, 667*(2), 192-200.

Javitt, D. C., Strous, R. D., Grochowski, S., Ritter, W., & Cowan, N. (1997). Impaired precision, but normal retention, of auditory sensory (" echoic") memory information in schizophrenia. *Journal of Abnormal Psychology, 106*(2), 315-324.

Javitt, D. C., & Sweet, R. A. (2015). Auditory dysfunction in schizophrenia: integrating clinical and basic features. *Nature Reviews Neuroscience, 16*(9), 535-550.

Jia, H., Rochefort, N. L., Chen, X., & Konnerth, A. (2010). Dendritic organization of sensory input to cortical neurons in vivo. *Nature, 464*(7293), 1307-1312.

Jones, L. P., Wei, S.-k., & Yue, D. T. (1998). Mechanism of auxiliary subunit modulation of neuronal α1E calcium channels. *Journal of General Physiology, 112*(2), 125-143.

Josephson, I. R., & Varadi, G. (1996). The beta subunit increases Ca2+ currents and gating charge movements of human cardiac L-type Ca2+ channels. *Biophysical Journal, 70*(3), 1285-1293.

Juraska, J. M. (1984). Sex differences in developmental plasticity in the visual cortex and hippocampal dentate gyrus. *Progress in Brain Research 61*, 205-214.

Kantrowitz, J. T., Epstein, M. L., Beggel, O., Rohrig, S., Lehrfeld, J. M., Revheim, N., . . . Silipo, G. (2016). Neurophysiological mechanisms of cortical plasticity impairments in schizophrenia and modulation by the NMDA receptor agonist D-serine. *Brain, 139*(12), 3281-3295.

Kantrowitz, J. T., Hoptman, M. J., Leitman, D. I., Moreno-Ortega, M., Lehrfeld, J. M., Dias, E., . . . Javitt, D. C. (2015). Neural substrates of auditory emotion recognition deficits in schizophrenia. *Journal of Neuroscience, 35*(44), 14909-14921.

Kantrowitz, J. T., Leitman, D. I., Lehrfeld, J. M., Laukka, P., Juslin, P. N., Butler, P. D., . . . Javitt, D. C. (2011). Reduction in tonal discriminations predicts receptive emotion processing

deficits in schizophrenia and schizoaffective disorder. *Schizophrenia Bulletin, 39*(1), 86-93.

Kapitein, L. C., Yau, K. W., Gouveia, S. M., van der Zwan, W. A., Wulf, P. S., Keijzer, N., . . . Hoogenraad, C. C. (2011). NMDA receptor activation suppresses microtubule growth and spine entry. *Journal of Neuroscience, 31*(22), 8194-8209.

Kasai, H., Matsuzaki, M., Noguchi, J., Yasumatsu, N., & Nakahara, H. (2003). Structure–stability–function relationships of dendritic spines. *Trends in Neurosciences, 26*(7), 360-368.

Kasai, K., Shenton, M. E., Salisbury, D. F., Hirayasu, Y., Onitsuka, T., Spencer, M. H., . . . McCarley, R. W. (2003). Progressive decrease of left Heschl gyrus and planum temporale gray matter volume in first-episode schizophrenia: a longitudinal magnetic resonance imaging study. *Archives of General Psychiatry, 60*(8), 766-775.

Kato, A., Hojo, Y., Higo, S., Komatsuzaki, Y., Murakami, G., Yoshino, H., . . . Kawato, S. (2013). Female hippocampal estrogens have a significant correlation with cyclic fluctuation of hippocampal spines. *Frontiers in Neural Circuits, 7*, 149. doi:10.3389/fncir.2013.00149

Kato, A. S., Zhou, W., Milstein, A. D., Knierman, M. D., Siuda, E. R., Dotzlaf, J. E., . . . Nicoll, R. A. (2007). New transmembrane AMPA receptor regulatory protein isoform, γ-7, differentially regulates AMPA receptors. *Journal of Neuroscience, 27*(18), 4969-4977.

Keshavan, M. S., Anderson, S., & Pettergrew, J. W. (1994). Is schizophrenia due to excessive synaptic pruning in the prefrontal cortex? The Feinberg hypothesis revisited. *Journal of Psychiatric Research, 28*(3), 239-265.

Klemmer, P., Smit, A. B., & Li, K. W. (2009). Proteomics analysis of immuno-precipitated synaptic protein complexes. *Journal of Proteomics, 72*(1), 82-90.

Klugbauer, N., Dai, S., Specht, V., Lacinová, L., Marais, E., Bohn, G., & Hofmann, F. (2000). A family of γ-like calcium channel subunits. *FEBS Letters, 470*(2), 189-197.

Knott, G., & Holtmaat, A. (2008). Dendritic spine plasticity—current understanding from in vivo studies. *Brain Research Reviews, 58*(2), 282-289.

Kolb, B., Gibb, R., & Gorny, G. (2003). Experience-dependent changes in dendritic arbor and spine density in neocortex vary qualitatively with age and sex. *Neurobiology of Learning and Memory, 79*(1), 1-10.

Koss, W. A., Belden, C. E., Hristov, A. D., & Juraska, J. M. (2014). Dendritic remodeling in the adolescent medial prefrontal cortex and the basolateral amygdala of male and female rats. *Synapse, 68*(2), 61-72.

Krishnan, G. P., Hetrick, W. P., Brenner, C., Shekhar, A., Steffen, A., & O'Donnell, B. F. (2009). Steady state and induced auditory gamma deficits in schizophrenia. *NeuroImage, 47*(4), 1711-1719.

Kubicki, M., Shenton, M. E., Salisbury, D. F., Hirayasu, Y., Kasai, K., Kikinis, R., . . . McCarley, R. W. (2002). Voxel-based morphometric analysis of gray matter in first episode schizophrenia. *NeuroImage, 17*(4), 1711-1719.

Kwon, J. S., O'donnell, B. F., Wallenstein, G. V., Greene, R. W., Hirayasu, Y., Nestor, P. G., . . . McCarley, R. W. (1999). Gamma frequency–range abnormalities to auditory stimulation in schizophrenia. *Archives of General Psychiatry, 56*(11), 1001-1005.

Lally, J., & MacCabe, J. H. (2015). Antipsychotic medication in schizophrenia: a review. *British Medical Bulletin, 114*(1), 169-179.

Lambert, J. T., Hill, T. C., Park, D. K., Culp, J. H., & Zito, K. (2017). Protracted and asynchronous accumulation of PSD95-family MAGUKs during maturation of nascent dendritic spines. *Developmental Neurobiology, 77*(10), 1161-1174.

Lang, C., Barco, A., Zablow, L., Kandel, E. R., Siegelbaum, S. A., & Zakharenko, S. S. (2004). Transient expansion of synaptically connected dendritic spines upon induction of hippocampal long-term potentiation. *Proceedings of the National Academy of Sciences, 101*(47), 16665-16670.

Lao, Q. Z., Kobrinsky, E., Liu, Z., & Soldatov, N. M. (2010). Oligomerization of Cavβ subunits is an essential correlate of Ca2+ channel activity. *The FASEB Journal, 24*(12), 5013-5023.

Larkman, A., Mason, A. (1990). Correlations between morphology and electrophysiology of pyramidal neurons in slices of rat visual cortex. I. Establishment of cell classes. *Journal of Neuroscience, 10*(5), 1407-1414.

Larson, M. K., Walker, E. F., & Compton, M. T. (2010). Early signs, diagnosis and therapeutics of the prodromal phase of schizophrenia and related psychotic disorders. *Expert Review of Neurotherapeutics, 10*(8), 1347-1359.

Lee, A., Scheuer, T., & Catterall, W. A. (2000). Ca2+/calmodulin-dependent facilitation and inactivation of P/Q-type Ca2+ channels. *Journal of Neuroscience, 20*(18), 6830-6838.

Leitman, D. I., Foxe, J. J., Butler, P. D., Saperstein, A., Revheim, N., & Javitt, D. C. (2005). Sensory contributions to impaired prosodic processing in schizophrenia. *Biological Psychiatry, 58*(1), 56-61.

Leitman, D. I., Hoptman, M. J., Foxe, J. J., Saccente, E., Wylie, G. R., Nierenberg, J., . . . Javitt, D. C. (2007). The neural substrates of impaired prosodic detection in schizophrenia and its sensorial antecedents. *American Journal of Psychiatry, 164*(3), 474-482.

Leitman, D. I., Laukka, P., Juslin, P. N., Saccente, E., Butler, P., & Javitt, D. C. (2008). Getting the cue: sensory contributions to auditory emotion recognition impairments in schizophrenia. *Schizophrenia Bulletin, 36*(3), 545-556.

Leitman, D. I., Sehatpour, P., Higgins, B. A., Foxe, J. J., Silipo, G., & Javitt, D. C. (2010). Sensory deficits and distributed hierarchical dysfunction in schizophrenia. *American Journal of Psychiatry, 167*(7), 818-827.

Lemkuil, B. P., Head, B. P., Pearn, M. L., Patel, H. H., Drummond, J. C., & Patel, P. M. (2011). Isoflurane neurotoxicity is mediated by p75NTR-RhoA activation and actin depolymerization. *Anesthesiology: The Journal of the American Society of Anesthesiologists, 114*(1), 49-57.

Leung, A., & Chue, P. (2000). Sex differences in schizophrenia, a review of the literature. *Acta Psychiatrica Scandinavica, 101*(401), 3-38.

Levy, S., Beharier, O., Etzion, Y., Mor, M., Buzaglo, L., Shaltiel, L., . . . Katz, A. (2009). Molecular basis for zinc transporter 1 action as an endogenous inhibitor of L-type calcium channels. *Journal of Biological Chemistry, 284*(47), 32434-32443.

Lewis, D. A., & Levitt, P. (2002). Schizophrenia as a disorder of neurodevelopment. *Annual Review of Neuroscience, 25*(1), 409-432.

Lewis, D. A., & Lieberman, J. A. (2000). Catching up on schizophrenia: natural history and neurobiology. *Neuron, 28*(2), 325-334.

Li, H.-S., Wang, D., Shen, Q., Schonemann, M. D., Gorski, J. A., Jones, K. R., . . . Jan, Y. N. (2003). Inactivation of Numb and Numblike in embryonic dorsal forebrain impairs neurogenesis and disrupts cortical morphogenesis. *Neuron 40*(6), 1105-1118.

Lieberman, J. A., Perkins, D., Belger, A., Chakos, M., Jarskog, F., Boteva, K., & Gilmore, J. (2001). The early stages of schizophrenia: speculations on pathogenesis, pathophysiology, and therapeutic approaches. *Biological Psychiatry, 50*(11), 884-897.

Lieberman, J. A., Stroup, T. S., McEvoy, J. P., Swartz, M. S., Rosenheck, R. A., Perkins, D. O., . . . Lebowitz, B. D. (2005). Effectiveness of antipsychotic drugs in patients with chronic schizophrenia. *New England Journal of Medicine, 2005*(353), 1209-1223.

Light, G. A., Hsu, J. L., Hsieh, M. H., Meyer-Gomes, K., Sprock, J., Swerdlow, N. R., & Braff, D. L. (2006). Gamma band oscillations reveal neural network cortical coherence dysfunction in schizophrenia patients. *Biological Psychiatry, 60*(11), 1231-1240.

Lisman, J., Schulman, H., & Cline, H. (2002). The molecular basis of CaMKII function in synaptic and behavioural memory. *Nature Reviews Neuroscience, 3*(3), 175-190.

Liu, R. C., Linden, J. F., & Schreiner, C. E. (2006). Improved cortical entrainment to infant communication calls in mothers compared with virgin mice. *European Journal of Neuroscience, 23*(11), 3087-3097.

Liu, R. C., & Schreiner, C. E. (2007). Auditory cortical detection and discrimination correlates with communicative significance. *PLoS biology, 5*(7), e173. doi:10.1371/journal.pbio.0050173

Lohmann, C., & Bonhoeffer, T. (2008). A role for local calcium signaling in rapid synaptic partner selection by dendritic filopodia. *Neuron, 59*(2), 253-260.

Lohmann, C., Myhr, K. L., & Wong, R. O. L. (2002). Transmitter-evoked local calcium release stabilizes developing dendrites. *Nature, 418*(6894), 177-181.

Ludwig, A., Flockerzi, V., & Hofmann, F. (1997). Regional expression and cellular localization of the α1 and β subunit of high voltage-activated calcium channels in rat brain. *Journal of Neuroscience, 17*(4), 1339-1349.

Luebke, J. I. (2017). Pyramidal neurons are not generalizable building blocks of cortical networks. *Frontiers in Neuroanatomy, 11*. doi:10.3389/fnana.2017.00011

MacDonald, M. L., Alhassan, J., Newman, J. T., Richard, M., Gu, H., Kelly, R. M., . . . Wills, Z. P. (2017). Selective loss of smaller spines in schizophrenia. *American Journal of Psychiatry, 174*(6), 586-594.

MacLean, B., Tomazela, D. M., Shulman, N., Chambers, M., Finney, G. L., Frewen, B., . . . MacCoss, M. J. (2010). Skyline: an open source document editor for creating and analyzing targeted proteomics experiments. *Bioinformatics, 26*(7), 966-968.

Majewska, A. K., & Sur, M. (2006). Plasticity and specificity of cortical processing networks. *Trends in Neurosciences, 29*(6), 323-329.

Maltez, J. M., Nunziato, D. A., Kim, J., & Pitt, G. S. (2005). Essential Ca v β modulatory properties are AID-independent. *Nature Structural & Molecular Biology, 12*(4), 372-377.

Markham, J. A., & Juraska, J. M. (2002). Aging and sex influence the anatomy of the rat anterior cingulate cortex. *Neurobiology of Aging, 23*(4), 579-588.

Marlin, B. J., Mitre, M., D'amour, J. A., Chao, M. V., & Froemke, R. C. (2015). Oxytocin enables maternal behaviour by balancing cortical inhibition. *Nature, 520*(7548), 499-504.

Matsuzaki, M., Honkura, N., Ellis-Davies, G. C. R., & Kasai, H. (2004). Structural basis of long-term potentiation in single dendritic spines. *Nature, 429*(6993), 761-766.

Matus, A. (1990). Microtubule-associated proteins and the determination of neuronal form. *Journal de Physiologie, 84*(1), 134-137.

McCarley, R. W., Faux, S. F., Shenton, M. E., Nestor, P. G., & Adams, J. (1991). Event-related potentials in schizophrenia: their biological and clinical correlates and new model of schizophrenic pathophysiology. *Schizophrenia Research, 4*(2), 209-231.

McCarley, R. W., Wible, C. G., Frumin, M., Hirayasu, Y., Levitt, J. J., Fischer, I. A., & Shenton, M. E. (1999). MRI anatomy of schizophrenia. *Biological Psychiatry, 45*(9), 1099-1119.

McCarthy, M. M., Arnold, A. P., Ball, G. F., Blaustein, J. D., & De Vries, G. J. (2012). Sex differences in the brain: the not so inconvenient truth. *Journal of Neuroscience, 32*(7), 2241-2247.

McCarthy, M. M., & Konkle, A. T. M. (2005). When is a sex difference not a sex difference. *Frontiers in Neuroendocrinology, 26*(2), 85-102.

McEnery, M. W., Copeland, T. D., & Vance, C. L. (1998). Altered expression and assembly of N-type calcium channel α1B and β subunits in epileptic lethargic (lh/lh) mouse. *Journal of Biological Chemistry, 273*(34), 21435-21438.

McEnery, M. W., Vance, C. L., Begg, C. M., Lee, W.-L., Choi, Y., & Dubel, S. J. (1998). Differential expression and association of calcium channel subunits in development and disease. *Journal of Bioenergetics and Biomembranes, 30*(4), 409-418.

McKinney, B. C., MacDonald, M. L., Newman, J. T., Shelton, M. A., DeGiosio, R. A., Kelly, R. M., . . . Sweet, R. A. (2019). Density of small dendritic spines and microtubule-associated-protein-2 immunoreactivity in the primary auditory cortex of subjects with schizophrenia. *Neuropsychopharmacology, 44*(6), 1055-1061.

McLean, A. C., Valenzuela, N., Fai, S., & Bennett, S. A. (2012). Performing vaginal lavage, crystal violet staining, and vaginal cytological evaluation for mouse estrous cycle staging identification. *JoVE* (67), e4389. doi:10.3791/4389

Meir, A., Bell, D. C., Stephens, G. J., Page, K. M., & Dolphin, A. C. (2000). Calcium channel β subunit promotes voltage-dependent modulation of α1B by Gβγ. *Biophysical Journal, 79*(2), 731-746.

Michie, P. T., Budd, T. W., Todd, J., Rock, D., Wichmann, H., Box, J., & Jablensky, A. V. (2000). Duration and frequency mismatch negativity in schizophrenia. *Clinical Neurophysiology, 111*(6), 1054-1065.

Miranda-Laferte, E., Gonzalez-Gutierrez, G., Schmidt, S., Zeug, A., Ponimaskin, E. G., Neely, A., & Hidalgo, P. (2011). Homodimerization of the Src homology 3 domain of the calcium channel β-subunit drives dynamin-dependent endocytosis. *Journal of Biological Chemistry, 286*(25), 22203-22210.

Mong, J. A., Roberts, R. C., Kelly, J. J., & McCarthy, M. M. (2001). Gonadal steroids reduce the density of axospinous synapses in the developing rat arcuate nucleus: an electron microscopy analysis. *Journal of Comparative Neurology, 432*(2), 259-267.

Moyer, C. E., Delevich, K. M., Fish, K. N., Asafu-Adjei, J. K., Sampson, A. R., Dorph-Petersen, K.-A., . . . Sweet, R. A. (2012). Reduced glutamate decarboxylase 65 protein within primary auditory cortex inhibitory boutons in schizophrenia. *Biological Psychiatry, 72*(9), 734-743.

Moyer, C. E., Delevich, K. M., Fish, K. N., Asafu-Adjei, J. K., Sampson, A. R., Dorph-Petersen, K.-A., . . . Sweet, R. A. (2013). Intracortical excitatory and thalamocortical boutons are

intact in primary auditory cortex in schizophrenia. *Schizophrenia Research, 149*(1), 127-134.

Moyer, C. E., Erickson, S. L., Fish, K. N., Thiels, E., Penzes, P., & Sweet, R. A. (2015). Developmental trajectories of auditory cortex synaptic structures and gap-prepulse inhibition of acoustic startle between early adolescence and young adulthood in mice. *Cerebral Cortex, 26*(5), 2115-2126.

Moyer, C. E., Shelton, M. A., & Sweet, R. A. (2015). Dendritic spine alterations in schizophrenia. *Neuroscience Letters, 601*, 46-53.

Muly, E. C., Smith, Y., Allen, P., & Greengard, P. (2004). Subcellular distribution of spinophilin immunolabeling in primate prefrontal cortex: localization to and within dendritic spines. *Journal of Comparative Neurology, 469*(2), 185-197.

Nakao, A., Miki, T., Shoji, H., Nishi, M., Takeshima, H., Miyakawa, T., & Mori, Y. (2015). Comprehensive behavioral analysis of voltage-gated calcium channel beta-anchoring and-regulatory protein knockout mice. *Frontiers in Behavioral Neuroscience, 9*, 141. doi:10.3389/fnbeh.2015.00141

Namkung, Y., Smith, S. M., Lee, S. B., Skrypnyk, N. V., Kim, H.-L., Chin, H., . . . Shin, H.-S. (1998). Targeted disruption of the Ca2+ channel β3 subunit reduces N-and L-type Ca2+ channel activity and alters the voltagedependent activation of P/Q-type Ca2+ channels in neurons. *Proceedings of the National Academy of Sciences, 95*(20), 12010-12015.

Navone, F., Jahn, R., Di Gioia, G., Stukenbrok, H., Greengard, P., & De Camilli, P. (1986). Protein p38: an integral membrane protein specific for small vesicles of neurons and neuroendocrine cells. *Journal of Cell Biology, 103*(6), 2511-2527.

Neef, J., Gehrt, A., Bulankina, A. V., Meyer, A. C., Riedel, D., Gregg, R. G., . . . Moser, T. (2009). The Ca2+ channel subunit β2 regulates Ca2+ channel abundance and function in inner hair cells and is required for hearing. *Journal of Neuroscience, 29*(34), 10730-10740.

Nestler, E. J., & Hyman, S. E. (2010). Animal models of neuropsychiatric disorders. *Nature Neuroscience, 13*(10), 1161-1169.

Nimchinsky, E. A., Sabatini, B. L., & Svoboda, K. (2002). Structure and function of dendritic spines. *Annual Review of Physiology, 64*(1), 313-353.

O'Donnell, B., Vohs, J., Hetrick, W., Carroll, C., & Shekhar, A. (2004). Auditory event-related potential abnormalities in bipolar disorder and schizophrenia. *International Journal of Psychophysiology, 53*(1), 45-55.

Obermair, G. J., Schlick, B., Di Biase, V., Subramanyam, P., Gebhart, M., Baumgartner, S., & Flucher, B. E. (2010). Reciprocal interactions regulate targeting of calcium channel β subunits and membrane expression of α1 subunits in cultured hippocampal neurons. *Journal of Biological Chemistry, 285*(8), 5776-5791.

Ohana, E., Sekler, I., Kaisman, T., Kahn, N., Cove, J., Silverman, W. F., . . . Hershfinkel, M. (2006). Silencing of ZnT-1 expression enhances heavy metal influx and toxicity. *Journal of Molecular Medicine, 84*(9), 753-763.

Ojeda, N., Sánchez, P., Elizagárate, E., Yöller, A., Ezcurra, J., Ramirez, I., & Ballesteros, J. (2007). Course of cognitive symptoms in schizophrenia: a review of the literature. *Actas espanolas de psiquiatria, 35*(4), 263-270.

Okamoto, K.-I., Nagai, T., Miyawaki, A., & Hayashi, Y. (2004). Rapid and persistent modulation of actin dynamics regulates postsynaptic reorganization underlying bidirectional plasticity. *Nature Neuroscience, 7*(10), 1104-1112.

Pakkenberg, B. (1993). Total nerve cell number in neocortex in chronic schizophrenics and controls estimated using optical disectors. *Biological Psychiatry, 34*(11), 768-772.

Palmer, L. M. (2014). Dendritic integration in pyramidal neurons during network activity and disease. *Brain Research Bulletin, 103*, 2-10.

Parker, E. M., Kindja, N. L., Cheetham, C. E. J., & Sweet, R. A. (2020). Sex differences in dendritic spine density and morphology in auditory and visual cortices in adolescence and adulthood. *Scientific Reports, 10*(1), 1-11. doi:10.1038/s41598-020-65942-w

Parker, E. M., & Sweet, R. A. (2018). Stereological assessments of neuronal pathology in auditory cortex in schizophrenia. *Frontiers in Neuroanatomy, 11*, 131. doi:10.3389/fnana.2017.00131

Patil, P. G., Brody, D. L., & Yue, D. T. (1998). Preferential closed-state inactivation of neuronal calcium channels. *Neuron, 20*(5), 1027-1038.

Pekkonen, E., Katila, H., Ahveninen, J., Karhu, J., Huotilainen, M., & Tiihonen, J. (2002). Impaired temporal lobe processing of preattentive auditory discrimination in schizophrenia. *Schizophrenia Bulletin, 28*(3), 467-474.

Penzes, P., Buonanno, A., Passafaro, M., Sala, C., & Sweet, R. A. (2013). Developmental vulnerability of synapses and circuits associated with neuropsychiatric disorders. *Journal of Neurochemistry, 126*(2), 165-182.

Penzes, P., Cahill, M. E., Jones, K. A., VanLeeuwen, J.-E., & Woolfrey, K. M. (2011). Dendritic spine pathology in neuropsychiatric disorders. *Nature Neuroscience, 14*(3), 285-293.

Perez-Reyes, E. (2003). Molecular physiology of low-voltage-activated T-type calcium channels. *Physiological Reviews, 83*, 117-161.

Perez-Reyes, E. (2006). Molecular characterization of T-type calcium channels. *Cell Calcium 40*, 89-96.

Peris, L., Bisbal, M., Martinez-Hernandez, J., Saoudi, Y., Jonckheere, J., Rolland, M., . . . Bosc, C. (2018). A key function for microtubule-associated-protein 6 in activity-dependent stabilisation of actin filaments in dendritic spines. *Nature Communications, 9*(1), 1-15.

Peters, A., & Kaiserman-Abramof, I. R. (1970). The small pyramidal neuron of the rat cerebral cortex. The perikaryon, dendrites and spines. *American Journal of Anatomy, 127*(4), 321-355.

Petersen, C. C. H., & Crochet, S. (2013). Synaptic computation and sensory processing in neocortical layer 2/3. *Neuron, 78*(1), 28-48.

Petkova, E., Lu, F., Kantrowitz, J., Sanchez, J. L., Lehrfeld, J., Scaramello, N., . . . Su, Z. (2014). Auditory tasks for assessment of sensory function and affective prosody in schizophrenia. *Comprehensive Psychiatry, 55*(8), 1862-1874.

Phifer, C. B., & Terry, L. M. (1986). Use of hypothermia for general anesthesia in preweanling rodents. *Journal of Physiology Behavior, 38*(6), 887-890.

Pichler, M., Cassidy, T. N., Reimer, D., Haase, H., Kraus, R., Ostler, D., & Striessnig, J. (1997). β subunit heterogeneity in neuronal L-type Ca2+ channels. *Journal of Biological Chemistry, 272*(21), 13877-13882.

Platholi, J., Herold, K. F., Hemmings Jr, H. C., & Halpain, S. (2014). Isoflurane reversibly destabilizes hippocampal dendritic spines by an actin-dependent mechanism. *PloS One, 9*(7), e102978. doi:10.1371/journal.pone.0102978

Poplawski, G. H. D., Tranziska, A.-K., Leshchyns' ka, I., Meier, I. D., Streichert, T., Sytnyk, V., & Schachner, M. (2012). L1CAM increases MAP2 expression via the MAPK pathway to promote neurite outgrowth. *Molecular and Cellular Neuroscience, 50*(2), 169-178.

Prange-Kiel, J., Jarry, H., Schoen, M., Kohlmann, P., Lohse, C., Zhou, L., & Rune, G. M. (2008). Gonadotropin-releasing hormone regulates spine density via its regulatory role in hippocampal estrogen synthesis. *Journal of Cell Biology, 180*(2), 417-426.

Purcell, S. M., Moran, J. L., Fromer, M., Ruderfer, D., Solovieff, N., Roussos, P., . . . Kähler, A. (2014). A polygenic burden of rare disruptive mutations in schizophrenia. *Nature, 506*(7487), 185-190.

Ramón y Cajal, S. (1888). Estructura de los centros nerviosos de las aves. *Rev Trim Histol Norm Pat, 1*, 1-10.

Ramón y Cajal, S. (1890). Textura de las circunvolutiones cerebrales de los mamíferos inferiores. Nota preventiva. *Gaceta Medica Catalana, 1*.

Ramón y Cajal, S. (1893). Neue Darstellung vom histologischen Bau des Centralnervensystems. *Arch Anat u Physiol Anat Abt*, 319-428.

Ripke, S., O'Dushlaine, C., Chambert, K., Moran, J. L., Kähler, A. K., Akterin, S., . . . Fromer, M. (2013). Genome-wide association analysis identifies 13 new risk loci for schizophrenia. *Nature Genetics, 45*(10), 1150-1159.

Risher, W. C., Ustunkaya, T., Alvarado, J. S., & Eroglu, C. (2014). Rapid Golgi analysis method for efficient and unbiased classification of dendritic spines. *PloS One, 9*(9), e107591. doi:10.1371/journal.pone.0107591

Rochefort, N. L., & Konnerth, A. (2012). Dendritic spines: from structure to in vivo function. *EMBO reports, 13*(8), 699-708.

Roger, B., Al-Bassam, J., Dehmelt, L., Milligan, R. A., & Halpain, S. (2004). MAP2c, but not tau, binds and bundles F-actin via its microtubule binding domain. *Current Biology, 14*(5), 363-371.

Rojo, C., Leguey, I., Kastanauskaite, A., Bielza, C., Larranaga, P., DeFelipe, J., & Benavides-Piccione, R. (2016). Laminar Differences in Dendritic Structure of Pyramidal Neurons in the Juvenile Rat Somatosensory Cortex. *Cerebral Cortex, 26*(6), 2811-2822.

Sabatini, B. L., & Svoboda, K. (2000). Analysis of calcium channels in single spines using optical fluctuation analysis. *Nature, 408*(6812), 589-593.

Salisbury, D. F., Kuroki, N., Kasai, K., Shenton, M. E., & McCarley, R. W. (2007). Progressive and interrelated functional and structural evidence of post-onset brain reduction in schizophrenia. *Archives of General Psychiatry, 64*(5), 521-529.

Schizophrenia Working Group of the Psychiatric Genomics Consortium. (2014). Biological insights from 108 schizophrenia-associated genetic loci. *Nature, 511*(7510), 421-427.

Schlick, B., Flucher, B., & Obermair, G. (2010). Voltage-activated calcium channel expression profiles in mouse brain and cultured hippocampal neurons. *Neuroscience, 167*(3), 786-798.

Schulman, H. (2004). Activity-dependent regulation of calcium/calmodulin-dependent protein kinase II localization. *Journal of Neuroscience, 24*(39), 8399-8403.

Schultz, S. K., Miller, D. D., Oliver, S. E., Arndt, S., Flaum, M., & Andreasen, N. C. (1997). The life course of schizophrenia: age and symptom dimensions. *Schizophrenia Research, 23*(1), 15-23.

Schwarz, J. M., Liang, S.-L., Thompson, S. M., & McCarthy, M. M. (2008). Estradiol induces hypothalamic dendritic spines by enhancing glutamate release: a mechanism for organizational sex differences. *Neuron, 58*(4), 584-598.

Scott, V. E., De, M. W., Liu, H., Gurnett, C. A., Venzke, D. P., Lennon, V. A., & Campbell, K. P. (1996). Beta subunit heterogeneity in N-type Ca2+ channels. *Journal of Biological Chemistry, 271*(6), 3207-3212.

Segal, D., Ohana, E., Besser, L., Hershfinkel, M., Moran, A., & Sekler, I. (2004). A role for ZnT-1 in regulating cellular cation influx. *Biochemical and Biophysical Research Communications, 323*(4), 1145-1150.

Selden, S. C., & Pollard, T. D. (1983). Phosphorylation of microtubule-associated proteins regulates their interaction with actin filaments. *Journal of Biological Chemistry, 258*(11), 7064-7071.

Shelley, A. M., Ward, P. B., Catts, S. V., Michie, P. T., Andrews, S., & McConaghy, N. (1991). Mismatch negativity: an index of a preattentive processing deficit in schizophrenia. *Biological Psychiatry, 30*(10), 1059-1062.

Shelton, M. A., Newman, J. T., Gu, H., Sampson, A. R., Fish, K. N., MacDonald, M. L., . . . Sweet, R. A. (2015). Loss of microtubule-associated protein 2 immunoreactivity linked to dendritic spine loss in schizophrenia. *Biological Psychiatry, 78*(6), 374-385.

Sheng, Z.-H., Westenbroek, R. E., & Catterall, W. A. (1998). Physical link and functional coupling of presynaptic calcium channels and the synaptic vesicle docking/fusion machinery. *Journal of Bioenergetics and Biomembranes, 30*(4), 335-345.

Shenton, M. E., Dickey, C. C., Frumin, M., & McCarley, R. W. (2001). A review of MRI findings in schizophrenia. *Schizophrenia Research, 49*(1), 1-52.

Shepard, K. N., Chong, K. K., & Liu, R. C. (2016). Contrast enhancement without transient map expansion for species-specific vocalizations in core auditory cortex during learning. *eNeuro, 3*(6). doi:10.1523/ENEURO.0318-16.2016

Shors, T. J., Chua, C., & Falduto, J. (2001). Sex differences and opposite effects of stress on dendritic spine density in the male versus female hippocampus. *Journal of Neuroscience, 21*(16), 6292-6297.

Smith, C. C., Vedder, L. C., & McMahon, L. L. (2009). Estradiol and the Relationship between Dendritic Spines, NR2B Containing NMDA Receptors, and the Magnitude of Long-Term Potentiation at Hippocampal CA3-CA1 Synapses. *Psychoneuroendocrinology, 34*, S130-S142.

Somogyi, P., & Cowey, A. (1981). Combined Golgi and electron microscopic study on the synapses formed by double bouquet cells in the visual cortex of the cat and monkey. *Journal of Comparative Neurology, 195*(4), 547-566.

Spacek, J., & Harris, K. M. (1998). Three-dimensional organization of cell adhesion junctions at synapses and dendritic spines in area CA1 of the rat hippocampus. *Journal of Comparative Neurology, 393*(1), 58-68.

Stark, A. K., Uylings, H. B., Sanz-Arigita, E., & Pakkenberg, B. (2004). Glial cell loss in the anterior cingulate cortex, a subregion of the prefrontal cortex, in subjects with schizophrenia. *American Journal of Psychiatry, 161*(5), 882-888.

Stoica, L., Ahmed, S. S., Gao, G., & Esteves, M. S. (2013). AAV-mediated gene transfer to the mouse CNS. *Current Protocols in Microbiology, Chapter 14*, Unit 14D.15.

Stotz, S. C., Barr, W., McRory, J. E., Chen, L., Jarvis, S. E., & Zamponi, G. W. (2004). Several structural domains contribute to the regulation of N-type calcium channel inactivation by the β3 subunit. *Journal of Biological Chemistry, 279*(5), 3793-3800.

Subramanyam, P., Obermair, G. J., Baumgartner, S., Gebhart, M., Striessnig, J., Kaufmann, W. A., . . . Flucher, B. E. (2009). Activity and calcium regulate nuclear targeting of the calcium channel beta4b subunit in nerve and muscle cells. *Channels, 3*(5), 343-355.

Sweet, R. A., Bergen, S. E., Sun, Z., Marcsisin, M. J., Sampson, A. R., & Lewis, D. A. (2007). Anatomical evidence of impaired feedforward auditory processing in schizophrenia. *Biological Psychiatry, 61*(7), 854-864.

Sweet, R. A., Bergen, S. E., Sun, Z., Sampson, A. R., Pierri, J. N., & Lewis, D. A. (2004). Pyramidal cell size reduction in schizophrenia: evidence for involvement of auditory feedforward circuits. *Biological Psychiatry, 55*(12), 1128-1137.

Sweet, R. A., Henteleff, R. A., Zhang, W., Sampson, A. R., & Lewis, D. A. (2009). Reduced dendritic spine density in auditory cortex of subjects with schizophrenia. *Neuropsychopharmacology, 34*(2), 374-389.

Sweet, R. A., Pierri, J. N., Auh, S., Sampson, A. R., & Lewis, D. A. (2003). Reduced pyramidal cell somal volume in auditory association cortex of subjects with schizophrenia. *Neuropsychopharmacology, 28*(3), 599-609.

Szebenyi, G., Bollati, F., Bisbal, M., Sheridan, S., Faas, L., Wray, R., . . . Brady, S. T. (2005). Activity-driven dendritic remodeling requires microtubule-associated protein 1A. *Current Biology, 15*(20), 1820-1826.

Taft, C. E., & Turrigiano, G. G. (2014). PSD-95 promotes the stabilization of young synaptic contacts. *Philosophical Transactions of the Royal Society B, 369*(1633), 20130134.

Takahashi, E., Mitsuhiro, I., & Nagasu, T. (2004). Effect of Genetic Background on Cav2 Channel α1 and β Subunit Messenger RNA Expression in Cerebellum of N-Type Ca2+ Channel α1B Subunit-Deficient Mice. *Comparative Medicine, 54*(6), 690-694.

Tanaka, O., Sakagami, H., & Kondo, H. (1995). Localization of mRNAs of voltage-dependent Ca2+-channels: four subtypes of α1-and β-subunits in developing and mature rat brain. *Molecular Brain Research, 30*(1), 1-16.

Tasaka, G.-i., Feigin, L., Maor, I., Groysman, M., DeNardo, L. A., Schiavo, J. K., . . . Mizrahi, A. (2019). Temporal Association Cortex-A Cortical Hub for Processing Infant Vocalizations. *SSRN Electronic Journal*. doi:10.2139/ssrn.3385122

Tasaka, G.-i., Guenthner, C. J., Shalev, A., Gilday, O., Luo, L., & Mizrahi, A. (2018). Genetic tagging of active neurons in auditory cortex reveals maternal plasticity of coding ultrasonic vocalizations. *Nature Communications, 9*(1), 871.

Thune, J. J., Uylings, H. B. M., & Pakkenberg, B. (2001). No deficit in total number of neurons in the prefrontal cortex in schizophrenics. *Journal of Psychiatric Research, 35*(1), 15-21.

Tija, M., Yu, X., Jammu, L. S., Lu, J., & Zuo, Y. (2017). Pyramidal Neurons in Different Cortical Layers Exhibit Distinct Dynamics and Plasticity of Apical Dendritic Spines. *Frontiers in Neural Circuits, 11*(43). doi:10.3389/fncir.2017.00043

Todd, B. J., Schwartz, J. M., Mong, J. A., & McCarthy, M. M. (2007). Glutamate AMPA/Kainate receptors, not GABAA receptors, mediate estradiol-induced sex differences in the hypothalamus. *Developmental Neurobiology, 67*, 304-315.

Trachtenberg, J. T., Chen, B. E., Knott, G. W., Feng, G., Sanes, J. R., Welker, E., & Svoboda, K. (2002). Long-term in vivo imaging of experience-dependent synaptic plasticity in adult cortex. *Nature, 420*(6917), 788-794.

Villa, K. L., Berry, K. P., Subramanian, J., Cha, J. W., Oh, W. C., Kwon, H.-B., . . . Nedivi, E. (2016). Inhibitory synapses are repeatedly assembled and removed at persistent sites in vivo. *Neuron, 89*(4), 756-769.

Vita, A., De Peri, L., Deste, G., & Sacchetti, E. (2012). Progressive loss of cortical gray matter in schizophrenia: a meta-analysis and meta-regression of longitudinal MRI studies. *Translational Psychiatry, 2*, e190. doi:10.1038/tp.2012.116

Walker, D., Bichet, D., Campbell, K. P., & De Waard, M. (1998). A β4 isoform-specific interaction site in the carboxyl-terminal region of the voltage-dependent Ca2+ channel α1A subunit. *Journal of Biological Chemistry, 273*(4), 2361-2367.

Walker, D., Bichet, D., Geib, S., Mori, E., Cornet, V., Snutch, T. P., . . . De Waard, M. (1999). A New β Subtype-specific Interaction in α1ASubunit Controls P/Q-type Ca2+ Channel Activation. *Journal of Biological Chemistry, 274*(18), 12383-12390.

Weinhard, L., Neniskyte, U., Vadisiute, A., di Bartolomei, G., Aygün, N., Riviere, L., . . . Gross, C. (2018). Sexual dimorphism of microglia and synapses during mouse postnatal development. *Developmental Neurobiology, 78*(6), 618-626.

Wexler, B. E., Stevens, A. A., Bowers, A. A., Sernyak, M. J., & Goldman-Rakic, P. S. (1998). Word and tone working memory deficits in schizophrenia. *Archives of General Psychiatry, 55*(12), 1093-1096.

Wissman, A. M., May, R. M., & Woolley, C. S. (2012). Ultrastructural analysis of sex differences in nucleus accumbens synaptic connectivity. *Brain Structure Function, 217*(2), 181-190.

Wittemann, S., Mark, M. D., Rettig, J., & Herlitze, S. (2000). Synaptic localization and presynaptic function of calcium channel β4-subunits in cultured hippocampal neurons. *Journal of Biological Chemistry, 275*(48), 37807-37814.

Wong, A., & Van Tol, H. (2003). Schizophrenia: from phenomenology to neurobiology. *Neuroscience and Biobehavioral Reviews, 27*(3), 269-306.

Wong, A. H. C., & Van Tol, H. H. (2003). Schizophrenia: from phenomenology to neurobiology. *Neuroscience & Biobehavioral Reviews, 27*(3), 269-306.

Woolley, C. S., Gould, E., Frankfurt, M., & McEwen, B. S. (1990). Naturally occurring fluctuation in dendritic spine density on adult hippocampal pyramidal neurons. *Journal of Neuroscience, 10*(12), 4035-4039.

Woolley, C. S., & McEwen, B. S. (1992). Estradiol mediates fluctuation in hippocampal synapse density during the estrous cycle in the adult rat. *Journal of Neuroscience, 12*(7), 2549-2554.

Wright, C. L., Burks, S. R., & McCarthy, M. M. (2008). Identification of prostaglandin E2 receptors mediating perinatal masculinization of adult sex behavior and neuroanatomical correlates. *Developmental Neurobiology, 68*(12), 1406-1419.

Wright, C. L., Schwarz, J. S., Dean, S. L., & McCarthy, M. M. (2010). Cellular mechanisms of estradiol-mediated sexual differentiation of the brain. *Trends in Endocrinology Metabolism, 21*(9), 553-561.

Xiao, Z., Qiu, T., Ke, X., Xiao, X., Xiao, T., Liang, F., . . . Chu, K. (2014). Autism spectrum disorder as early neurodevelopmental disorder: Evidence from the brain imaging abnormalities in 2–3 years old toddlers. *Journal of Autism and Developmental Disorders, 44*(7), 1633-1640.

Yasuda, R., Sabatini, B. L., & Svoboda, K. (2003). Plasticity of calcium channels in dendritic spines. *Nature Neuroscience, 6*(9), 948-955.

Yasuda, T., Lewis, R. J., & Adams, D. J. (2004). Overexpressed Cavβ3 inhibits N-type (Cav2. 2) calcium channel currents through a hyperpolarizing shift of "ultra-slow" and "closed-state" inactivation. *The Journal of General Physiology, 123*(4), 401-416.

Yeon, J.-H., Park, C.-G., Hille, B., & Suh, B.-C. (2018). Translocatable voltage-gated Ca2+ channel β subunits in α1–β complexes reveal competitive replacement yet no spontaneous dissociation. *Proceedings of the National Academy of Sciences, 115*(42), E9934-E9943.

Yuste, R. (2011). Dendritic spines and distributed circuits. *Neuron, 71*(5), 772-781.

Yuste, R., Majewska, A., & Holthoff, K. (2000). From form to function: calcium compartmentalization in dendritic spines. *Nature Neuroscience, 3*(7), 653-659.

Zamponi, G. W. (2005). *Voltage-gated calcium channels*: Springer.

Zhang, W., Peterson, M., Beyer, B., Frankel, W. N., & Zhang, Z.-w. (2014). Loss of MeCP2 from forebrain excitatory neurons leads to cortical hyperexcitation and seizures. *Journal of Neuroscience, 34*(7), 2754-2763.

Zhang, Y., Chen, Y.-h., Bangaru, S. D., He, L., Abele, K., Tanabe, S., . . . Yang, J. (2008). Origin of the voltage dependence of G-protein regulation of P/Q-type Ca2+ channels. *Journal of Neuroscience, 28*(52), 14176-14188.

Zhang, Y., Mori, M., Burgess, D. L., & Noebels, J. L. (2002). Mutations in high-voltage-activated calcium channel genes stimulate low-voltage-activated currents in mouse thalamic relay neurons. *Journal of Neuroscience, 22*(15), 6362-6371.

Zhao, Y., Sivaji, S., Cheng, A., Ali, H., Guo, Z., Reed, A., . . . Wills, Z. P. (2017). Amyloid beta peptides block new synapse assembly by nogo receptor mediated inhibition of t-type calcium channels. *Neuron, 96*(2), 355-372.

Zhou, Q., Homma, K. J., & Poo, M.-m. (2004). Shrinkage of dendritic spines associated with long-term depression of hippocampal synapses. *Neuron, 44*(5), 749-757.

Ziermans, T. B., Schothorst, P. F., Sprong, M., & van Engeland, H. (2011). Transition and remission in adolescents at ultra-high risk for psychosis. *Schizophrenia Research, 126*(1-3), 58-64.

Zuo, Y., Lin, A., Chang, P., & Gan, W.-B. (2005). Development of long-term dendritic spine stability in diverse regions of cerebral cortex. *Neuron, 46*(2), 181-189.